KWAME NKRUMAH UNIVERSITY OF SCIENCE AND TECHNOLOGY

Mechanistic Studies and Mathematical Models for Mycolactone Toxin and Autoinhibitory WASP: Model Mechanisms for Buruli ulcer Initiation and Spread.

By
Peter Romeo Nyarko
(PG8107512)

A DISSERTATION SUBMITTED TO THE DEPARTMENT OF MATHEMATICS, KWAME NKRUMAH UNIVERSITY OF SCIENCE AND TECHNOLOGY IN PARTIAL FULFILLMENT OF THE REQUIREMENT FOR THE DEGREE OF DOCTOR OF PHILOSOPHY IN APPLIED MATHEMATICS

August 2015

DECLARATION

I declare that I have done this study on my own and that no other sources than those listed in the references have been used.

Peter Romeo Nyarko	.....	.....
	Signature	Date

Student Name
Certified By:

Professor. I.K. Dontwi	.....	.....
Supervisor	Signature	Date

Professor D.E. Bentil	.....	.....
Co-supervisor	Signature	Date

Professor. S.K. Amponsah	.....	.....
Head of Department	Signature	Date

ABSTRACT

The Wiskott-Aldrich Syndrome Protein (WASP) has been implicated in many diseases such as Wiskott-Aldrich Syndrome (WAS) and Buruli ulcer. *Mycobactrium*

ulcerans is the main causative organism of Buruli ulcer (BU) disease. The bacteria secretes a polyketide lipid toxin (*Mycolactone*). The toxin not only diffuses through the cell membranes, but also binds, hijacks and disrupts the normal functions of WASP in the cytoplasm leading to over polymerization of actin filament, cytoskeletal rearrangement and eventually cell death through necrosis. In pre-ulcerative BU disease, toxins extend beyond the actual size of the lesion. A mathematical model is developed to describe the binding mechanism of the two conformations of WASP and the complexes formed using the idea of isomerization. The formulation utilizes ligand concentration-dependence (ligand-receptor), equilibrium and conservation principles. By this approach, we are able to determine the fractional response of WASP against change in concentration of its activators; Cell division cycle 42 (Cdc42) and *Mycolactone*. There is a lag phase is the analysis of the binding process which explains the breaking of bonds between the GTPase-binding domain (GBD) and the VCA

(verprolin, cofilin, acidic) of WASP. The analyses confirm the results obtained by Laure et al. [2013] and the need for competitive inhibitors of *Mycolactone* toxin, to prevent *Mycolactone* from binding to the hydrophobic region of WASP for effective treatment of BU. To further understand the intracellular behavior of the toxin and WASP binding, the reaction-diffusion system arising from the binding process is solved in the cell cytoplasm. A periodic geometry is introduced for computing quasi-periodicity. Computational time and CPU memory have been drastically reduced as a result of simulating only one cell as a true representation of a layer of tissue, which consists of millions of cells. The complex system of coupled Partial Differential Equations (PDEs) arising from the Cdc42-WASP-*Mycolactone* binding is

implemented in Comsol Multiphysics. In the numerical simulation, two different geometrical representation of the cell membrane are implemented. The numerical results from the two implementations were identical. From the analysis the extent of diffusion of the toxin in the tissue can be predicted with time. To further probe the numerical results, the performance of three direct sparse solvers namely: UMFPACK, SPOOLES, and PARDISO were compared, mainly for their time, and CPU memory requirements in computing solutions. The PARDISO solver is found to perform better than the other two in the present study. The numerical solutions confirm experimental findings on BU disease, and further augment the understanding of the role of WASP in polymerization of actin filament and cytoskeletal rearrangement.

DEDICATION

The work is dedicated to my love, Leticia Nyarko for her prayers, support and encouragement to do this work.

ACKNOWLEDGEMENT

My humble thanks go to God whose constant love and blessings enabled me to complete this important research work. I am very grateful to God for seeing me through this phase of my career.

I would like to gratefully and wholeheartedly, acknowledge the support and guidance of my lead supervisor Professor. Dr. Isaac Kwame Dontwi, without his guidance and encouragement, this work would not have been accomplished. I appreciate the freedom he gave me, to explore and develop ideas while working on my research (I see him as a father). My sincere thanks go to Professor Dr. Daniel E. Bentil; University of Vermont, USA, who gave me the excellent insight into the real mathematical biology. I have benefited immensely from his authority in the field to get my taught right. His patience, suggestions and motivation during the writing of this thesis were excellent. I thank Dr. Amoako-Yirenkyi for assisting with mathematical analysis, and for providing feedback on my modeling endeavors.

Over the past three years I have had the opportunity to collaborate with several researchers and I would like to acknowledge their contribution to this work. In particular, I would like to thank; Dr. William Philips of KCCR and Komfo Anokyi teaching hospital Kumasi, Ghana and Professor Dr. Pamela L. C. Small; Department of Microbiology, Knoxville, Tennessee, USA, for their many discussions on the Pathogenesis of *Mycobacterium ulcerans* infection. I thank Dr Osei Asante for helpful discussions about cell Biology.

Many thanks go to all the lecturers in the department of mathematics KNUST, especially Professor S. K. Amponsah for the encouragement and friendly atmosphere created during the course of writing this thesis. To all my PhD colleagues at KNUST; Parker, Edem, Justice and Anokye, I say God richly bless you. My life would not have been so exciting and memorable without your company.

To my parents; Mr. Joseph Kwadwo Nyarko and Mrs. Akua Asantewaa, for instilling in me the love for learning, I say I love you. I appreciate your love and support during the up and down periods.

Finally, I owe my loving thanks to my friend and wife, Leticia Nyarko, for her unflinching love, encouragement, prayers and faith in me. Her soothing words always made me feel better and urged me on. It is not surprising that I dedicate this thesis to her. To my wonderful kids: Kwasi and Afia Nyarko, I say thank you for the unconditional love.

TABLE OF CONTENTS

LIST OF FIGURES

Figure

CHAPTER 1

INTRODUCTION

1.1 Background

Buruli ulcer (BU), is an infectious disease in immunocompetent humans that is caused by *Mycobacterium ulcerans (M. ulcerans)*. The World Health Organization (WHO) defines BU as an infectious disease involving the skin and the subcutaneous adipose tissue, characterized by a painless nodule, papule, plaque, which normally evolves into a painless ulcer with characteristically undermined edges. If left untreated it can lead to massive skin ulceration and complication such as disfiguring, loss of certain organs such as eyes, hands, limbs and ears. There is significant psychological burden on the patient and complicated cases require between three to eighteen months hospitalization for treatment [Siegmund et al., 2005]. The disease is one of the most *neglected tropical diseases* that largely affect the poor in remote rural areas [Siegmund et al., 2005, Richard et al., 2005]. BU is the third mycobacteriosis in prevalence, after leprosy and tuberculosis [Meyers, 1996]. The disease was first discovered in 1897, by Sir Albert Cook in Uganda when he described skin ulcers consistent with Buruli ulcer and in 1948, MacCallum, published the first confirmed case of the disease in Australia. In Australia, the disease was called Bairnsdale ulcer after the main town in the original endemic region. In Africa, it is called Buruli ulcer, named after a county in Uganda where large number of BU cases were reported in the 1950s [Portaels et al., 2001, Clancey et al., 1962].

In March 2004, the WHO report indicated that BU has been reported or suspected in over 30 countries with tropical and subtropical climates worldwide [WHO, 2004]. BU has emerged as an important cause of human suffering. In BU endermic countries, the efficient use of scarce health care resources are undermined and knowledge, awareness, mode of transmission and spread of the disease, both within the medical community and among the general public is limited. Therefore the resultant effects are under-recognition and underreporting [WHO, 2004].

It is reported that after inoculation into the skin, *M. ulcerans* proliferates the extracellular region and exudes a polyketide lipid toxin (*Mycolactone*), that enters the cells by passive diffusion and causes necrosis of the dermis, panniculus, and deep fascia. Early lesions are closed, but as the necrosis spreads, the overlying dermis and epidermis eventually ulcerate, with undermined edges and a necrotic slough in the base of the ulcer (see Fig1.1). Histopathologic sections reveal a contiguous coagulation necrosis of the deep dermis and panniculus, with destruction of nerves, appendages, and blood vessels. Clumps of extracellular acid-fast bacilli are plentiful and are frequently limited to the base of the ulcer and adjacent necrotic subcutaneous tissues. In active lesions, inflammatory cells are conspicuously few, presumably as a result of the immunosuppressive activity of the toxin. After healing, there is a granulomatous response, and the ulcerated area is eventually replaced by a depressed

scar.

Currently, West Africa appears to be the most affected region. About 70 percent of those affected are children under the age of 15 years. Unfortunately, the epidemiology of the disease remains unclear [Boleira et al., 2010]. Furthermore, the

prevalence of the disease is not accurately known [Portaels et al., 2001]. Therefore, there is frequent misclassification and delayed diagnosis of BU disease with considerable socioeconomic impact in terms of treatment cost due to prolonged hospitalization [Siegmund et al., 2005].

Over 15,000 cases of BU were recorded in Cote d'Ivoire between 1978 and 1999 with an estimated 16 percent prevalence rates in some communities. About 4000 cases of BU were reported in Benin over a period of ten years and in Ghana, studies show about 6000 reported BU cases, and all 10 regions of the country are affected, with the Ashanti region recording the highest percentage. BU cases have also been reported in other West African countries such as Burkina Faso, Togo, and Guinea [WHO., 2001, Amofah et al., 2002].

1.2 Problem Statement

In Boleira et al. [2010], the authors report that *M. ulcerans* is capable of producing *Mycolactone*, an immunomodulatory macrolide toxin that causes tissue necrosis and destroys the skin and soft tissues (from the cell level) with the formation of large ulcers, often in the arms or legs (although other parts of the body can equally be affected). An *in vivo* studies on a guinea pig model suggests that *Mycolactone* is responsible for both the extensive tissue damage and immunosuppression observed in Buruli ulcer cases [George et al., 1999]. In general, patients who do not seek early medical treatment often suffer functional disabilities and disfiguring originating from self-healing processes or surgical treatment, with majority of patients having deformities in their joints restricting their ability to execute and participate in every

day activities. Therefore, early diagnosis and specific treatment for BU associated disease with interventions that prevent disabilities are crucial. In the work of Simona et al.

[2006] on the detection of *Mycobacterium Ulcerans* DNA in the margin of an excised BU lesion, they found that after an en bloc surgical removal of a clinically diagnosed BU, analysis conducted for the spread of *Mycobacterium ulcerans* and toxins in the margin of 2 to 3cm of healthy-looking tissue was positive. In pre-ulcerative BU disease, toxins extend beyond the actual size of the lesion [Bretzel et al., 2011]. The question is, to what margin must the surgeon cut to remove all infected tissue to prevent re-occurrence of the disease?

This study provides a mathematical model that predicts the kinetics of the toxin and the reaction-diffusion of the *Mycolactone* and it metabolites in the tissue. The model can be used to predict the extent of infection and therefore be used for the treatment and eradication of Buruli Ulcer. The study proposes a ligand-receptor binding that models the kinetics of the polyketide lipid toxin in the cell.

1.3 Research Objectives

In this thesis, the objective is to study ligand-receptor kinetics and to determine active fractions of WASP complexes, in order to predict actin filament polymerization. Secondly, to investigate the binding mechanism of WASP, Cdc42 and *Mycolactone* to identify specific targets for drug discovery for BU disease. Thirdly, numerically solve the reaction-diffusion problem arising from the *Mycolactone*,

ligand and the receptor protein binding in the cytoplasm of the cell. The BU disease is as shown in Figure 1.1

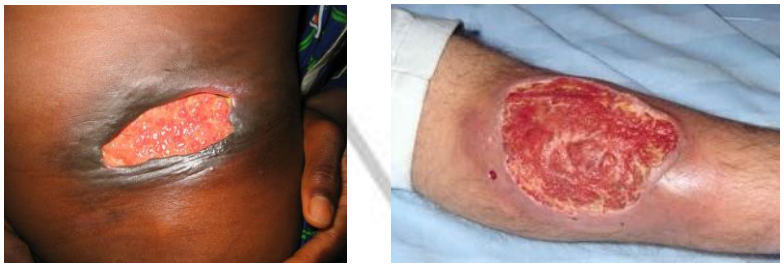

(a) (b)

Figure 1.1: Taken with permission from [WHO]

1.4 Methodology

Singular Perturbation Methods will be used to compute various complexes formed from Enzyme-substrate binding. Two time scales evolve in this approach which are not experimentally measurable. This becomes a limitation to the current study on computing active WASP complexes. An alternative approach is to apply the Law of Detri (see Chapter 3) to compute the fraction of the various complexes in the binding process.

The concept of isomerixation is used to construct binding mechanisms for WASPCdc42, and WASP-Cdc42-*Mycolactone* binding respectively. The fractional activation of WASP at varying concentrations of Cdc42 and *Mycolactone* will be approximated to give an idea of the etiology of the BU disease.

The law of Mass Action and the Fick's Law are applied to write a system of reactiondiffusion equations from the binding mechanisms. The coupled system of

reactiondiffusion equations are solved numerically using Finite Element Method. The model is implemented in Comsol Multiphysics. The numerical results of three direct solvers are compared in the numerical solution.

1.5 Overview of current BU models

Most existing mathematical models for BU have been concentrated on economic and regional predictions. A thermal model has been developed and validated by Braxmeier et al. [2009], for the heat treatment of *Mycobacterium ulcerans* infection (Buruli ulcer). The heat application device is based on a phase change material (pcm). The first prototype trial in Cameroon produced good results consistent with available data. The thermal model allowed for the prediction of skin surface temperatures and the amount of pcm with respect to discharge time could be evaluated and optimized. Imran and Hal [2006] developed a model of a bacterial colonization of host tissue. The model took into account nutrient availability and innate immune response. Their model features a local infection-free state, which is not globally attracting, implying that there exist a super-threshold bacterial inoculum required for successful colonization and tissue infection. Hillen and Mark [2014] developed a model for cell movement in a network of tissues. They formulated the problem as an evolution equation in a Banach space of measure-valued functions and used methods from semigroup theory to show the global existence of mild and classical solutions. Their model revealed the existence of biologically meaningful measure valued solutions, which correspond to tissue and cell alignment. Siegmund et al. [2005], developed a dry-reagent-based PCR (Polymerase chain reaction) formulation for the early detection of *M. ulcerans* in a diagnostic specimen at the Bernard Nocht Institute for

Tropical Medicine. Currently this formulation is being used at the Kumasi Center for Collaborative Research in Tropical Medicine (KCCR). It gives information on the amount of bacterial load in tested tissues but can not predict the extent of infection with time. Schunk et al. [2009] studied the frequency and treatment outcome after surgery of Buruli Ulcer Disease (BUD) with or without antimycobacterial treatment in Ghana. They used the chi-square and the student t-test in their statistical analysis. Their investigation did not establish any relationship between recurrences and clinical or treatment specific factors, but they did emphasize the need for more research into the development and treatment of the wounds. In a paper by Bretzel et al. [2011], on post-surgical assessment of excised tissue from patients with Buruli ulcer, tissue samples were subjected to PCR and histopathology analysis. Although they determined the excision size microscopically by unrealistically assuming a complete removal of all infected tissues, they found the bacterial load to decrease from the center to periphery of the wound. Additionally, their study suggest a correlation between surgical techniques and local recurrences. Furthermore, their study shows that the removal of all infected tissues cannot always be visualized by the surgeon. These are the motivating factors for the proposed research work. It is worth mentioning that none of the works cited above have considered a reaction-diffusion mechanism of the *Mycolactone* and receptor protein binding within cell tissues as is proposed in this study.

In this thesis the words binding and reaction as well as compartment and domain will be used synonymously.

1.6 Thesis outline

In the introductory chapter, a short overview of BU disease, review of related BU models and motivation for the current study of BU is outlined. The idea is to give some fundamental concepts so that the reader may understand the remaining chapters easily. In chapter 2, the cell, constituent structures and species involved in the pathogenesis of BU are discussed. In chapter 3 the concept of ligand-receptor binding mechanisms and fraction of bound receptor sites are introduced. In chapter 4, models for ligand-receptor and ligand-receptor-lipid binding mechanisms to model Cdc42-WASP, and Cdc42-WASP-Mycolactone respectively, are discussed. In chapter 5, steady state of the model and parameterization of the species are discussed. In chapter 6 the reaction diffusion system from the binding mechanisms, is solved in the cytoplasm of the cell. Chapter 7 is a summary of the main results, recommendations and directions for future work.

CHAPTER 2

Biological Background

In this chapter, the cell, constituent structures, proteins and species involved in the pathogenesis of BU are discussed.

2.1 The Cell

The cell is the basic structural, functional and biological unit of all known living organisms. Cells are the smallest unit of life that can replicate independently. They are often called the building blocks of life. The cell has a cytoskeleton that acts to organize and maintain the cell's shape, anchors organelles in place and move parts of the cell in processes of growth and mobility [Bruce et al., 2008]. The structure of the cell is as shown on Figure 2.1 [Seer].

Within the cell is the cytoplasm and the cytoskeletal apparatus. The cytoskeleton's varied functions depends on the behavior of three families of protein molecular assemblies, namely: Intermediate, Microtubules and Actin filaments. Like our ligaments, bones and muscles work together, so do the three filament families work together to promote the proper function of the cytoskeleton. The three filaments, (Intermediate, Microtubules and Actin filaments), provide mechanical strength, determine the position of the membrane-enclosed organelles, direct intracellular transport, determine the shape of the cell surface and locomotion, respectively [Bruce

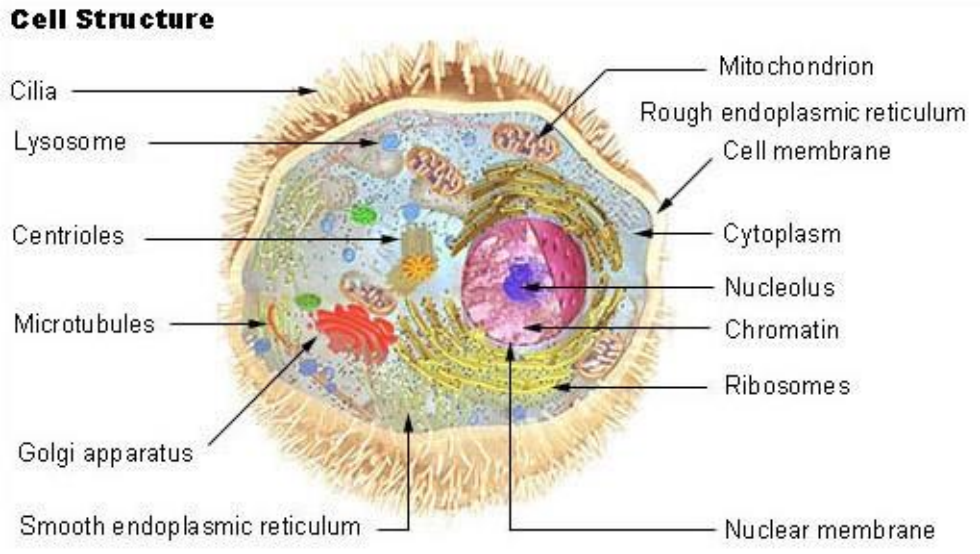

Figure 2.1: Structure of the cell

et al., 2008] (pg 965).

The actin filament is positioned under the plasma membrane of animal cells providing strength and shape to the cell through the lipid bilayer [Helfand et al., 2003, Howard, 2001]. The filaments form many types of cell surface projections of dynamic structures, such as the lamellipodia and filopodia that enable cells to explore and pull themselves around.

With time, the actin-based contractile ring assembly divide cells into two or more stable arrays that allow cells to brace themselves against injury and enable muscle to contract. The intermediate filaments line the inner surface of the nuclear envelope and forms a protective cage for the cell's Deoxyribonucleic acid (DNA). In the cytoplasm (cytosol), they are twisted into strong cables and can hold epithelial cell sheets together. The filaments allow cells to build large cytoskeletal structures that extend from one end to the other [Bruce et al., 2008]. The cytoskeletal filament

(assembly of subunits) form using a combination of end-to-end and side-to-side protein contacts.

Covalent linkages between their subunits hold together many biological polymers, including DNA, RNA and proteins. In contrast, weak non-covalent interactions hold together the three types of cytoskeletal filaments. Consequently, their assembly and disassembly can occur rapidly, without covalent bond being formed or broken. It is important to note that filaments are formed from linkage of protein subunits. These subunits can move in the cytosol because of their small size, but filaments do not move, rather they can be rearranged [Luby-Phelps, 2000, Mitchison, 1995, Hill and Kirschner, 1982, Shih and Rothfield, 2006].

2.2 Protein Subunits are joined by Covalent Linkages

A simple association reaction generally link protein subunits together to form a filament. A free subunit binds to the end of a filament that contains N subunits to generate a filament of length (N + 1). The initial aggregation of subunits, that is stabilized by many subunit-subunit contacts is called *Filament Nucleation*. As with other specific protein-protein interactions, many hydrophobic interaction and weak non-covalent bonds hold the subunit in a cytoskeletal filament together. There is a time lag (lag phase) and a saturation phase in the filament formation depending on how many subunits must come together to form the nucleus [Bruce et al., 2008].

The survival of eucaryotic cells depends on the balance assembly and disassembly of highly conserved cytoskeletal filaments formed from actin and tubuli. These two

types of filaments and proteins bind to initiate filament polymerization. The latter are frequent targets of natural toxins. Generally the toxins either disrupt filament polymerization reaction process or bind tightly to either the filament form or the free subunit form of the polymer driving the assembly reaction in the direction that favors the form to which the toxin binds. Therefore, either a net polymerization or depolymerization of the actin filament is formed and therefore the whole cell function is disrupted [Bruce et al., 2008]. The cytoskeleton is a dynamic structure in living cells that is maintained by a rapid and continual exchange of subunits between the soluble and filamentous forms. The subunit flux is necessary for normal cytoskeletal function [Bradshaw and Dennis, 2003, Palade, 1975]. Cells regulate the length and stability of their cytoskeletal filaments as well as their number and geometry [Howard, 2001]. By regulating the attachment to one another, and to other components of the cell, the filaments form a network of higher-order structures. Through direct covalent modification of filaments, subunits regulate some filament properties, most of the regulation is performed by a large array of accessory proteins that bind to either the filament or their free subunits. The nucleation of actin filament is catalysed by two different types of regulatory factors namely: the Actin related complex (Arp) and the formins. Arp is a complex of proteins that include Arp2/3 which nucleate actin filament growth. In animals, the Arp2/3, complex is located in the lamellipodia and intracellular signaling molecules, and in the cytosolic face of the plasma membrane (i.e. regions of active filament growth) [Bruce et al., 2008].

2.3 The Rho Protein Family and Cytoskeletal Rearrangements

Cell directional migration require long distance communication between one end of the cell and the other. Carefully controlled polarization processes are required for oriented cell divisions in tissue, and in formation of a coherent, organized multicellular structure [Bruce et al., 2008]. For the cytoskeleton, diverse cell surface receptors trigger global structural rearrangements in response to external signals. But all these signals seem to converge inside the cell group of a closely related monomeric GTPases that are members of the Rho-protein family (Cdc42, Rac, and Rho) [Bruce et al., 2008] (pg. 1042). Rho proteins act as molecular switches to control cell processes by cycling between an active GTP-bound state and an inactive GDP-bound state [Howard, 2001]. Activation of Cdc42 on the plasma membrane triggers actin polymerization. Each of these molecular switches bind specific target protein and cause a dramatic structural change in the actin organization in the cell. Some key targets of the activated Cdc42 are members of the Wiskott- Aldrich Syndrome Proteins (WASP) family. Human patients, deficient in WASP suffer from Wiskott-Aldrich Syndrom, a severe form of immunodeficiency where immune system cells have abnormal actin-based motility and platelets do not form normally. Secondly, mutations in the gene encoding WASP, results in an immune system disorder and affected individuals die unless they receive bone marrow transplant. Other related disorders like thrombocytopenia, eczema, and immunodeficiency in humans also exist due to specific mutations in WASP [Martinez et al., 2001, Bruce et al., 2008].

WASP can exist in an inactive, folded and active open conformations. Association with Cdc42-GTP stabilizes the open form of WASP, enabling it to bind to the Arp2/3

complex thus strongly enhancing this complex's actin-nucleating activity. In this way, activation of Cdc42 increases actin nucleation [Bruce et al., 2008, Higgs and Pollard, 2000, 2001]. In the literature [Clin, 2013, Bozzo, 2010], *Mycolactone* is believed to operate by hijacking the WASP family of actin-proteins and disrupting the auto-inhibition WASP leading to an uncontrolled filament formation in the cell. Therefore it will not be out of place to speculate in this work that the covalent binding of *Mycolactone* toxin to WASP induces the immunodeficiencies, and the lack of acute inflammatory response observed in Buruli ulcer patients.

2.4 A survey of Autoinhibitory Protein Functions in the Cell

2.4.1 Autoinhibition

Autoinhibition is a widespread phenomenon that plays a key role in the regulation of proteins by facilitating the response to signaling pathways. The precise regulation of protein activities is essential for normal growth and development. A common regulatory strategy to modulate protein function is provided by intramolecular interactions between separable domains (elements) within a single protein. Specifically one region of a protein interacts with another to negatively regulate its activity. Defining the mechanism of inhibition and the clarification of how the autoinhibition is counteracted or reinforced requires extensive mathematical modeling and additional experimental investigation. There are many examples of self-inhibited, induced and autoinhibited protein models but our main concern in this study is on inhibition of protein-protein interactions (example WASP, SNARE and ERM proteins). Within this diversity, there is a common thread in the mechanism of autoinhibition, that is an intramolecular interaction that either directly or allosterically interferes with the function of a *targeted* domain. The functional

domain could be directly blocked from a necessary ligand interaction or constrained in a nonfunctional conformation by a more indirect mechanism. In general, one can conclude that the modular organization of proteins facilitates regulation by autoinhibition.

Autoinhibitory domains are regions of protein that negatively regulate the function of other domains via intramolecular interactions. Autoinhibition is a potent regulatory mechanism that provides tight *on-site* repression. The discovery of autoinhibition mechanisms have given rise to valuable clues as to how proteins are regulated. Mechanisms that counteract the autoinhibition of proteins often represent central regulatory pathways, and affect many downstream processes. Some instances in which autoinhibition acts in cell regulation include for example ERM, SNARE and WASP [Miles et al., 2002].

The modular design of proteins has several implications for the autoinhibitory phenomenon. First, autoinhibitory domains are distinct from domains that are the target of the inhibition. However, the relationship of an autoinhibitory domain to other domains vary. The autoinhibitory domain can be one whose sole purpose is inhibition or it can be a domain that mediates inhibition but also performs a second activity. Alternatively, there can be mutual inhibition between two domains that possess other activities. A second feature of the modularity of proteins is that domains are often linked by flexible regions. The transition from the inhibited to the activated state usually requires this flexibility. Also , a distinguishing feature for a module that functions as an autoinhibitory domain is the set of intramolecular interactions. Although most protein modules can function in isolation, an

autoinhibitory domain is structurally coupled to the targeted domain. Its inhibitory function is inextricably linked to the function of the remainder of the protein [Miles et al., 2002]. Furthermore the autoinhibitory domain restrains the targeted domain in a secure off state. In some cases, this is the default state, but there exist regulatory strategy that counteract the inhibition. Autoinhibition of a molecule presents a reversible barrier that prevents spurious activation of a signaling pathway. Among the various mechanisms for counteracting inhibition, the most common are the displacement of the inhibitory domain by a second molecule, thus replacing the intramolecular interaction with an intermolecular interactions and or binding of small molecules that allosterically alter the inhibitory domain. However, even this simple formulation comes with surprising diversity (e.g WASP, and SNAREs) as we shall see in chapter

three.

Though there are extremely divergent biological settings for known autoinhibitory phenomena, most mechanistic models of autoinhibition predict the existence of intramolecular interactions between the inhibitory elements and the functional domain [Buck et al., 2001, Miles et al., 2002]. Knowledge of species that activate, presumably by disrupting these interactions, and the mode of activation are informative. This intramolecular interaction model can be tested experimentally. Furthermore a variety of protein-protein interaction assays can also demonstrate intermolecular binding of an inhibitory domain to the targeted functional domain in experiments.

2.4.2 Wiscott-Aldrich Syndrome Protein (WASP)

As mentioned in section 2.3, WASP regulate actin assembly via activation of the Arp2/3 complex. The activation function is masked by autoinhibition. The dynamic assembly and disassembly of actin filaments controls the shape of the membrane within a cell. In addition to providing a structural scaffold, actin filaments are involved in changing membrane shape in cell division, vesicular transport, and motility. Each of these processes requires characteristic networks of actin filaments [Chen et al., 2000].

The WASP family catalyzes actin nucleation and polymerization at the membrane by activating the Arp2/3 complex. The Arp2/3 complex alone nucleates actin poorly and requires the presence of an activator, including members of the WASP family [Higgs and Pollard, 2000, Zalevsky et al., 2001b,a]. The conserved C terminus of all WASP family members, termed the VCA domain (verprolin homology, cofilin homology, acidic region), is necessary for this activation (see Fig.2.2). The VCA domain has been shown to bind directly to the Arp2/3 complex, inducing a conformational change that converts Arp2/3 complex into an active form [Zalevsky et al., 2001b, Volkmann et al., 2001]. In isolation the VCA is fully active, but the activity of the VCA domain is inhibited in the context of the full-length protein by the N terminus [Higgs and Pollard, 2001].

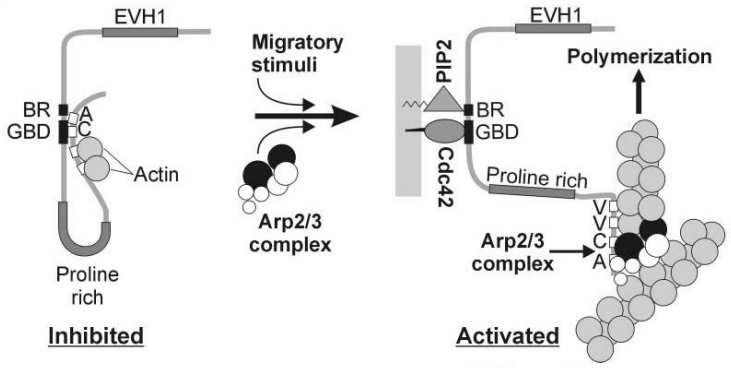

Figure 2.2: left WASP in Autoinhibition state, migration of activators, right activation of the Arp2/3 complex and actin polymerization. Image from Higgs and Pollard [2001], Miles et al. [2002] with permission

Figure 2.2, shows the domain structure of WASP. Notice the inhibited and activated region of WASP (the VCA domain stimulates actin polymerization and branching by activating the Arp2/3 complex). Intramolecular interactions between inhibitory elements, BR-GBD, and the VCA domain mask the activating function of WASP (left). Activated GTPase-Cdc42 and PIP2 displace the inhibitory elements GBD and BR (Basic Region), allowing the VCA domain to activate the Arp2/3 complex, which induces actin polymerization and actin branching, both necessary for the formation of filopodia [Miki et al., 1998]. Some biochemical studies further indicate that the binding of the GBD to Cdc42 and the VCA are mutually exclusive. Together, these studies indicate that the GBD is stabilized either intramolecularly by the VCA domain to create an inhibited WASP or intermolecularly by Cdc42 to create an activated WASP [Kim et al., 2000a].

Amide exchange experiments using a GBD-VCA fragment indicate that the GBD is only partially displaced by Cdc42, which again suggests that multiple inputs are necessary to relieve autoinhibition [Buck et al., 2004].

WASP and its ubiquitously expressed homolog N-WASP share similar biochemical, biophysical, and structural features. In this introduction, my efforts is to summarize their general function and regulation instead of distinguishing their differences.

2.5 Introduction to Actin Related Proteins of the Cell

The actin cytoskeleton of the cell play major roles in numerous cellular processes and it plays a key role in maintaining cell activity and function. More than a hundred actin-related proteins have evolved in eukaryotic cells to regulate the actin cytoskeleton in both space and time [Siripala and D., 2007].

2.5.1 Regulated Dynamics of the Actin Cytoskeleton

One of the most fundamental and abundant protein to life and death is the actin in eukaryotic cells. The cytoskeleton is a dynamic filament network that is essentially responsible for cell movement during embryo development, polymerization, cell division, immune system function and in the metastasis of cancer cells. Cells harness various actin binding proteins to build varied cellular structures and utilize the force generated by actin polymerization to drive these diverse processes.

Cells regulate actin cytoskeleton dynamics in response to extracellular stimulation. These regulated pathways modulate actin assembly and disassembly by switching on the Rho family GTPases. During actin assembly, activated Rho GTPases (Rac and Cdc42) stimulate the actin nucleation and branching factor Arp2/3 complex via members of the Wiskott-Aldrich Syndrome Protein (WASP) family [Jaffe and A., 2005, Hall, 1998, Bruce et al., 2008, Pollard and Cooper, 2009]. WASP is involved in the

pathogenesis of many immune-related disorders and it is a key regulator of actin dynamics.

It is not surprising that toxic substances, bacteria and viruses have evolved mechanisms to interrupt or hijack and usurp the host actin machinery (e.g. cytoskeleton) to serve their own needs during infection. Toxins and pathogens often target the host actin cytoskeleton as a means to facilitate intimate attachment to host membranes and mediate their entry into host cells [Munter et al., 2006, Stevens et al., 2006].

2.5.2 WASP Function in Actin Dynamics

WASP family play a major role in regulating actin dynamics in cells. They are defined by a VCA domain. This protein family consists of WASP, N-WASP (neuronal WASP), WAVE (WASP family verprolin homolog) isoforms 1-3, and WASH (WASP/Scar homolog). All these proteins share similar C-terminal VCA domains, which are required for the biochemical activity of promoting actin polymerization by nucleation and branching factor Arp2/3 complex, but nearly all of them differ in their N-terminal domain organization, indicating that each member has distinct cellular localizations, modes of regulation, and biological functions [Bruce et al., 2008]. WASP is composed of an N-terminal, a basic region (BR), a GTPase binding domain (GBD) and a C-terminal VCA region. The VCA is the activity-bearing domain of WASP, whereas the other N-terminal domains mainly serve regulatory functions. WASP spatially and temporally coordinates numerous signal inputs via its various regulatory domains to give a specific functional output through the VCA. This process turns on the actin nucleating Arp2/3 complex. The major nucleation promoting activity of WASPs VCA is modulated by its N-terminal and the GBD. These regions

receive or engage with various active complexes to link extracellular stimulation to intracellular actin machinery.

An important feature of WASP is its allosteric mechanism. The Rho-family small GTPase Cdc42, phosphatidylinositol 4,5-bisphosphate (PIP2), and SH2 domaincontaining proteins are all major allosteric activators of WASP (see Figure 2.3). WASP is the gene product responsible for the pathogenesis of Wiskott-Aldrich Syndrome, an X-linked recessive, immunosuppressive disease characterized by small platelet size, *thrombocytopenia* (low platelet count), *eczema*, and recurrent infections [Hussain and Jenna, 2001, Derry and Ochs, 1994]. Mainly WASP, is found in haematopoietic cell lineages, such as platelets, B cells, T cells, and monocytes [Stewart and Treiber-Held., 1996].

It has been reported that, the polyketide lipid toxin (*mycolactone*), the main virulence of Buruli ulcer operates by hijacking WASP thereby leading to an uncontrolled polymerization of actin filament in eukaryotic cells. Therefore a detailed study of WASP may provide insights into the pathogenesis of Buruli Ulcer (BU) and other WASP-related diseases. It may also explain the basis of immunosuppression and acute inflammatory response observed in BU patients. To summarize this section: activities of WASP resides in the VCA, which coordinates with Arp2/3 complex to nucleate actin filaments (Figure2.4). These WASP regulators and the nature of their interactions with WASP are reviewed below.

2.5.3 WASP is Autoinhibited via Intramolecular Interactions between GBD and VCA Domains

WASP alone is autoinhibited because the activity bearing VCA is masked by the GBD. The VCA binds to the GBD, but this interaction can be weakened by addition of activated Cdc42 that binds to the GBD [Miki et al., 1998, Kim et al., 2000a].

The activity of WASP in actin assembly is enhanced by the presence of activated Cdc42. In contrast, the isolated VCA fragment at low nanomolar concentrations has at least a hundredfold higher activity than the full-length protein. The full length WASP does exhibit any detectable interaction with Arp2/3 complex, while under the conditions of isolated VCA it displays a strong binding interaction with Arp2/3 complex. Data in the literature support the notion that WASP and N-WASP are autoinhibited via intramolecular interactions between their GBD and VCA. Binding to activated Cdc42 releases this inhibition and allows the VCA to bind and activate Arp2/3 complex (Figure 2.4). The question is how this autoinhibition is achieved. In the research works of Kim et al. [2000a], Panchal et al. [2003], the authors report on the Nuclear Magnetic Resonance (NMR) of actin polymerization show that when Cdc42 binds the VCA of WASP the intramolecular interaction sequesters the C region of the VCA and blocks residues needed for Arp2/3 activation, thus inhibiting WASP.

2.5.4 The Rho family GTPase Cdc42 releases WASP Autoinhibition

The works of Lamarche and Tapon [1996], show that Cdc42 binds to the WASP GBD, with a high affinity in the GTP state. This interaction links Cdc42 to the actin cytoskeleton in cells. Cdc42 competes with the VCA for binding to the GBD [Miki et al., 1998]. Importantly, this binding interaction is required for stimulation of WASP activity in actin assembly. In the active state, the GBD-VCA is largely unfolded and the VCA is readily able to bind and activate Arp2/3 complex; whereas in the closed and inactive state, interactions between the GBD and the VCA blocks the accessibility of the VCA to Arp2/3 complex.

Research works from Buck et al. [2001], Abdul-Manan [1999], Kim et al. [2000a], have established a two-state allosteric equilibrium models to explain WASP

regulation. In these models binding of activated Cdc42 to the GBD, shifts the equilibrium to the open state and globally destabilizes the autoinhibited fold, hence releasing the VCA and activating WASP to stimulate actin assembly by Arp2/3 complex.

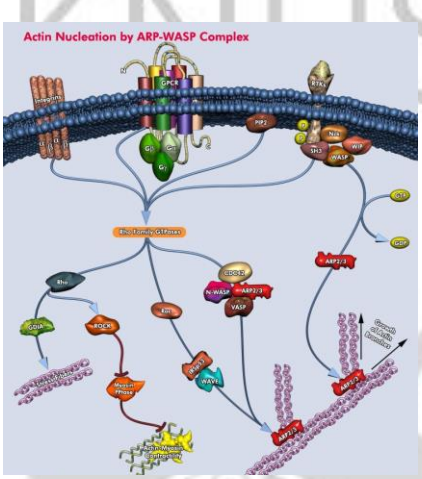

Figure 2.3: Actin Nucleation by ARP WASP complex Qiagen

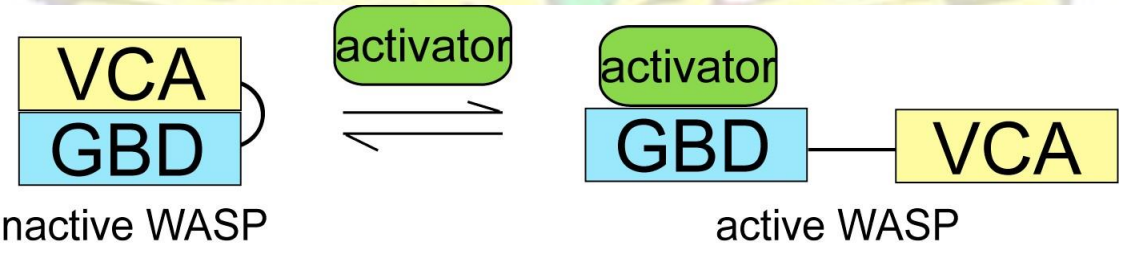

Figure 2.4: Autoinhibitory equilibrium of WASP

The proposed model for WASP regulation invokes an isomeric constant *M* and afinity constant *C* to control intramolecular contacts between the regulatory GTPase Binding Domain (GBD) and the activity-bearing VCA domain of the protein. WASP activators (e.g. Cdc42) relieves autoinhibition allosterically by disrupting the intramolecular contact between GBD-VCA of WASP, enabling the VCA to activate Arp2/3 complex (Figure 2.4).

These observations suggest that important mechanism(s) of regulating the activity of WASP toward Arp2/3 complex, in addition to allostery, remain to be discovered.

2.6 Effect of Mycolactone on WASP leads to Cytoskeletal Rearrangement

Mycolactone is a diffusible lipid secreted by the human pathogen *Mycobacterium* ulcerans, which induces the formation of open skin lesions referred to as Buruli ulcers [Kathleen et al., 2000, McCallum et al., 1948]. *Mycolactone* operates by hijacking the Wiskott-Aldrich syndrome protein (WASP) family of actin-nucleating factors. By disrupting WASP autoinhibition, *Mycolactone* leads to uncontrolled activation of Arp2/3-mediated assembly of actin in the cytoplasm. In epithelial cells, *Mycolactone*-induced stimulation of Arp2/3 concentrated in the perinuclear region, resulting in defective cell adhesion and directional migration.

In vivo, the injection of *Mycolactone* into mouse ears consistently altered the junctional organization and stratification of keratinocytes, leading to epidermal thinning, followed by rupture. These results clarify the molecular basis of *Mycolactone* activity and provide a mechanism for Buruli ulcer pathogenesis [Clin, 2013, Belinda et al., 2014, Laure et al., 2011, Demangel et al., 2009]. *In vitro*, *Mycolactone* diffuses passively into the cytoplasm of mammalian cells to induce apoptotic cell death, although with highly variable efficacy [Hong et al., 2008]. Anchorage-dependent cells are the most susceptible to *Mycolactone* toxicity, which proceeds through cytoskeletal rearrangements and detachment [Bozzo, 2010, George et al., 2000, Snyder and Small, 2003, Laure et al., 2013]. *Mycolactone* gains access to WASP by passive diffusion through the plasma membrane [Snyder and Small, 2003] and it binds to WASP 100fold more strongly than its major regulator,

Cdc42 [Leung and Rosen, 2005], leading to a much greater capacity to stimulate actin assembly in vitro.

Mycolactone is believed to relieve/ disrupt the intramolecular contacts that maintain WASP autoinhibition [Clin, 2013].

2.6.1 Implications of Disrupted Autoinhibition for Human Disease

Autoinhibition can be disrupted in disease states. In a genetic disease, a mutated gene could be altered within the region that encodes the inhibitory element or the surface that interacts with the autoinhibitory domain. The mutated gene could direct synthesis of a protein that is constitutively active, having lost the negative control afforded by the intramolecular network. An example is the case of a human disease and WASP [Devriendt et al., 2001]. The position of the mutation suggests that it could result in release of VCA inhibition, leading to constitutive activation of Arp2/3 and mis-regulated actin polymerization [Devriendt et al., 2001].

Because an autoinhibitory mechanism is specific to the regulation of a particular activity within a unique protein, it is suitable for targeted therapeutics. An autoinhibitory domain could be targeted for either activation or further repression by a small molecule. The drug would be directed to a single protein to intervene with its unique regulatory mechanism. An understanding of the full repertoire of regulatory strategies for a particular protein, including autoinhibition, should facilitate such pharmaceutical research efforts.

CHAPTER 3

Kinetics and Model Mechanism for Ligand-Receptor Binding

3.1 Introduction

In this chapter, we will consider the kinetics of ligand-receptor binding, and develop model mechanisms for fractions of bound receptor complexes.

The modeling process begins with the enzyme-substrate kinetics proposed by Henry Michaelis and Menten (HMM). In the HMM model, two time scales appear in the solution of the complexes formed, which are experimentally not measurable, therefore an approach to find fractions of bound ligand-receptor complexes is introduced. This way, we are able to determine the fraction of bound WASP complex that can activate Arp2/3 complex to initiate polymerization of actin filament in the cell. The approach was first proposed by Briggs-Haldane (1925) using the law of adsorption and desorption. We find in the analysis that in ligand-receptor kinetics, the flux, though proportional to concentration gradient, is also proportional to the bound conformation(s) of the ligand-receptor complex(es).

The model will be a formulation of concentration-dependent steady-state (equilibrium) formalism based on conservation principles. By the equilibrium approach, we distinguish between functional and binding response of receptors against a change in concentration of the ligand, or as fractional response of receptors against a change in concentration of the ligands. Obviously in biochemical reaction, just because there is a conformational change in the receptor unit when a ligand binds, this conformational change is not necessarily the one which activates (or inhibits) the receptive unit for function. Meanwhile since theories on binding and function have many overlapping and identical expressions, their analysis are easily confounded Bindslev [2008].

From the law of reciprocity, if binding affects activation, then activation must affect binding (Colquhoun 1998). This law allows us to formulate reversible reactions at equilibrium. Before we develop the model for WASP, Cdc42 and *Mycolactone* toxin binding we give, a brief introductory theory of equilibrium reactions and chemical kinetics.

3.1.1 Guldberg and Waag Law of Chemical Equilibrium (GWCE)

Often many biological reactions are not completely irreversible and the transformation of the products back to reactants and reactants to products is possible. In biology it is often required to describe the kinetics of complex formulations (e.g. binding of ligand to receptor or binding of substrate to an enzyme). A precise example is given by:

$$[C_1] + [C_2] \underset{k_{-1}}{\overset{k_1}{\rightleftharpoons}} [C_3]$$

Where $[C_1]$,$[C_2]$,$[C_3]$ are receptor, ligand and product concentrations, respectively. Here k_1 and k_{-1} are the reaction rate constants. At equilibrium, the rate of production of $[C_3]$ by combining $[C_1]$ and $[C_2]$ is just as fast as the elimination of $[C_3]$ over the time generating $[C_1]$ and $[C_2]$.

From the law of mass action, the equilibrium concentration of the products and reactants is characterized by the equilibrium dissociation or association constant at steady state as:

$$K_d = \frac{[C_1][C_2]}{[C_3]}, \quad \text{or} \quad K_a = \frac{[C_3]}{[C_1][C_2]} = \frac{1}{K_d} \tag{3.1.1}$$

The equilibrium dissociation constant ($K_d = \frac{k_{-1}}{k_1}$) has unit of concentration and the equilibrium association constant K_a has unit of per concentration $\left(\frac{1}{\text{concentration}}\right)$. Equation (3.1.1) has no unit of time. The right hand side of equation (3.1.1) states that the ratio between occupied receptive site C_3 and non-occupied receptive site C_1 is equal to the ligand concentration C_2 times the ratio of association rate constant (k_1) and dissociation rate constant (k_{-1}). It is important to draw a distinction between k_1 and k_{-1} in reaction kinetics. The equation (3.1.1) for the reaction above will not hold if any of the reactants and or products is volatile or forms a precipitate or is consumed in other chemical reactions.

3.1.2 Reaction Kinetics

The complexity of biological and biochemical processes is such that the development of simplifying models and reaction schemes are essential in trying to understand the phenomenon under consideration. For such models and reactions, it is important to use reaction mechanisms which are plausible biochemically.

Biochemical reactions are continually taking place in all living organism and most of them involve proteins called enzymes/receptors, ligands etc. The most important features of enzymes are: regulatory, specificity on substrate and catalytic power. The clearest example is haemoglobin in red blood cells is an enzyme and oxygen, with which it combine is a substrate.

In this study, reaction kinetics are introduced since the ideas mirror some general types of reactions or binding phenomena and their corresponding mathematical realization. A knowledge of these is essential in constructing a mathematical model

to reflect specific known biochemical properties of a mechanism. Next the HMM model for enzyme-substrate reaction is discussed in detail.

3.1.3 Chemical reaction equilibrium approximation: HMM equation

Below, the HMM model for enzyme-substrate reaction is described. HMM in (1913) proposed the reaction mechanism for the enzyme-catalyzed biochemical reaction based on experimental observations. In their model, an enzyme (E) reacts with a substrate (S) to form an intermediate complex (ES). This intermediate complex breaks down, not only to form back the reactants (E) and (S), but forms also the product (P), and the remaining enzyme (E), is recouped. In this work such a substrate is referred to as having one binding site

3.1.4 Reaction of Proteins with One Binding-Site

In this work the Michealis-Menten equation is referred to as one binding site substrate / protein reaction mechanism. See for example Murray [2001]. The reaction scheme is given by:

$$[E] + [S] \underset{k_{-1}}{\overset{k_1}{\rightleftharpoons}} [ES] \xrightarrow{k_2} [E] + [P]$$

From the law of mass action, the equations describing the reaction mechanism can be written as:

$$\begin{cases} \frac{ds}{dt} &= -(k_1 s)e + k_{-1}c \\ \frac{de}{dt} &= -(k_1 s)e + (k_{-1} + k_2)c \\ \frac{dc}{dt} &= (k_1 s)e - (k_{-1} + k_2)c \\ \frac{dp}{dt} &= k_2 c \end{cases} \tag{3.1.2}$$

The initial concentrations are:

$$[S(0)] = s_0, [E(0)] = e_0, [SE(0)] = [P(0)] = 0$$

where the [.] are concentrations and k_i, i = 1,2 are reaction rate constants. Small letters are used to represent concentrations, $s = [S]$, $e = [E]$, $c = [SE]$ and $p = [P]$. The last equation in (3.1.2) is uncoupled and can be solved provided c is known.

$$p(t) = k_2 \int_0^t c(t')dt' \tag{3.1.3}$$

Since part of the enzyme is used up in the formation of the intermediate complex (c) we can deduce from the conservation law that:

$$e(t) = e_0 - c(t) \tag{3.1.4}$$

Equation (3.1.4) shows that from an initial concentration of the enzyme (e_0), part of it is used up to form the intermediate complex (c). The concentration of the intermediate complex will increase to a maximum (very fast) whiles the enzyme concentration decreases until the complex begins to break down to form the product and reactants since it is a reversible reaction process.

Introducing the dimensionless quantities;

$$u = \frac{s}{s_0}, \qquad v = \frac{c}{e_0},$$
$$\epsilon = \frac{e_0}{s_0}, \qquad \lambda = \frac{k_2}{k_1 s_0}$$
$$\tau = k_1 e_0 t, \qquad K_m = \frac{k_{-1} + k_2}{k_1}, \quad \text{and} \quad K = \frac{k_{-1} + k_2}{k_1 s_0} \tag{3.1.5}$$

where K_m is the Michaelis constant and $\epsilon \approx 10^{-9}$. Substituting (3.1.4) and (3.1.5) into (3.1.2) we obtain its dimensionless equivalent as:

$$\frac{du}{d\tau} = -u + (u + K - \lambda)v \quad \text{and} \quad \epsilon\frac{dv}{d\tau} = u - (u + K)v \tag{3.1.6}$$

with the initial conditions

$$u(0) = 1, \quad \text{and} \quad v(0) = 0. \tag{3.1.7}$$

Using 3.1.4 to eliminate the second equation in (3.1.2), equation (3.1.6) is obtained from the first and third of 3.1.2. Note that $K - \lambda > 0$ from (3.1.6). The solutions $u(\tau)$ and $v(\tau)$ immediately gives the solutions to equations (3.1.3) and (3.1.4). Since $|\epsilon| \ll 1$, the model system (3.1.6) is singular.

Using singular perturbation techniques, we look for solutions to (3.1.6) of the form:

$$u(\tau, \epsilon) = \sum_{n=0}^{\infty} \epsilon^n u_n(\tau)$$
$$v(\tau, \epsilon) = \sum_{n=0}^{\infty} \epsilon^n v_n(\tau) \tag{3.1.8}$$

The $O(1)$ order solution of (3.1.8) is given by:

$$v_0 = \frac{u_0}{u_0 + K}$$
$$u_0(\tau) + K \ln u_0(\tau) = -\lambda\tau + 1 \tag{3.1.9}$$

Notice that the first solution in (3.1.9) does not uniformly satisfy the initial condition in (3.1.7) since $v_0(0) = \frac{1}{1+K}$ $/$= 0. Inclusion of higher order terms in does not remedy the problem. Therefore, the assumption that$\epsilon \approx 10^{-9}$ is very small, which made $\epsilon \frac{dv}{d\tau} \approx 0$ is reframed to include solutions near $\tau \to 0$ (for $v(\tau)$). Secondly, the assumption that the initial concentration of the enzyme-substrate complex is zero ($c(0) = 0$) is a mathematical interpretation since in reality, life (protein and enzyme binding) is a continuous process and such complexes can not be zero. This will be achieved by introducing a magnification factor around $\tau \to 0$. Let the new time scale be given by:

$$\varphi = \frac{\tau}{\epsilon} \quad \Rightarrow \epsilon \to 0 \quad \varphi \to \infty \tag{3.1.10}$$

Using the new time scale, equation (3.1.6) can be written as:

$$\begin{cases} \frac{dU}{d\varphi} & = \epsilon \left[-U + (U + K - \lambda) V \right] \\ \frac{dV}{d\varphi} & = U - [V + K] \\ U_0(0) & = 1, \qquad U_n(0) = 0 \quad n \geq 1 \\ V_n(0) & = 0 \qquad \forall n \in \mathbb{N} \end{cases} \tag{3.1.11}$$

Similarly, we look for solutions of the form:

$$\begin{aligned} U(\varphi, \epsilon) &= \sum_{n=0}^{\infty} \epsilon^n U_n(\varphi) \\ V(\varphi, \epsilon) &= \sum_{n=0}^{\infty} \epsilon^n V_n(\varphi) \end{aligned} \tag{3.1.12}$$

Up to $O(1)$, the system becomes

$$\begin{cases} \frac{dU_0}{d\varphi} = 0 \\ \frac{dV_0}{d\varphi} = U_0 - [U_0 + K]V_0 \\ U_0(0) = 1 \qquad V_0(0) = 0 \end{cases} \tag{3.1.13}$$

The solution to equation (3.1.13) is of the same order as (3.1.12) and given by

$$U_0(\varphi) = C, \Rightarrow U_0(\varphi) = 1$$
$$V_0(\varphi) = \frac{1}{1+K}[1 - \exp -(1-K)\varphi] \tag{3.1.14}$$

In most biological applications $0 < \epsilon \ll 1$, therefore we only need the 0(1) order terms. The $O(\epsilon)$ order terms contributions are negligible [Murray, 2001].

The matching conditions are given by:

$$O(1) : \lim_{\varphi\to\infty}[U(\varphi,\epsilon), V(\varphi,\epsilon)] = \lim_{\tau\to 0}[u(\tau,\epsilon), v(\tau,\epsilon)], \quad \forall\epsilon \tag{3.1.15}$$

The two time scales give an inner and outer solution as follows:

$$u(\tau, \ ) = \ u_0(\tau) + 0(\ \ ) \quad \tau \geq 0$$
$$v(\tau, \ ) = \begin{cases} V_0(\phi) + 0(\ \ ) & 0 < \tau \ \ 1 \\ \text{Innersolution} & \\ v_0(\tau) + 0(\ \ ), & \tau \ \ 1 \\ \text{Outer solution} & \end{cases} \tag{3.1.16}$$

where $u_0(\tau)$ and $v_0(\tau)$ are given by the first and implicitly by the second equation in (3.1.9) respectively, and $V_0(\phi)$ is given by the second equation of (3.1.14).

Remark: Generally, problems involving two time scales as the one discussed above, singular perturbation techniques are very important and powerful methods for determining asymptotic solutions of such systems of equations for small . The asymptotic solutions are remarkable approximations to the exact solutions. The

disadvantage in this current scenario is that the rapid changes in the enzyme-substrate complexes in both dimensionless and dimensional times are so small that they are experimentally not measurable. Secondly we have assumed in the discussion above that $\epsilon \approx 0$, and therefore, mathematically $\epsilon \frac{dv}{d\tau} \approx 0$. The question is what happens if the ratio of enzyme to substrate ($\frac{e_0}{s_0}$) is not so small? This was studied by De Boer and Perelson (1994) for a situation that involved T-cell proliferation in response to an antigen. The model proposed in this study is analogous to that of De Boer and Perelson.

Therefore, since it is our aim to determine the total concentrations of bound WASP and GTPase-Cdc42 complex as well as bound WASP and *Mycolactone* complexes in real time, this method can not be used.

In the next section, a general approach is used to investigate a reaction system of enzyme/receptor and substrates binding without any assumption on the enzymesubstrate ratio. The approach can lead to the determination of fractions of concentrations of all the complexes in real time. Next the introduction of quasi-steady state assumptions.

3.1.5 Quasi-Steady State Assumption (QSSA)

It is assumed in the derivation of 3.1.2 that the formation of the complex (*c*) is very fast, such that it is in instantaneous equilibrium with the substrate *s*. Therefore,

$$k_1, k_{-1} \gg k_2 \qquad \text{Thus} \qquad k_1 se = k_{-1} c \tag{3.1.17}$$

From equation (3.1.17), applying the law of Detri, (i.e. if $\frac{a}{b} = \frac{c}{d},\ b = d\ /= 0$, then $\frac{a}{b+a} = \frac{c}{d+c}$) the fraction of the complex [*ES*] can be written as:

$$c = \frac{e_T . s}{K_d + s} \tag{3.1.18}$$

where e_T is the total concentration of enzymes (bound and unbound), $e_T = e + c$. K_d is the equilibrium dissociation constant. Since the last equation in (3.1.2) is not coupled, we can write:

$$V = k_2 c = \frac{k_2 . e_T s}{K_d + s} \tag{3.1.19}$$

where $V = \frac{dp}{dt}$ is the speed at which the product (p) is formed and it is equivalent to equation (3.1.3).

3.1.6 Quasi-Steady State Assumption: Briggs-Haldane Equation

From the reaction scheme in 3.1.2, Briggs and Haldane (1925) suggested an alternative hypothesis: If the enzyme is present in catalytic amounts ($e \ll s$), then shortly after mixing e and s, a steady state is established in which the concentration of c remains essentially constant with time, therefore

$$\frac{dc}{dt} = \frac{de}{dt} = 0 \tag{3.1.20}$$

From equation (3.1.2) and the condition given by (3.1.20) and $e_T = e + c$ we can write:

$$k_1 se - k_{-1} c - k_2 c = 0. \quad \text{as} \quad c = \frac{e_T s}{s + b} \tag{3.1.21}$$

where $b = \frac{k_{-1} + k_2}{k_1}$, and thus

$$c = \frac{e_T s}{s + K_m} \tag{3.1.22}$$

Equation (3.1.22) is time independent and can also be substituted into (3.1.3) to compute the product $p(t)$. Notice that equation (3.1.1) from GWCE in section 3.1.1 can also be rewritten as:

$$C_3 = \frac{C_2}{K_d + C_2}$$

where $C_3 = c, C_2 = s, C_1 = e$. Thus,

$$\frac{\text{Occupied receptive site}}{\text{Total receptive sites}} = \frac{C_3}{C_1 + C_3} = \frac{C_2}{K_d + C_2} \quad (3.1.23)$$

If we replace $K_d = \frac{1}{K_a}$ in equation (3.1.23) where K_a is the equilibrium association constant we get:

$$\text{Occupied receptive sites} = \frac{C_{tot}.C_2.K_a}{1 + C_2.K_a} \quad (3.1.24)$$

where $C_{tot} = C_1 + C_3$. Equation (3.1.24) is equivalent to the experimentally confirmed Langmuir (1918) equation for adsorption and desorption.

Equations (3.1.24) and (3.1.23) suggests that the fraction of occupied (or bound) receptive sites is not a simple proportional function of the ligand concentration as in the Law of Mass Action.

Again from the conservation of mass we can substitute (3.1.4) into the first equation of (3.1.2) as:

$$\frac{ds}{dt} = -k_1 e_0 s - (k_1 s - k_{-1})c \quad (3.1.25)$$

If the intermediate reaction is very fast, substituting equation (3.1.22) into (3.1.25), and performing some algebraic manipulations lead to

$$\frac{ds}{dt} = \frac{-Qs}{s + K_m} \quad (3.1.26)$$

where $Q = K_2 e_0$. Note that from equation (3.1.26), the term $\frac{s}{K_m + s}$ is a saturation function, which tends to unity as $s \to \infty$. Equation 3.1.26 has a solution of the form:

$$s(t) + K_m \ln(s) = -Qt + A \quad (3.1.27)$$

where K_m is the HMM equilibrium dissociation constant, Q and A are constants to be determined. The time-dependent concentration of the complex [ES] can be obtained with time if we substitute (3.1.27) into (3.1.22).

The analysis above shows that enzymatic reactions do not necessarily follow the law of mass action directly. As the concentration of the substrate is increased, the rate of the reaction increases, reaching a maximal (saturation) reaction velocity at high substrate concentration.

This is in contrast with the law of mass action which, when applied directly to the reaction with the enzyme predicts that the velocity increases linearly as the substrate concentration increases. Notice that if the desorption is faster ($k_{-1} \gg k_2$) then $K_m \rightarrow K_d$, and the HMM constant equals the equilibrium dissociation constant. Secondly the HMM equations are time-dependent expressions of initial concentrations. They become equal, at the steady state, to the GW model.

3.2 Introduction to Ligand-Receptor Binding

A receptor is a protein which may have more than one (active or inactive) binding sites. When a ligand is bound to a receptor binding site, there will be a conformational change in the receptor unit. The binding of a ligand to a receptor binding site may or may not influence the binding of another ligand to a second site on the receptor unit. Here we discuss two cases of a receptor with two binding sites: (1) the two binding sites are mutually exclusive (independent) and (2) they are mutually inclusive (cooperativity). The reaction mechanism is shown in Figure 3.1.

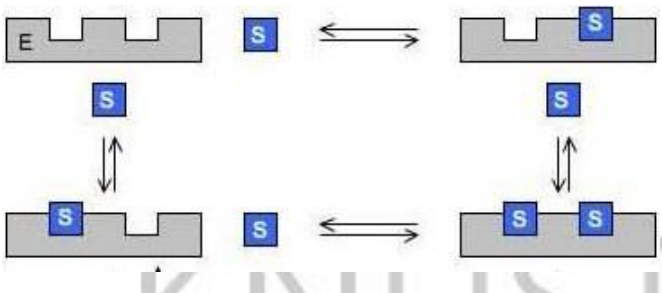

Figure 3.1: Reaction mechanism for receptor with two binding sites

Let C_1 denote a receptor bound on one site by a ligand and C_2 denote a receptor bound on the two sites by ligand. The subscripts {1,2} indicates the number of sites on the receptor bound by ligand(s). The reaction scheme for such a reaction is shown as:

$$2[[S] + [E] \underset{k_{-1}}{\overset{k_1}{\rightleftharpoons}} [C_1]] \underset{k_{-2}}{\overset{k_2}{\rightleftharpoons}} 2[[S] + [C_1] \rightleftharpoons [C_2]]$$

From the law of mass action we get

$$\begin{cases} \frac{ds}{dt} &= 2\left(-k_1 se - k_2 sc_1 + k_{-1}c_1 + k_{-2}c_2\right) \\ \frac{dc_1}{dt} &= 2\left(k_1 se - k_{-1}c_1 - k_2 sc_1\right) \\ \frac{dc_2}{dt} &= 2\left(k_2 sc_1 - k_{-2}c_2\right) \end{cases} \tag{3.2.28}$$

where e and s are concentrations of receptor/protein, and substrate/ligand respectively. $c_1 = [C_1]$ and $c_2 = [C_2]$ are receptor and substrate complexes:

3.2.1 Case I: Two Mutually Exclusive Binding Sites

Let

$$e_t = e + 2c_1 + c_2$$

Applying the quasi-steady state assumption,

$$\frac{dc_1}{dt} = \frac{dc_2}{dt} = 0 \tag{3.2.29}$$

and denoting

$$K_1 = \frac{k_{-1}}{k_1}, \quad \text{and} \quad K_2 = \frac{k_{-2}}{k_2} \tag{3.2.30}$$

$$k_1 = k_2 = k_+ \quad \text{and} \quad k_{-1} = k_{-2} = k_-,$$

and

$$K = K_1 = K_2 = \frac{k_- + k_+}{k_+}$$

it holds that

$$c_1 = \frac{se}{K_1}, \quad \text{and} \quad c_2 = \frac{sc_1}{K_2} = \frac{s^2 e}{K_1^2}. \tag{3.2.31}$$

Therefore the fraction of receptor sites in the bound states will be given by:

$$\frac{\text{bound receptor sites } (F)}{\text{total receptor sites (unbound plus bound)}} = \frac{2c_1 + 2c_2}{e + 2c_1 + c_2} \tag{3.2.32}$$

In the right hand side of (3.2.32), the first 2 stands because there are 2 forms of c_1, while the second 2 stands for the fact that there are 2 bound sites on c_2.

Substituting (3.2.31) into (3.2.32) we have:

$$\frac{F}{e_{tot}} = \frac{2\left(\frac{se}{K_1} + \frac{s^2 e}{K_1^2}\right)}{e + 2\left(\frac{se}{K_1}\right) + \frac{s^2 e}{K_1^2}} \tag{3.2.33}$$

Equation (3.2.33) simplifies to

$$F = \frac{2e_t s}{K + s} \tag{3.2.34}$$

The equation (3.2.34) is two times (3.1.23), where $F = C_3, C_2 = s,$ and $e_t = C_1 + C_3$ (i.e. the equation for a receptor with one binding site). This is similar to the Michaelis- Menten equation for ($k_{-1} \gg k_p$).

3.2.2 Case II: Two Mutually Inclusive Binding Sites

In this scenario, the binding of a ligand to a receptor site favors the binding of other ligands to the other receptor sites (cooperativity). In the reaction scheme above ,

$$k_1 \gg k_2$$

Therefore, we can write

$$k_2 = \beta k_1 \tag{3.2.35}$$

where $\beta \ll 1$. β is a dimensionless cooperativity constant. From the condition in (3.2.35), it holds that:

$$c_1 = \frac{se}{K_1}, \quad \ll c_2 = \frac{s^2 e}{\beta K_1^2} \tag{3.2.36}$$

$$\frac{F}{e_{tot}} = \frac{2\left(\frac{s}{K_1} + \frac{s^2}{\beta K_1^2}\right)}{1 + \frac{2s}{K_1} + \frac{s^2}{\beta K_1^2}} \tag{3.2.37}$$

Since $\beta \ll 1$, we can assume that C_2 dominates. Then, equation (3.2.37) reduces to:

$$\frac{F}{E_{tot}} \simeq \frac{\frac{2s^2}{\beta K_1^2}}{1 + \frac{s^2}{\beta K_1^2}} \tag{3.2.38}$$

$$F = \frac{e_t s^2}{\beta K_1^2 + s^2} \tag{3.2.39}$$

Notice that equation (3.2.39) is time independent, and secondly cooperative binding does not follow the Michaelis-Menten function. The function in (3.2.39) has a

sigmoidal shape. Below, we generalize equation (3.2.39) for a receptor with N-finite cooperative binding sites.

3.3 Receptor with N-finite Cooperative Binding Site

We derive an equation for a receptor with N-finite cooperative binding sites. We assume that the more ligand molecules are already bound, the easier the binding of additional ligand molecules. (i.e. cooperativity implies $k_i > k_{i+1}$). Let K_i denote the equilibrium (dissociation) constant of the ith step of binding ($K_i = \frac{k_{-i}}{k_{+i}}$). The receptor conformation is changed to favor the binding of more ligands to the receptor.

We start with a receptor with four binding sites. The reaction mechanism is below.

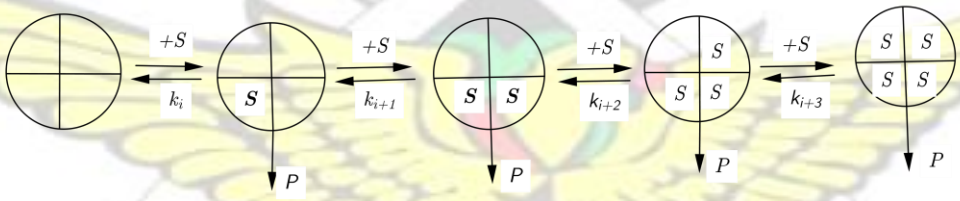

Figure 3.2: Co-operative mechanism for ligand-receptor binding

For a receptor with N cooperative binding sites, we can write

$$k_i = \beta_i k_{i-1} \tag{3.3.40}$$

where cooperativity in this case means

$$k_i > k_{i+1}$$

If we assume that all forms of the ligand-receptor complexes are possible, then a general equation for the fraction of bound receptive sites is given by:

$$F = \frac{e_t s^n}{K^n + s^n}, \quad n > 0 \tag{3.3.41}$$

.

where K is a function of K_i, $K^n = K_1^n \prod_{i=1}^{n} \beta_i^{n-i}, n > 0.$

In enzyme kinetics n is called the Hill coefficient. Notice that equation (3.3.41) reduces to (3.1.22) if n = 1. Secondly, as S ' K, we can evaluate K in a plot of experimental data (ie when half of the total receptor sites are bound by ligands). Thirdly, equation (3.3.41) is sigmoidal and saturates as $S \rightarrow \infty$. Fourth, the curve for equation (3.3.41) is similar to a Hill function.

If the cooperativity between binding sites is very strong, then n is equal to the number of binding sites on the receptor. As stated earlier, the receptor has finite number of binding sites. A plot of equation (3.3.41) for different parameter values is shown in Figure 3.3.

In Figure 3.3(a) the plot shows different values of the equilibrium dissociation constant (K) for the interval ($0.5 \leq K \leq 10$) and n = 1. In Figure 3.3(b), the plot shows n = 4 at same values of K as in Figure 3.3(a). When half of the total receptor sites are fully bound to ligands K_d can be computed.

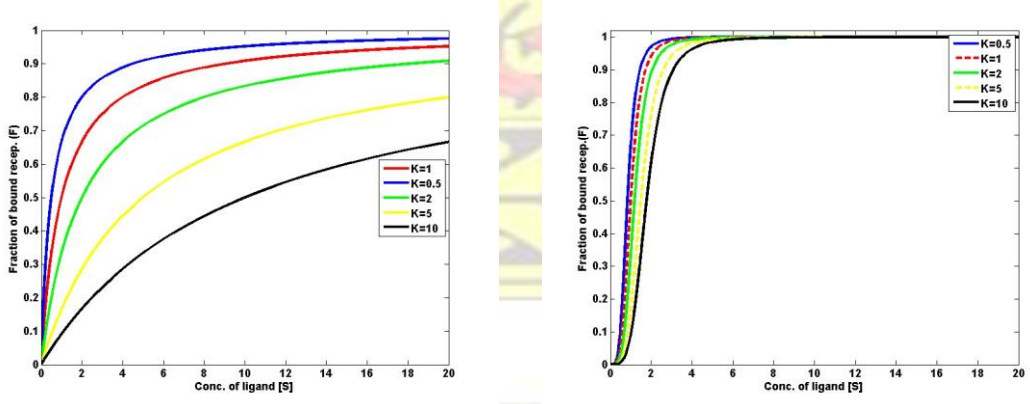

(a) (b)

Figure 3.3: Plot of the fraction of bound receptor sites against the concentration of the ligand S

.

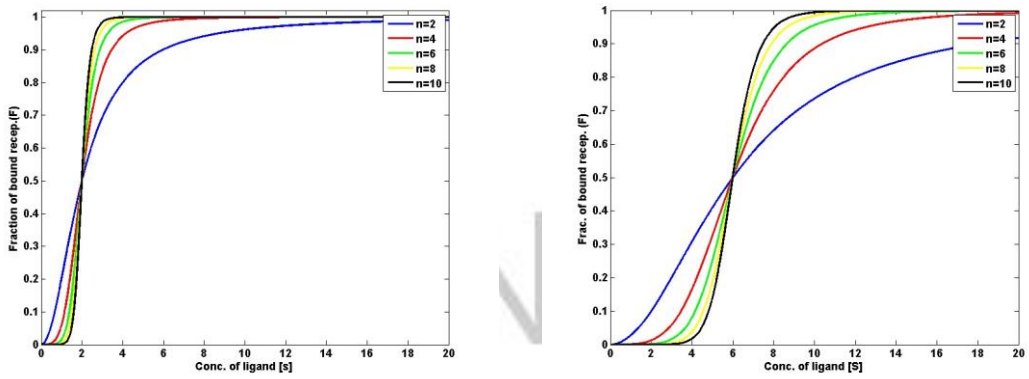

(a) (b)

Figure 3.4: Plot to show the effect of the parameter n on fraction of bound receptive unit against ligand concentration (a) $K = 2$ and (b) $K = 6$.

Figure 3.4 shows the effect of the parameter n on the fraction of bound receptor sites F against concentration of [S]. In Figure 3.4(a) the plot show the effect of parameter n on saturation as n varies from 2 to 10 in steps of 2 while $K = 2$. In Figure 3.4(b) $K = 6$ and $2 < n < 10$. For small values of K the receptor protein saturates faster. The legend shows the values of n and the corresponding colors respectively.

If the formation of the intermediate complex is fast, as assumed by the MichaelisMenten model, then the equilibrium dissociation or association constants can not be obtained from the graphs above. In both plots of Figure 3.4, all the curves pass through the point when the concentration of the ligand equals the equilibrium dissociation constant ($K = [S]$). At this point, the fraction of bound receptor sites equals half. Equation (3.3.41) can be linearized using the Lineweaver-Burk approach to approximate K.

$$\log\left(\frac{F}{e_{tot} - F}\right) = n \log s - n \log K \tag{3.3.42}$$

The two parameters *n* and *K* have a strong effect on the saturation of the bound states. Secondly, as the parameter $K \gg 1$ increases, more products are dissolved to form reactants, and the graph shift towards the right. The shift indicates a lag phase in reaching the steady state (saturation) since more products are dissolved to form reactants. The reverse is true for decreasing *K*.

Binding of proteins/receptors to ligands have the ability to activate or inhibit the binding of other molecules.

In the next section we introduce the concept of allostery in receptor binding.

3.4 Allosteric Effect in Ligand-Receptor Binding

The concept of isomerization and conformational changes in receptor and ligand complexes reveals that allostery and cooperativity in reactions are similar. This notion is supported by Monod et al. [1963], in their study of cooperative and allosteric phenomena. Monod et al. [1963] concluded that the two were closely related and that conformational flexibility probably accounted for both. Subsequently, Monod et al. [1963] proposed a model to explain allostery / cooperativity phenomena in protein binding. Their allosteric model starts from the observation that each molecule of a typical cooperative protein contains several subunits. We will denote by α the number of subunits. A simple reaction scheme for allostery is shown below. (see for example Maurizio [2011], Jean-Pierre [2013], Bindslev [2008]).

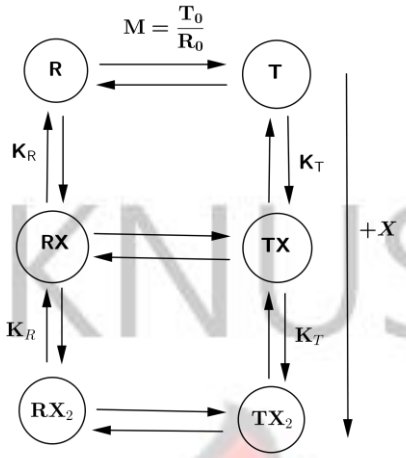

Figure 3.5: Allosteric reaction scheme The R and T represent relaxed and tense states of the protein.

3.4.1 Assumptions of the model:

1. Each subunit can exist in two different conformations (isomers), denoted R and T.

2. All subunits of the protein must be in one of two conformation at any time. Therefore, for a dimeric protein (with two binding sites) the conformational states R and T, are the only ones permitted, the mixed conformation RT being forbidden (this condition becomes much more restrictive when the protein (receptor) counts more than 2 subunits (e.g. for $\alpha = 4$ the allowed states are R_4 and T_4, while R_3T, R_2T_2, RT_3 are all forbidden).

3. The ratio of the two conformational states of the protein in basal form (inactive T and active R), will be given by the constant $M = \frac{[T_0]}{[R_0]}$. We refer to M as an isomerisation constant. In the basal form of the protein, M is a ratio of inactive and active states of the protein as we shall see later.

4. A ligand (*X*) can bind to a subunit in either conformation, but the equilibrium dissociation constant are different: $K_R = \frac{[R][X]}{[RX]}$ for each R subunit; $K_T = \frac{[T][X]}{[TX]}$ for each T subunit. The ratio $C = \frac{K_R}{K_T}$. C is the cooperativity constant or the affinity constant.

If $0 < C < 1$, the affinity of *X* to *R* is strong whiles if $C > 1$, the affinity of *X* to *R* is weak. Note that *C* is a ratio of two equilibrium dissociation constants. In other words the value of *C* indicates the affinity of *X* to the protein (*R*).

The resulting equations from the above scheme are given by

$$\begin{cases} \frac{d[R]}{dt} = -k_1[R][X] + k_{-1}[RX] \\ \frac{d[T]}{dt} = -k_2[T][X] + k_{-2}[TX] \\ \frac{d[RX]}{dt} = k_1[R][X] - k_{-1}[RX] \\ \frac{d[TX]}{dt} = k_2[T][X] - k_{-2}[TX] \\ \frac{d[RX]}{dt} = -k_1[RX][X] + k_{-1}[RX_2] \\ \frac{d[TX]}{dt} = -k_2[TX][X] + k_{-2}[TX_2] \\ \frac{d[RX_2]}{dt} = k_1[RX][X] - k_{-1}[RX_2] \\ \frac{d[TX_2]}{dt} = k_2[TX][X] - k_{-2}[TX_2] \end{cases} \tag{3.4.43}$$

with initial conditions,

$$R(0) = R_0, \quad T(0) = T_0, \; RX = TX = RX_2 = TX_2 = 0 \tag{3.4.44}$$

where $K_R = \frac{k_{-1}}{k_1}$ and $K_T = \frac{k_{-2}}{k_2}$.

We describe here the derivation of the equations for the case of a dimeric protein with 2 subunits. We assume that the equilibrium dissociation constant K_R are the same for *X* binding to *R* to form *RX*, and *X* binding to *RX* to form RX_2 and same for the *T* binding complexes. We then discuss the generalization to the case of α

subunits.

At steady state, we obtain the following useful concentrations and system constants from equation (3.4.43):

$$\begin{cases} [RX] & = \frac{2[R][X]}{K_R} \\ [RX_2] & = \frac{1}{2}\frac{[RX][X]}{K_R} = \frac{[R][X]^2}{K_R^2} \\ [T] & = M[R] \\ [TX] & = \frac{2[T][X]}{K_T} = \frac{2M[R][X]}{K_T} \\ [TX_2] & = \frac{1}{2}\frac{[TX][X]}{K_T} = \frac{M[R][X]^2}{K_T^2} \end{cases} \tag{3.4.45}$$

In each equation, the factor 2,1/2 and 1 results from the fact that the dissociation constants are defined in terms of individual sites, but the expression are written for the complete molecules and receptor sites with two bound ligand count twice We define the fraction of sites bound by the ligand (f_r) as:

$$fr = \frac{\text{Number of sites bound by ligand}}{\text{Total number of limited receptive sites}} \tag{3.4.46}$$

$$fr = \frac{[RX] + 2[RX_2] + [TX] + 2[TX_2]}{2\left([R] + [RX] + [RX_2] + [T] + [TX] + [TX_2]\right)} \tag{3.4.47}$$

In the numerator the concentration of each molecule is counted according to the number of occupied sites it contains (the empty sites are not counted), but in the denominator, each molecule is counted according to how many sites it contains, whether it is occupied or not. Substituting the concentrations from (3.4.45) into (3.4.47).

$$fr = \frac{\frac{[X]}{K_R} + \frac{[X]^2}{K_R^2} + \frac{M[X]}{K_T} + \frac{M[X]^2}{K_T^2}}{1 + 2\frac{[X]}{K_R} + \frac{[X]^2}{K_R^2} + M + 2\frac{M[X]}{K_T} + \frac{M[X]^2}{K_T^2}} = \frac{\left(1 + \frac{[X]}{K_R}\right)\frac{[X]}{K_R} + M\left(1 + \frac{[X]}{K_T}\right)\frac{[X]}{K_T}}{\left(1 + \frac{[X]}{K_R}\right)^2 + M\left(1 + \frac{[X]}{K_T}\right)^2} \quad (3.4.48)$$

Let $\chi = \frac{[X]}{K_R}$ and $Y = \frac{[X]}{K_T}$ be normalized concentrations. Then, for the general case where the protein has *α* subunits, Equation (3.4.48) becomes:

$$fr = \frac{(1+\chi)^{\alpha-1}\chi + M(1+Y)^{\alpha-1}Y}{(1+\chi)^{\alpha} + M(1+Y)^{\alpha}} \quad (3.4.49)$$

The shape of the saturation curve defined by equation (3.4.49) depends on the values of *α,M,K*$_R$ and *K*$_T$, as can be illustrated by assigning some extreme values to these constants. If the value of *M* is significantly different from zero, the graph of *fr* as a function of *χ* is sigmoidal. If *α* = 1, (i.e. only one binding site on the protein) then (3.4.49) simplifies to:

$$fr = \frac{\chi}{K_{RT} + \chi}, \qquad K_{RT} = \frac{K_R(1+M)}{1+MC} \quad (3.4.50)$$

where *K*$_{RT}$ is the apparent dissociation constant for initial concentrations of both *R* and *T* in the binding process. The complexity of this dissociation constant does not however alter the fact that it is a constant, and thus no cooperativity is possible if *α* = 1.

If *M* = 0, the *T* form of the protein does not exist under any condition, *K*$_{RT}$ = *K*$_R$ and the factor $(1+\chi)^{\alpha-1}$ cancels between the numerator and the denominator, leaving

$$fr = \frac{\chi}{K_R + \chi} \quad (3.4.51)$$

which predicts hyperbolic (non-cooperative) binding with dissociation constant *K*$_R$. A similar simplification occurs if *M* approaches infinity, (i.e. if the *R* → 0). In the second case,

$$fr = \frac{\chi}{(K_T + \chi).} \tag{3.4.52}$$

It follows that both *R* and *T* forms are needed if cooperativity is to be possible for a dimeric protein. It is also necessary for the two forms to be functionally different from each other, i.e. K_R 6= K_T. If K_R = K_T it is again possible to cancel the common factor $(1 + \chi)^{\alpha-1}$, leaving a hyperbolic expression. This illustrates the reasonable expectation that if the ligand binds equally well to the two states of the receptor, the relative proportion in which they exist are irrelevant to the binding behaviour.

If $K_T \gg K_R$, i.e. if X binds only to the *R* state, we find:

$$fr = \frac{(1 + \chi)\,\chi}{M + (1 + \chi)^2.} \tag{3.4.53}$$

where *M* is an intrinsic isomeric constant that describe the equilibrium of *R* and *T* in the absence of *x*.

CHAPTER 4

Mathematical Model Mechanism for BU

In this chapter, the mathematical models for the kinetics of polyketide lipid toxin (Mycolactone), and WASP binding is developed. *Mycolactone* has been implicated as the main virulence of the Buruli ulcer (BU) disease. Literature on BU suggests that the lipid toxin diffuses passively into the cell, binds the WASP and hijacks the autoinhibition of the WASP leading to an uncontrolled polymerization of actin filament and cytoskeletal rearrangement in eukaryotic cells [Laure et al., 2013].

WASP in its basal form exist in two conformations: an inactive (folded) conformation and an active (unfolded) conformation, which become stabilized on binding to Cdc42 [Kim et al., 2000b]. The active complex then binds the Arp2/3 complex to initiate the polymerization of actin filament. The autoinhibition mechanism of WASP controls the actin polymerization in the cell for proper cell function. The identification of autoinhibitory domains in proteins derives primarily from functional studies. However for mathematical modeling, structural data is very essential. WASP, has a structural information for both the inhibited and activated species. Structural data for many proteins highlight the essential role of conformational change in the autoinhibitory mechanism. In the simplest model, the inhibitory domain sterically masks the active site on the targeted domain, and a conformational change unmasks the active site during activation. In WASP, the structure of the inhibitory GDB domain is induced by both the intramolecular and intermolecular interactions. Most models

approximate this with a simple model, showing two juxtaposed domains moving with respect to each other (see for example Buck et al. [2004], Devreotes and Sherring [1985]). However, the conformational changes are usually more complex, although there exist conformational flexibility of elements within a single domain.

Mathematical modeling connects the fields of research in biology especially the lower levels of aggregation in biology (cell, tissue, organs) with tremendous progress in experimental data. There is no doubt that the role of mathematical modeling is becoming more and more significant, since modeling is the natural way to deduce insight into the mechanisms underlying the many processes driving living systems. In contrast to experimental approaches that characterize an autoinhibition phenomenon, mathematical modeling that considers the distinctive function of the protein within its biological context must be considered. A detailed mechanistic and structural model of autoinhibition is an invaluable tool in exploring and understanding the critical functions and allosteric effects of proteins as we provide in this study.

4.1 Overview of past and current WASP-Cdc42 related models

A mechanism, that involves destabilization of an autoinhibited structure on binding to Cdc42, has been proposed for the activation of p21-activated kinase (PAK) [Lei et al., 2000], another CRIB motif-containing effector. However, the regions of the structure that are affected by Cdc42 binding and the magnitude of their destabilization have not been determined and documented yet.

In this study we use the concept of isomerization (Same chemical content but different conformations) and present the WASP as existing in two isomeric conformations: an active unfolded isomeric conformation and an inactive folded isomeric conformation. We denote the WASP as receptor (R) and the Cdc42 will be referred to as the ligand (A). The model proposed by Buck et al. [2004], considers the two states of WASP as independent and mutually exclusive but for the model proposed in this work, the concept of Isomerization is used to model WASP. This way, we are able to model both mutually inclusive, and exclusiveness of the protein and ligand binding.

4.2 Modeling WASP Auto-inhibition and Cdc42 Binding

The GTPase-Cdc42 is a member of the Rho subfamily of Ras proteins that can signal to the cytoskeleton through its receptors. The WASP is a receptor of Cdc42 and its activation results in localized polymerization of new actin filaments. NMR on structures of WASP peptide models in the Cdc42-bound and free states suggest that GTPase binding weakens autoinhibitory contacts between the GTPase binding domain (GBD) and the C-terminal actin regulatory (VCA) region of the protein [Buck et al., 2001]. GTPases in the Ras super family function as molecular switches in diverse systems, controlling processes such as cytoskeletal change, cell growth, adhesion, motility, and vesicle transport [Hall, 1998, Johnson, 1999, Burbelo et al., 1995]. Research in recent years have discovered multiple effectors for many members of this supper family. It is generally believed that the subset of these molecular targets, utilized in response to a particular stimulus, determines the resultant specific cellular response. But the structural and biophysical factors that

determine the engagement of a particular effector and the means by which interaction is coupled to activation are poorly understood [Boguski and McCormick, 1993]. The WASP is a CRIB (Cdc42/Rac Interactive Binding) motif-containing Cdc42 effector and a critical component of pathways that link extracellular signals to the actin cytoskeleton [Buck et al., 2001, Abdul-Manan et al., 1999, Mott et al., 1999, Morreale et al., 2000, Kim et al., 2000a, Lei et al., 2000, Carlier et al., 1999, Machesky and Insall, 1999,

Higgs and Pollard, 2001]

We develop a concentration-dependent mathematical model for the autoinhibited WASP and Cdc42 binding that controls actin filament polymerization and the cytoskeleton rearrangement of a human cell (eukaryotic cell). In the reaction scheme 4.2 below, WASP is the receptor unit (R) and GTPase-Cdc42 is the ligand (A). As mentioned above, WASP can exist in two isomeric conformations: active unfolded conformation (R^*) and an inactive folded conformation (T). (see for example Monod et al. [1963, 1965], Blum [1955]), who were the pioneers in this area of research. By this notation they meant that protein had to relax (R-state) in order to bind substrate and in the tense (T-state) it is inactive. This does not mean the T-state isomeric conformation does not bind; it is rather inactive. Let R^* denote the active part of the WASP to make it different from the receptor WASP (R). Therefore, these two isomeric conformation will constitute the two states of WASP (T or R^*). The ligand (A) can bind to either sides of R independently or simultaneously (ie the concept of mutually exclusive and inclusive protein binding). Let us denote the binding of A to the left side of R (i.e. AR) as TA and the binding of A to the right side of R (i.e. RA) as R^*A. Here binding of a ligand to the left of R is assumed to prevent activation of the receptor unit, therefore the receptor conformations AR and ARA are possible but not active.

The AR^*A is the complex of a receptor unit with a ligand bound simultaneously to its left and right sites and it is assumed non-active.

In the scheme only the R^*A and R^* are active conformations and able to activate Arp2/3.

The model developed here follows the scheme:

Ligand → WASP → Arp complex → Actin filament

The proposed reaction mechanism for WASP autoinhibition is shown below:

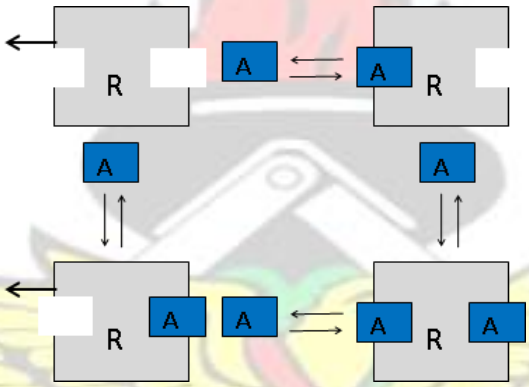

Figure 4.1: Reaction mechanism for Cdc42 WASP binding

Those complexes with arrows on them are active complexes and are assumed to activate Arp2/3 complex to initiate actin polymerization. The reaction scheme here is understood in the sense of *weak reversibility* because the rate constant for the formation of R^*A and AR are much bigger than the interconversion complex formation AR^*A. A detailed consideration of the complete reversible scheme and the interpretation of *weak reversibility* is treated in Chapter five.

The reaction scheme for the reaction mechanism shown above (see Figure 4.1) can be written as:

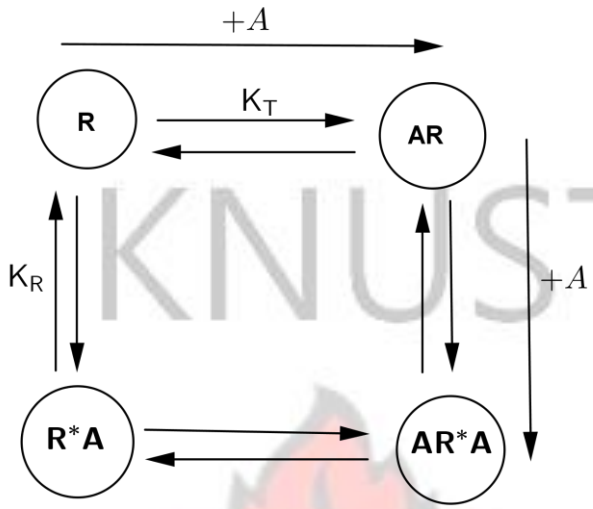

Figure 4.2: Reaction scheme for figure 4.1

We make the following assumptions:

as1: Binding may precede conformational change.

as2: The concentration of ligand is inexhaustible **as3**:

There is a finite number of receptor sites.

For an equilibrium reaction in a closed system , the sum of all conformations, bound and unbound (R_{tot}) is fixed **as3**. There will be a fixed number of bombardment of a *finite* number of receptor sites by ligand molecules with varying intensities as the ligand concentration varies **as2**. By this finite number of receptor sites we are able to determine the fraction of bound WASP at varying ligand concentration. This adsorption process is saturable because there is a limited number of binding sites.

From the Law of Mass Action, the following set of equations can be written from the scheme of Figure 4.2 as:

$$\begin{cases} \frac{d[R^*A]}{dt} & = k_1[R^*][A] - k_{-1}[R^*A], \\ \frac{d[AR]}{dt} & = k_2[A][R] - k_{-2}[AR], \\ \frac{d[AR^*A]}{t} & = k_2[R^*A][A] - k_{-2}[AR^*A] \end{cases} \tag{4.2.1}$$

Initial conditions

$$R^*A = AR = AR^*A = 0 \text{at} t = 0 \tag{4.2.2}$$

where $K_R = \frac{k_{-1}}{k_1}$ and $K_T = \frac{k_{-2}}{k_2}$. Similar equation can be written for *R* and *A*. It is assumed that the binding of a second ligand to the active complex supersedes that of binding the inactive complex. Let the following receptor conformations and system constants be defined as:

$$\begin{cases} M = \frac{[T_0]}{[R_0^*]}, & [R^*A] & = \frac{[R^*][A]}{K_R}, \\ S = \frac{[A]}{K_R}, & [AR^*A] & = R^* \left(\frac{[A]}{K_R}\right) \frac{[A]}{K_T} \\ C = \frac{K_R}{K_T}, & [AR] & = \frac{[A][R]}{K_T} = \frac{[T][A]}{K_T} = \frac{M[R^*][A]}{K_T} \end{cases} \tag{4.2.3}$$

[AR^*A] is a result of mutually inclusive binding (cooperativity), *C* is the affinity constant and also called the cooperative factor in this model. [R^*A] and [*AR*] are both receptor complexes with different equilibrium dissociation constants K_R and K_T respectively. The concentration symbols [.] will be dropped for convenience. There will be three scenarios of fractional-activation function responses namely: *self activation*, *activation induced on Cdc42 binding*, and *complete activation and inhibition of the WASP* (sum of first two). Only the last two will be considered since our interest is on the effect of the ligand on the receptor.

Scenario One: Fractional Activation of WASP Induced on Cdc42 Binding

Functionally, we distinguish between the fraction of WASP in the active conformation induced on Cdc42 binding and the fraction of active protein in the

whole reaction scheme. We have assumed that in basal form WASP has an active part (R^*) and an inactive part T. The fraction of active conformation induced on Cdc42 binding is:

$$\frac{f_r}{R_{tot}} = \frac{R^*A}{R^* + R^*A + AR + AR^*A + MR^*} \quad (4.2.4)$$

Substituting equations (4.2.3) into (4.2.4) gives:

$$F_r = \frac{S}{1 + S + MSC + S^2C + M} \quad (4.2.5)$$

Where $F_r = \frac{f_r}{R_{tot}}$ and $R_{tot} = R^* + R^*A + AR + AR^*A + MR^*$ and $S = \frac{A}{K_R}$ is a normalized concentration of the ligand (A).

Scenario Two: Self and Induced Fractional Activation of WASP on Cdc42 Binding The total fraction of WASP in active conformation is given by:

$$F_r = \frac{\text{[Free} - R^* - \text{state]} + \text{[bound} - R^* - \text{state]}}{\text{[Total R and T -states]}} \quad (4.2.6)$$

Therefore

$$F_r = \frac{R^* + R^*A}{R^* + R^*A + AR + AR^*A + MR^*} \quad (4.2.7)$$

Making substitution into (4.2.7) from equations (4.2.3), we get

$$F_r = \frac{1 + S}{1 + S + MSC + CS^2 + M} \quad (4.2.8)$$

Equation (4.2.5) shows the active fraction of WASP induced on GTPase-Cdc42 binding while equation (4.2.8) shows the total fraction of active conformation of WASP. It is realized from equation (4.2.8) that when $[A] = 0$ (i.e. in the absence of a ligand),

$$F_{r(0)} = \frac{1}{1 + M} \quad (4.2.9)$$

Secondly, at very high concentration of the ligand $[A] \rightarrow \infty$, we have:

$$F_{r(sat)} = \frac{1}{1 + C(M+1)} \tag{4.2.10}$$

where $F_{r(0)}$ and $F_{r(sat)}$ are the active fractions of WASP in the absence of a ligand and at saturating concentration of the ligand, respectively.

Equation (4.2.9) implies in the absence of a ligand, the WASP is regulated by the isomeric equilibrium constant M (it determines the stability of the reaction). If the concentration of the unfolded conformation of WASP far exceed the folded conformation, then the constant $M \approx 0, (T \ll 1)$ steadily from one, $F_{r(0)} \approx 1$, then the fraction of active conformation of the WASP complex and total WASP (R_{tot}) equalize and no binding occurs, there is saturation (Figure 4.3a). The reverse is also true if M rises steadily as unfolded conformation (R^*) decreases and we have all T conformation (i.e. $M \to \infty$), $F_{r(0)}$ decrease asymptotically, thus inhibition of the protein or inactive conformation of the protein (Figure 4.3b).

At saturating concentration of the ligand, the fraction of active conformation of WASP depends on affinity constant C and the isomeric equilibrium constant M. If $C < 1$, the affinity of the ligand A to R^* is increased as M decreases asymptotically, hence the fraction of active conformation increases (Figure 4.4a). The reverse is true for increasing C. As M becomes large (all T-state) the fraction of active conformation of WASP decreases asymptotically. The asymptotic decrease in the plots (Figure 4.4b) and (Figure 4.3b) show inhibition (or deactivation).

In Figure 4.3(b), the curve never touches the horizontal axis. This implies the fraction of active WASP complex does not reduce to zero. Biologically, it explains the importance of WASP in actin nucleation and control of cytoskeleton in the cell.

In Figure 4.5 fraction of active WASP in the absence of ligand ($F_r(0)$) is given

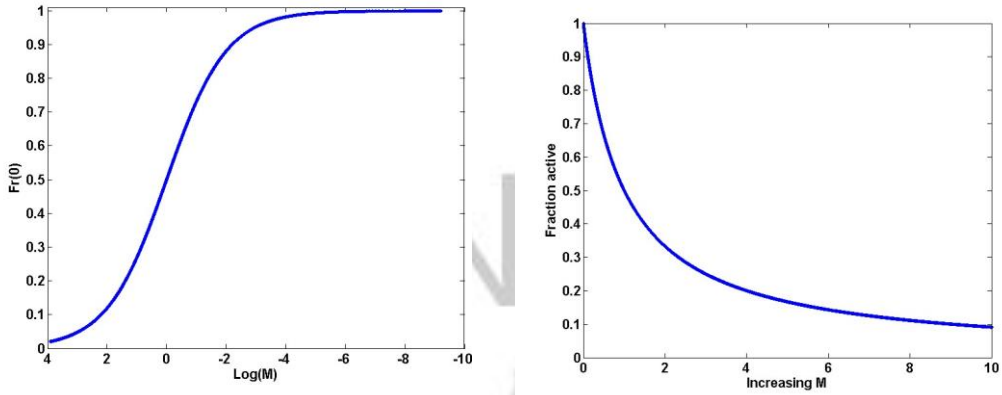

(a) (b)

Figure 4.3: Fraction of the free WASP ($Fr(0)$) in the active conformation as a function of M. (a) $M < 1$, (b) $M > 1$.

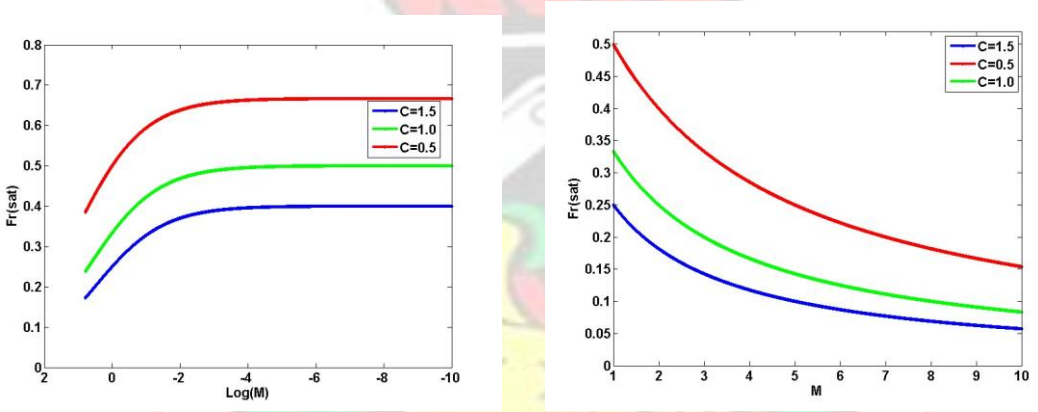

(a) (b)

Figure 4.4: Fraction of the saturated WASP ($Fr(sat)$) in the active conformation as a function of M. showing the effect of C (a) $M < 1$, (b) $M > 1$

by the blue curve, fraction of active WASP at saturation concentration of the ligand ($F_r(sat)$) is given by the red curve and the difference in the degree of activation due to Cdc42 binding ($Fr(sat) - Fr(0)$) is given by the green curve. The green curve explains the fact that there is activation and inhibition of the fraction of WASP on Cdc42 binding. Given that the Cdc42 binds the GBD domain of WASP to stabilize the active conformation of WASP, then stability of the active fraction increases from right

to left with the red curve ($Fr(sat)$) being the most stable. Equations (4.2.5) and (4.2.8) are plotted below:

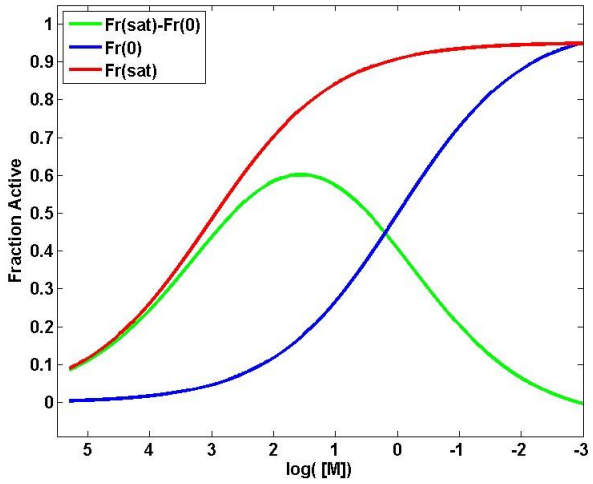

Figure 4.5: Plot of Fraction of active WASP at saturation ($Fr(sat)$) and absence of ligand ($Fr(0)$) vs stability log([M]). C = 0.05,

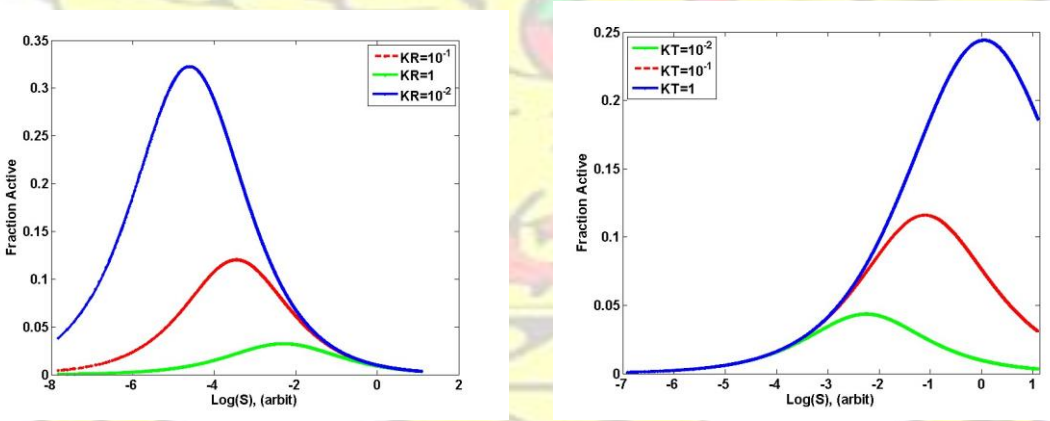

(a) (b)

Figure 4.6: The plot shows Fraction of Active WASP complex vs Ligand concentration.

In Figure 4.6(a) the equilibrium dissociation constant is in the range is $10^{-2} \leq K_R \leq 1$, $K_T = M = 1$ and $C = K_R$. The highest fraction of active WASP complex

corresponds to $K_R = 10^{-2}$ and decreases as K_R increases. It is observed that there is activation and inhibition of the fraction of WASP as the concentration of the ligand increases. This implies that in ligand-receptor binding where the protein can exist in two isomeric conformations (active and inactive), if the absorption rate is greater than the desorption rate, there will be an increase in the fraction of active WASP complex (ready to activate Arp2/3 complex) up to a certain maximum depending on the parameters $M,C,K_R,$ and K_T any further increase in the ligand concentration inhibits the protein. It also means that if all active sites on the WASP are bound, any additional concentration of ligand inhibits the protein. In figure 4.6(b) K_T is varied in the range $10^{-2} \leq K_T \leq 1$ in steps of 10 whiles $K_R = M = 1$ and $1 \leq C \leq 100$. Here, the highest fraction of active WASP complex corresponds to $K_T = 1$ and decreases in that order. If $K_T \geq 1$ it implies desorption of the inactive complex of the WASP is greater than absorption. Therefore, the fraction of active WASP complex increases though there is a delay (lag phase) and the curve shift to the right and the fraction is reduced is Figure 4.6(b) compared to Figure 4.6(a).

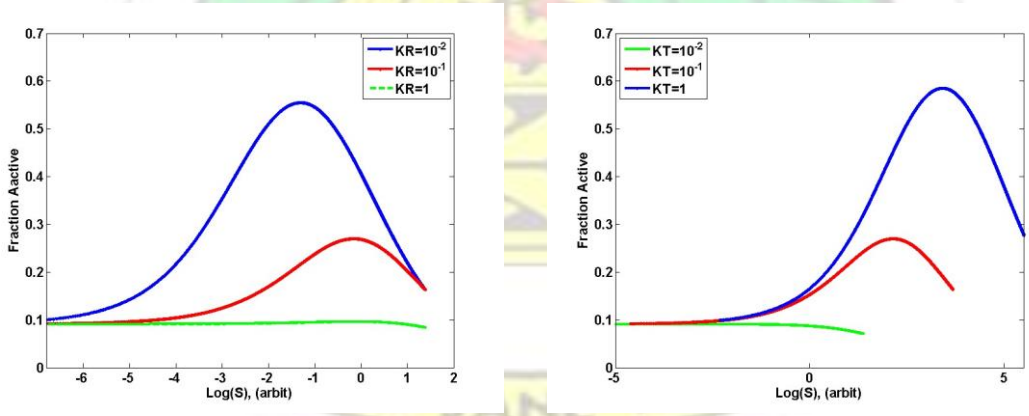

(a) (b)

Figure 4.7: The plot shows Fraction of Active WASP complex vs Ligand concentration.

Figure 4.7(a) and Figure 4.7(b) are plots of equation (4.2.8). Notice the rise in the fraction of active conformation of the WASP complex compared to Figure 4.6(a) and Figure 4.6(b) respectively. The fraction of active conformation of WASP complex Figure 4.6(a) increases by approximately 27% in Figure 4.7(a). In Figure 4.6(b) and Figure 4.7(b) notice that varying K_T shift the plots to the right. This is an indication of a delay (lag phase) in the formation of active WASP complex. The biologically implication is that first the GBD domain of WASP has high affinity for Cdc42 than VCA domain of WASP. The intramolecular interaction between the GBD and VCA domains of WASP autoinhibits the protein. We speculate that the lag phase observed in Figure 4.6(b) and Figure 4.7(b) is due to the breaking of this intramolecular interaction between the GBD and VCA when Cddc42 binds the GBD domain relieving the VCA domain. This result confirms the experimental report in the literature that the affinity of WASP GBD for Cdc42 is higher than its affinity for the VCA (affinity of GBD-Cdc42 > GBD-VCA) [Miki et al., 1998, Lamarche and Tapon, 1996, Buck et al., 2001, Bruce et al., 2008].

Secondly, the ligand may compete with the VCA to bind the GBD domain of WASP [Miki et al., 1998]. The model above is not limited to autoinhibition of WASP but can also predict the models of Haldane's and Laidler [Haldane, 1930, Laidler, 1958]. If the protein exist in only one conformational state, then $M = 0$, and the model can be used to predict Auto-intervention one state binding schemes.

Next we introduce the concept of binding and differentiate it from fraction of active receptor conformations/ complexes.

Binding

In this subsection an equation for fractions of bound WASP complexes in a concentration-binding regime is derived. Here receptor sites with two bound ligands count twice. The fraction of bound receptor sites is given by:

$$f_R = \frac{R^*A + AR + 2AR^*A}{R^* + T + R^*A + AR + 2AR^*A} \tag{4.2.11}$$

Equation (4.2.11) simplifies to

$$f_R = \frac{A\left(1 + M\frac{K_R}{K_T} + 2\frac{A}{K_T}\right)}{K_R(1+M) + A\left(1 + M\frac{K_R}{K_T} + 2\frac{A}{K_T}\right)} \tag{4.2.12}$$

Further simplification gives:

$$f_R = \frac{A}{A + K_R\frac{(1+M)}{\left(1+M\frac{K_R}{K_T}+2\frac{A}{K_T}\right)}} \tag{4.2.13}$$

It can be observed that equations (4.2.13) and (4.2.8) are different. Equation (4.2.8) is the fraction of active conformation of the receptor whiles equation (4.2.13) is the fraction of bound conformation of the receptor. Similar results of equation (4.2.13) is given by Haldane [1930], Laidler [1958, 1956] for their one state auto-regulation schemes where *M* = 0. We only write their results from Bindslev [2008] as:

$$f_R = \frac{\text{Occupancy}}{\text{total}} = \frac{S}{S + \frac{K_{ss}}{1+2S/K_{is}}} \tag{4.2.14}$$

where $K_R = K_{ss},\ K_{is} = K_T\ ,\ S = \frac{A}{K_R}$.

The plots of equation (4.2.13) and (4.2.14) are shown below for varying parameters.

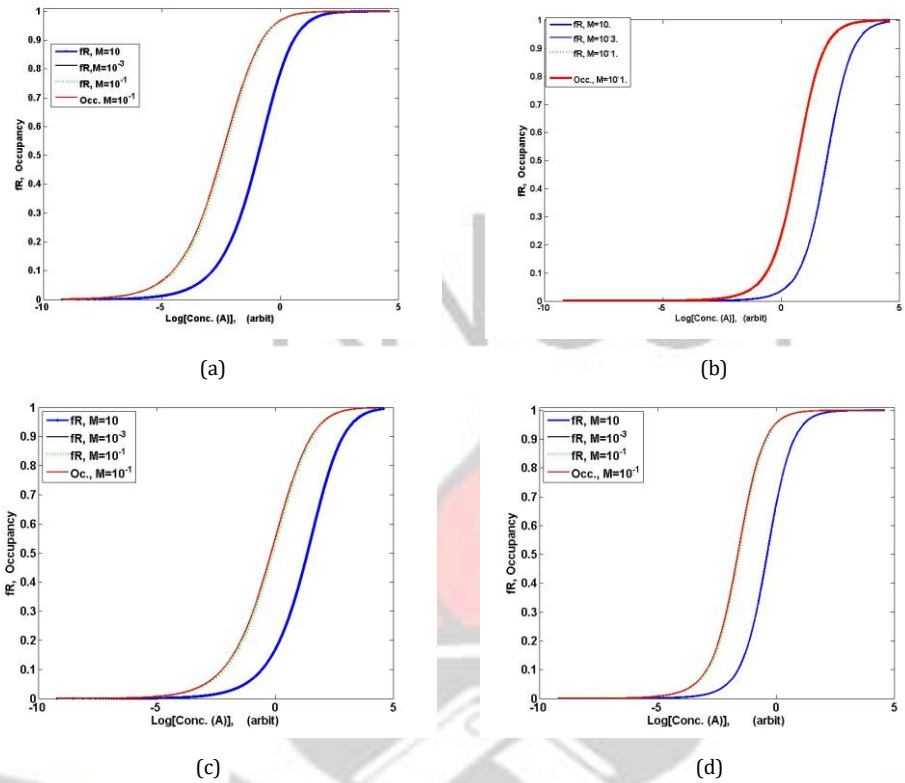

Figure 4.8: The plots show fraction of bound WASP complex verses ligand concentration

In Figure 4.8, M is varied to show the stability of the fractions of bound WASP at steady state. In Figure 4.8(a) $K_R = C = 10^{-1}$, $K_T = 1$ whiles $10^{-3} \leq M \leq 10$ in steps of 100. In all the plots above the black, green and blue curves correspond to an increase in M in the given steps respectively for equation (4.2.13). The red curve for equation (4.2.14), $K_{ss} = 10^{-1}$ coincide exactly with the black curve in the current model. In Figure 4.8(b) desorption is increased by increasing the equilibrium dissociation constant ($K_R = \frac{k_{-1}}{k_1} = 10$). The shift of the plot in Figure 4.8(b) to the right compared to the plots in Figure 4.8(a) is the effect of the equilibrium dissociation constant K_R. The plots in Figure 4.8(a) saturates faster and at lower concentration of the ligand compared to Figure 4.8(b) implying when the adsorption rate is less than the desorption rate, binding is slower. In the plots of Figure 4.8(c) and Figure

4.8(d), $K_R = C = 0.1$ and 10 whiles K_T take values 10 and 10^{-1} respectively.

4.3 Mycolactone Activation of WASP lead to Uncontrolled Polymerization of Actin Filament

In this section the polyketide lipid toxin (*Mycolactone*) is introduced as a second ligand (B) into the model. The lipid toxin (hydrophobic) sticks non-specifically to all lipids and most proteins. *Mycolactone* is the main virulence factor of the BU disease. *Mycolactone* is cytotoxic to fibroblasts and adipocyte cells in vitro and has a modulating activity on immune cell function [Belinda et al., 2014, Laure et al., 2011]. The effect of *Mycolactone* and the mechanism of its toxicity is presently not fully understood. However it is known that the toxin diffuses passively into the cytoplasm of mammalian cells to induce necrotic cell death by hijacking and or disrupting the functions of WASP. *Mycolactone* toxicity to cells proceeds through cytoskeletal rearrangement. In the proposed model we hypothesize that the lipid toxin, *Mycolactone*, binds to the hydrophobic region (VCA) of WASP. This abhorrent binding disrupts the autoinhibition of the WASP leading to an uncontrolled polymerization of actin filament. The reaction scheme Figure 4.9 describe the above process. Here it is proposed that the ligand Cdc42 (A) binds to WASP to form the active complex R^*A. The complex R^*A then binds to *Mycolactone* (B) to form the active complex BR^*A. The lipid toxin can also bind the active part of R to form the complex BR^*. In addition to the complexes R^* and R^*A, all the complexes formed on binding to the toxin (B) are active complexes that can bind Arp2/3 and actin monomers to initiate actin filament formation. The complexes BR^* and BR^*A are lipid-proteins and lipid-protein-protein respectively, whiles R^*A and AR are protein-protein complexes.

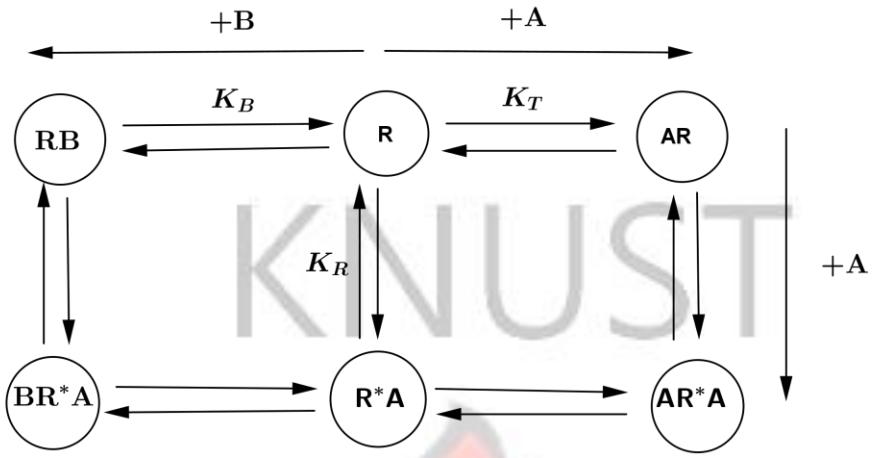

Figure 4.9: Reaction scheme for Mycolactone and Cdc42 binding to WASP

The dot(·) is used to indicate multiplication of two species. Secondly the concentration notation [·] used in the previous sections have been dropped for simplicity.

$$\begin{cases} \frac{dR^*A}{dt} &= (k_1R^*)A - k_{-1}R^*A, \\ \frac{dTA}{dt} &= (k_2T)A - k_{-2}TA \\ \frac{dAR^*A}{dt} &= (k_2R^*A)A - k_{-2}AR^*A, \\ \frac{dBR^*A}{dt} &= (k_3R^*A)B - k_{-3}BR^*A \\ \frac{dRB}{dt} &= (k_3R^*)B - k_{-3}RB \end{cases} \tag{4.3.15}$$

Initial conditions

$$TA = RB = R^*A = BR^*A = AR^*A = 0. \tag{4.3.16}$$

where $K_R = \frac{k_{-1}}{k_1}$, $K_T = \frac{k_{-2}}{k_2}$ and $K_B = \frac{k_{-3}}{k_3}$ are equilibrium dissociation constants

of the ligand binding to the right, left and the toxin binding respectively. The receptor conformations and system constants derived from the kinetic equations at quasi-steady state, are:

$$\begin{cases} S = \frac{A}{K_R}, & C = \frac{K_R}{K_T}, \\ K_B = \alpha K_R, & BR^*A = \frac{R^* \cdot A \cdot B}{\alpha K_R^2}, \\ R^*A = \frac{R^* \cdot A}{K_R}, & T = M \cdot R^* \\ AR^*A = \frac{R^* \cdot A^2}{K_R K_T}, & R^*B = \frac{B \cdot R^*}{\alpha K_R}, \quad B = \frac{B}{K_B} \\ TA = \frac{M \cdot R^* \cdot A}{K_T} \end{cases} , \tag{4.3.17}$$

It is assumed that the toxin binds at the same rate, therefore only one equilibrium dissociation constant (K_B) is used. Here α is a dimensionless co-operativity constant. In this case, the fraction of WASP complex in active conformation ready to bind the Arp2/3 complex to initiate polymerization of actin filament in the cell is given by:

$$\frac{f_m}{R_{tot}} = \frac{R^* + R^*A + BR^*A + BR^*}{R^* + AR + AR^*A + R^*A + BR^*A + BR^* + MR^*} \tag{4.3.18}$$

We have assumed in the reaction mechanism above that the binding is mutually inclusive (co-operative). Therefore substituting expressions from equation (4.3.17) into (4.3.18) and simplifying, we have

$$F_m = \frac{(1+S)(1+B)}{(1+S)(1+B) + M(1+SC) + S^2C} \tag{4.3.19}$$

where $F_m = \frac{f_m}{R_{tot}}$.

In the absence of a ligand ($A = 0$) and at saturating concentration of the ligand ($A \to \infty$) we have

$$F_m(0) = \frac{1+B}{1+B+M} \quad \text{and} \quad F_m(sat) = \frac{1}{1+C(1+M)}, \quad \text{respectively.} \tag{4.3.20}$$

In the absence of the lipid toxin (B = 0), equation (4.3.19) reduces to

$$F_m(A) = \frac{1+S}{1+S+M(1+SC)+S^2C} \tag{4.3.21}$$

Biologically the first expression on the left in equation (4.3.20) confirms that like Cdc42 the lipid toxin is able to activate WASP independently, confirming precisely experimental work in the literature [George et al., 1999, Bozzo, 2010, George et al., 2000, Snyder and Small, 2003]. Therefore, in the absence of Cdc42, fractions of active WASP complex will be formed and actin filaments nucleation will be initiated. There is a sharp saturation of WASP complex which depends on the concentration of the lipid toxin. The expression on the right of equation (4.3.20) is equal to (4.2.10). Therefore the analysis are similar. It is found that $F_m(sat)$ in equation (4.3.20), confirm that when all active sites on the WASP are fully bound, the lipid toxin has no effect.

From equation (4.3.19) it can be concluded that only a small amount / concentration of the lipid toxin is required to fully activate and saturate the fraction of active WASP complex. Data from Laure et al. [2013], support the view that ternary complex can be formed, through which GTPase-CDC42 and *Mycolactone* bind distinct sites on WASP. Though both *Mycolactone* and Cdc42 activate WASP by releasing the VCA from the GBD, the former has a 100-fold higher affinity and is a stronger activator than the later [Leung and Rosen, 2005]. Therefore the model confirms that the presence of the polyketide lipid toxin in the cell leads to an uncontrolled polymerization of the actin filament and cytoskeletal rearrangement, which is in agreement with experimental data.

The absence of the R conformation from equations (4.2.13), (4.3.19), (4.3.20) and (4.3.21) suggests that in actin filament polymerization, WASP is just needed to initiate the process and it is in itself not involved in the actin polymerization.

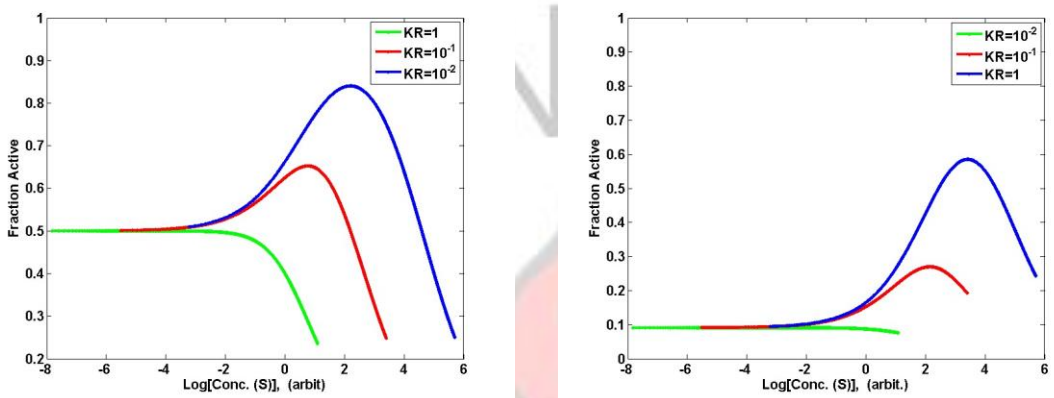

(a) (b)

Figure 4.10: Plot shows active fractions of WASP complex vs concentration of ligand (a) $C = K_R$, $B = 10^{-6}M$, $K_T = M = 1$, (b) $C = K_R$, $B = 10^{-9}M$, $K_T = 1$, and $M = 10$.

The value of the equilibrium dissociation constant (K_T) is maintained equal to one in most of the analysis. This idea is to ensure that in the worse case of WASP activation, adsorption and desorption are equal for the folded conformation.

In Figure 4.10(a), notice that the introduction of the lipid toxin, increases the fraction of active WASP complex. Increasing the concentration of the ligand, it is found that there is a lag phase in the fraction of active WASP complex, as the ligand concentration is increased. It is speculated in this work that this lag phase is the period of intramolecular disruption between the GBD-VCA domain of WASP when it binds the Cdc42 and toxin.

Egidio et al. [2007] in their study on microphage growth phase of *Mycobacterium ulcerans*, explains the observed lag phase as a *delay-type* hypersensitivity response in BU patients. Also, it can be concluded that the lipid toxin affects the steady-state

equilibrium and the stability of the model. Again, this confirms the claim that the binding of Cdc42 to the GBD of WASP stabilizes the unfolded conformation of the WASP complex.

The plots also confirm the claim by Buck et al. [2004], that the ligand (Cdc42) partially shift the GBD domain from the VCA domain in WASP and that further inputs are required to fully activate WASP. The shift of the plot to the right gives an indication of the affinity of the GBD of WASP for the ligand (Cdc42).

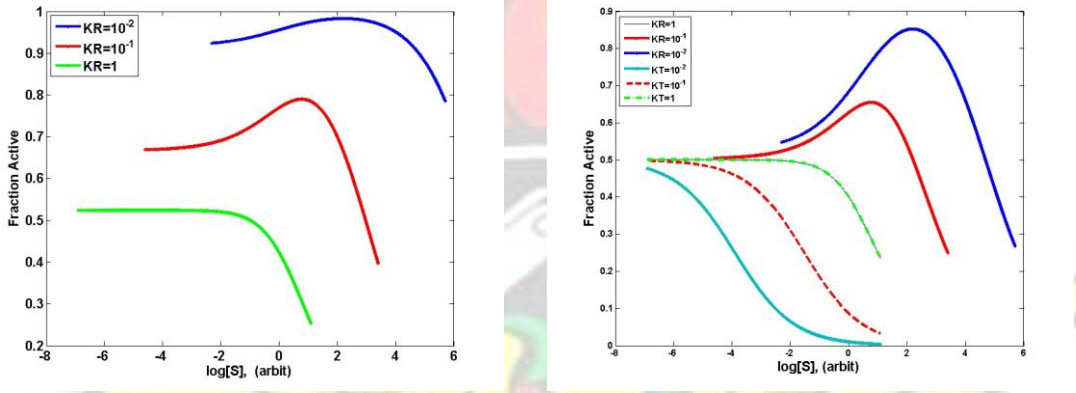

(a) (b)

Figure 4.11: (e) $B = 10^{-3}, M = 1, C = K_R$, $10^{-2} \leq K_R \leq 1$, (f) $B = 10^{-6}$, $M = 1$, $C = K_R$, $10^{-2} \leq K_R, K_T \leq 1$.

Figure 4.11(b), the concentration of the folded conformation is increased ($M = 10$), all other parameters remain the same as in Figure 4.11(a). In figure 4.11(a), the effect of the lipid toxin concentration ($B = 10^{-3}$) is shown. The highest fraction of WASP correspond to $K_R = 10^{-2}$. Figure 4.11(b), the effect of both dissociation constants are observed. $K_T = 10^{-2}$ correspond to the light blue curve at the bottom, which indicate inhibition while the highest fraction of active WASP complex correspond to $K_R = 10^{-2}$. The intermediates are shown in the legend. When both adsorption and desorption are equal for the two equilibrium dissociation constants

(i.e. $K_T = K_R = 1$) the green curve, there is a lag phase in the fraction of active WASP complex at a constant value 0.5, followed by a decease as the ligand concentration increases.

Further experimental work is required to explain the biological significance of this scenario. As the dissociation constant (K_T) decreases, the fraction of active WASP complex decreases, whiles a decrease in the dissociation constant (K_R) increases the fraction of active WASP complex, with an increasing concentration of the ligand (Cdc42).

From the analysis, it can be concluded that a competitive inhibitor of *Mycolactone* is needed to prevent the toxin from binding to the hydrophobic region of WASP as an effective way of treating BU.

The proposed model can produce results on existing protein model from Laidler and Haldane on dose response, and shows an improvement to the model of Buck et al. [2004] on two state allosteric model for WASP autoinhibition. While the model proposed in this study takes into account the isomeric conformation of WASPs, the Buck et al. [2004] model instead considers WASP as having two distinct juxtaposed domains moving with respect to each other. The mutually inclusive and exclusiveness of ligand-receptor binding are also fully captured by this model, whiles the Mathias model can only account for mutually exclusive binding of proteins.

The model further accounts for the equilibrium of this isomeric conformations and whether or not a particular isomeric conformation of the protein has strong affinity for a ligand over the other with the parameters M and C, respectively.

CHAPTER 5

Steady State Analysis of The WASP-Cdc42 Model

5.1 Steady State Analysis of the Ligand Receptor Model

In this Chapter, the effect of variation of ligand concentration on steady state of the model is analyzed. The complexes are parameterized and written in terms of the reaction rate constants. Values of the parameterized constants are then computed from experimental data and compared with existing models constants. For convenience the reaction rates for the complexes are represented as k_{ij} for the *ith* row and the *jth* column.

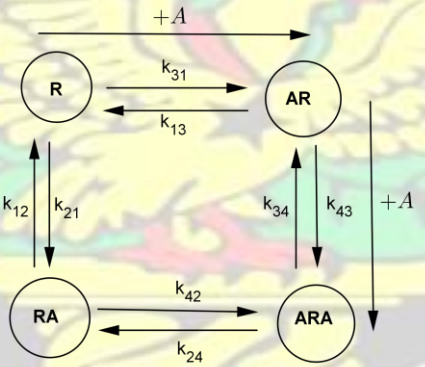

Figure 5.1: Reaction scheme

Let $RA \rightarrow C_1$, $AR \rightarrow C_2$ and $ARA \rightarrow C_3$.

The model equations for the reaction scheme in Figure 5.1 is given by:

$$\begin{cases} \frac{dR}{dt} &= -(k_{21}+k_{31})R.A + k_{13}C_2 + k_{12}C_1 \\ \frac{dC_1}{dt} &= -(k_{12}+k_{42})C_1 + k_{24}C_3 + k_{21}R.A \\ \frac{dC_2}{dt} &= -(k_{13}+k_{43})C_2 + k_{34}C_3 + k_{31}R.A \\ \frac{dC_3}{dt} &= -(k_{24}+k_{34})C_3 + k_{42}C_1 + k_{43}C_2 \end{cases} \quad (5.1.1)$$

From conservation of mass

$$\frac{dR}{dt} + \frac{dC_1}{dt} + \frac{dC_2}{dt} + \frac{dC_3}{dt} = 0 \quad (5.1.2)$$

Therefore,

$$R(t) + C_1(t) + C_2(t) + C_3(t) = R_0$$

The initial concentrations of the species are $R(0) = R_0, C_1(0) = C_2(0) = C_3(0) = 0$. Let m be the number of complexes in the reaction scheme. R forms C_1 and C_2 respectively whiles C_3 is a result of mutually inclusive binding. Consider the four complexes R, C_1, C_2, C_3 and assume the ligand A is in abundance. We adopt the word node from graph theory and use it to denote the positions of the complexes. Then each node $i = 1,....n$ is represented by a vector z_i. Each z_i contains the information on which individual species participate as reactants at each node. Thus $z_i \in R^n$ whose coordinates are $z_i = (z_{1i}, z_{2i}, ...z_{ni})^0$ with $z_{li} \neq 0$ if species y_i is part of the node z_i. In the specific problem, the $z_i^{'s}$ form the column vectors of the matrix $Z \in R_{n\times m}$.

$$Z := (z_1, z_2, ...z_m)$$

where $R + A$ z_1, C_1 z_2, C_2 z_3 and C_3 z_4.

$$z_1 = \begin{bmatrix} 1 \\ 0 \\ 0 \\ 0 \end{bmatrix}, z_2 = \begin{bmatrix} 0 \\ 1 \\ 0 \\ 0 \end{bmatrix}, z_3 = \begin{bmatrix} 0 \\ 0 \\ 1 \\ 0 \end{bmatrix}, z_4 = \begin{bmatrix} 0 \\ 0 \\ 0 \\ 1 \end{bmatrix}, \quad (5.1.3)$$

Therefore, the matrix Z is 4×4 identity matrix I_4. The links between individual nodes can now be represented by a matrix that contains all the kinetic constants. By this definition, if reactants in node z_i are products resulting from the reactant node z_j, then there is an arrow pointing from z_j to z_i with corresponding kinetic constant k_{ij}.

Let $K^F = k_{ij} \in R^{m \times m}$ be the matrix representing reactants ending at a node, where k_{ij} 6= 0, if and only if there exist an arrow from z_j to z_i.

A second matrix K^B which contains in its i_{th} diagonal entry the information on all the reactions that start from node z_i is given by:

$$K_B = \text{Diag}\left(\sum k_{j1}, \sum k_{j2}, \ldots \sum k_{jm}\right) \quad (5.1.4)$$

$$K_F = \begin{bmatrix} 0 & k_{12} & k_{13} & 0 \\ k_{21} & 0 & 0 & k_{24} \\ k_{31} & 0 & 0 & k_{34} \end{bmatrix} \quad (5.1.5)$$

$$\begin{bmatrix} & & & \\ & & & \\ 0 & k_{42} & k_{43} & 0 \end{bmatrix}$$

and

$$K_B = \begin{bmatrix} k_{21}+k_{31} & 0 & 0 & 0 \\ & & & \\ 0 & k_{12}+k_{42} & 0 & 0 \\ & & & \\ 0 & 0 & k_{13}+k_{43} & 0 \\ & & & \\ 0 & 0 & 0 & k_{24}+k_{34} \end{bmatrix} \quad (5.1.6)$$

The net contribution of both matrices is given by

$$K = K^F - K^B = \begin{bmatrix} -(k_{21}+k_{31}) & k_{12} & k_{13} & 0 \\ & & & \\ k_{21} & -(k_{12}+k_{42}) & 0 & k_{24} \\ & & & \\ k_{31} & 0 & -(k_{13}+k_{43}) & k_{34} \\ & & & \\ 0 & k_{42} & k_{43} & -(k_{24}+k_{34}) \end{bmatrix}$$

(5.1.7) Let θ be a matrix containing the complexes (mass action elemental events), then we define

$$\begin{bmatrix} y_{11}^{z_{11}} y_{21}^{z_{21}} \dots y_{n1}^{z_{n1}} \\ \\ y_{12}^{z_{12}} \quad y_{22}^{z_{22}} \quad \dots \quad y_{n2}^{z_{n2}} \\ \\ \\ \end{bmatrix}$$

$$\theta_I = \quad (5.1.8)$$

$$y_{z1m} \quad y_{z2m} \quad . \quad . \quad .$$
$$y_{nznm}\ y_1$$

Then for our model equation with $y = (R,C_1,C_2,C_3)$. $\theta_I(y)$ is given by

$$\theta_I(y) = \quad (5.1.9)$$

$$RA \quad C_1 \quad C_2 \quad C_3$$

The evolution equation for the concentration of the n species for the ligand-receptor model in equation (5.1.1) can then be written in compact form as:

$$\frac{dy}{dt} = KI\theta_I(y) \quad (5.1.10)$$

Equation (5.1.10) is equivalent to equation (5.1.1), but has the advantage that the information on the system is condensed into three objects: (1) The identity matrix which defines the nodes involved in the reactions, (2) The matrix K which specifies

the kinetic constants, and (3) The vector $\theta_I(y)$, which specifies the elemental events.

5.2 Steady-States

The steady state concentration of the component biochemical species given by the system of equations (5.1.10) are given by the vector $\bar{y} \in R^n$ defined by

$$\bar{f}(\bar{y}) = KI\theta_I(\bar{y}) = 0, \quad \forall \quad \bar{y} > 0 \quad \text{at coordinates} \quad i \tag{5.2.11}$$

Note that each of the steady states of the vector $\bar{y}$ is positive and globally asymptotically stable [Monod et al., 1963]. Next we find the steady states of the system of equations in (5.1.10) in terms of the kinetic constants k_{ij}.

Normalize the system of equations in (5.1.10) with the concentration $R.A$ at steady state and compute the scalars e_2, e_3, e_4 where the equivalent scaled terms are $C_1 = e_2, C_2 = e_3, C_3 = e_4$, give:

$$0 = -(k_{21} + k_{31}) + k_{12}e_2 + k_{13}e_3 \tag{5.2.12}$$

$$0 = k_{21} - (k_{12} + k_{42})e_2 + k_{24}e_4 \tag{5.2.13}$$

$$0 = k_{31} - (k_{13} + k_{43})e_3 + k_{34}e_4 \tag{5.2.14}$$

Then the components in the vector $\bar{y}$ can be computed as

$$e_3 = \frac{k_{31}k_{12}(k_{24} + k_{34}) + k_{34}k_{42}(k_{21} + k_{31})}{k_{12}k_{24}(k_{13} + k_{43}) + k_{13}k_{34}(k_{12} + k_{42})} \tag{5.2.15}$$ From equation 5.2.15 we have

$$e_2 = -e_3\frac{k_{13}}{k_{12}} + \frac{k_{21} + k_{31}}{k_{12}} \quad \text{and} \quad e_4 = \frac{k_{13} + k_{43}}{k_{34}}e_3 - \frac{k_{31}}{k_{34}} \tag{5.2.16}$$

The term $\frac{k_{21}+k_{31}}{k_{12}}$ is equivalent to the Henry Michaelis and Menten constant K_m.

The identity matrix I_4 has full column rank (i.e. vectors $z_1 \ldots\ldots z_m$ are linearly independent and none of its rows vanish).

Secondly the matrix K^F is irreducible (i.e. $\exists\ m > 0$ such that $(K^F)^m{}_{ij} > 0$). The second condition amounts to the requirement of *weak reversibility* [Feinberg, 1995]. There is a chemical pathway connecting each pair of nodes. For example there exist a

chemical pathway from nodes $R + A$ to node C_3 by passing through C_1 and it is possible to travel from C_2 to $R + A$ by another chemical pathway. Although our model happens to be all reversible, generally complete reversibility is not a necessary condition. The conditions on I_4 and K^F guarantee existence and uniqueness of steady state solutions for equation (5.1.10) [Monod et al., 1963, Feinberg, 1995]. This is essentially a mathematical way to describe the property of *weak reversibility* of a biochemical reaction. From conservation law it holds that

$$R(t) + C_1(t) + C_2(t) + C_3(t) = R_{tot} \quad \text{and} \quad R(0) + C_1(0) + C_2(0) + C_3(0) = R_{tot} \tag{5.2.17}$$

) Equation (5.2.17) is valid provided none of the reacting species or complexes formed vanish. Initially there are no ligand-receptor complexes hence

$$C_1(0) = C_2(0) = C_3(0) = 0 \tag{5.2.18}$$

Therefore, it follows that

$$R_0 = R_{tot} \tag{5.2.19}$$

Using similar analysis we define $A_0 = A_{tot}$ for the ligand. The constants e_2, e_3, e_4 in terms of the kinetic constants k_{ij} were obtained by using the concentration RA to scale the system of equation in (5.1.10) at steady state therefore, $e_1 = 1$.

Proposition: The vector y is a steady state if and only if the vector $\theta_I(y)$ belongs to the null space of K. To give characterization to the terms of the kinetic constants k_{ij}, let

$$_0\text{nullspace}(K) := \{e = (e_1, e_2, e_3, e_4) : Ke = 0\} \tag{5.2.20}$$

Then the steady state satisfy

$$y \in f(y) \Leftrightarrow \quad KI\theta_I(y) = 0 \Leftrightarrow \quad K\theta_I(y) = 0 \Leftrightarrow \quad \theta_I(y) \in \text{nullspace}(K) \tag{5.2.21}$$

where the second equivalence is justified because the matrix I_4 has full column rank and the third equivalence is simply the definition of the nullspace of K Monod et al. [1963].

It follows immediately that the nullspace of K is spanned by a positive vector. This means that the nullspace of K can be characterized by a scaling factor ℵ and positive constants e_2,e_3 and e_4 as:

$$_0\,\text{nullspace}(K) = \{ℵ(1,e_2,e_3,e_4) : ℵ \in R\} \qquad (5.2.22)$$

Note that R is an isomer and can exist in two conformations (R^*or$T$). Furthermore we have shown that the WASP itself does not take part in the actin polymerization, therefore it is useful to use this scaling. The parameters e_2,e_3,e_4 are positive constants that depend on the kinetic constants k_{ij} only.

There exist an appropriate positive value of ℵ for each steady state such that

$$\theta_I(\overline{y}) = ℵ \begin{pmatrix} 1 \\ e_2 \\ e_3 \\ e_4 \end{pmatrix} \qquad (5.2.23)$$

where ℵ depends on the initial condition $\overline{y}(0)$.

The complete characterization is given by the equations (5.2.17) and (5.2.23)

$$KI\theta_I(\overline{y}) = 0 \iff \begin{pmatrix} \widetilde{RA} \\ \widetilde{C_1} \\ \widetilde{C_2} \\ \widetilde{C_3} \end{pmatrix} = \aleph \begin{pmatrix} 1 \\ e_2 \\ e_3 \\ e_4 \end{pmatrix} \tag{5.2.24}$$

and

$$RAg + Cf_1 + Cf_2 + Cf_3 = R_{tot}, \qquad Ae + Cf_1 + Cf_2 + Cf_3 = A_{tot} \tag{5.2.25}$$

The parameter ℵ recast the ligand-receptor model in terms of products of the steady state amounts of the basic conformation R and free ligand A. The constants e_2, e_3, e_4 gives a summary of all the information needed about the kinetic constants. They group the eight kinetic constants K_{ij} and together with ℵ, provide a complete description of the steady state condition for the model with minimal number of parameters. The authors Woolf et al. [2001] remark that only three out of the eight constants that describe the network of reactions would be independent. Therefore, by this formulation we are able to find the dependent constants as well as their physical meaning.

Equation (5.2.24) confirms that the $e_i's$ are indeed equilibrium constants that give the fraction of the steady state values of the elemental events relative to one another. Example e_2 is the fraction of the steady state concentration of the ligand receptor complex C_1 relative to the value RA.

5.3 Steady State Activity of the Isomeric Receptor Model

Here the isomeric receptor model is examined in detail to obtain explicit expressions for the quantities of interest. We analyze the steady state for fractions of the complexes with varying concentrations of the ligand. It is realized from the steady state analysis that the model provides a good description for ligand-receptor

interactions by varying the relative values of the kinetic constants. The steady state response for different initial conditions of a similar model has been determined experimentally using ligand binding assays by Woolf et al. [2001]. Furthermore, a typical concentration response to determine the fraction of receptors in one of two possible state has been discussed by Bywater et al. [2002], Leo et al. [1971]. The authors plotted the concentration response curves: $\frac{\widetilde{R}+\widetilde{C}}{R_{tot}} \quad vs \quad logA$ as was done in Chapter

4 of this study (log plot of ligand because of the small amounts of the concentration).

Next, in explicit terms the steady state values of R,e C_{f1},C_{f2} and C_{f3} are solved for and expressed in terms of the kinetic constants k_{ij} and the initial concentration R_0 and A_0 from equations (5.2.24) and (5.2.25).

The system of equations in (5.1.10) can be solved numerically for the values e_2,e_3,e_4 but such a solution does not give explicitly the functional dependence of the variables at steady states on the kinetic constants (k_{ij}). The explicit solutions are necessary to confirm experimental results.

5.4 Fraction of Receptor Response at Steady State

In this section we examine the fractions of steady state response and dependence on the kinetic constants k_{ij}. From equation (5.2.24) we have

$$C_{f1} = \aleph e_2, \quad C_{f2} = \aleph e_3, \quad C_{f3} = \aleph e_4 \tag{5.4.26}$$

From conservation principles, an expression for the concentration of ligand can be written as

$$\widetilde{A} + \widetilde{C_1} + \widetilde{C_2} + \widetilde{C_3} = A_0, \quad \text{and} \quad A_e = A_0 - (e_2 + e_3 + e_4)\aleph \tag{5.4.27}$$

Then from equation (5.2.24) we can write

$$\widetilde{R} = \frac{\aleph}{A_0 - (e_2 + e_3 + e_4)\aleph} \tag{5.4.28}$$

Substituting equation (5.4.28) into equation (5.2.25) we have

$$\frac{\aleph}{A_0 - (e_2 + e_3 + e_4)\aleph} + (e_2 + e_3 + e_4)\aleph = R_0 \tag{5.4.29}$$

Equation (5.4.29) leads to a quadratic equation in $\aleph$. Let $V = (e_2 + e_3 + e_4)$

$$-(V\aleph)^2 + \aleph + A_0 V\aleph - R_0 V\aleph + R_0 A_0 = 0 \tag{5.4.30}$$

$$(V\aleph)^2 - [(A_0 + R_0)V + 1]\aleph + R_0 A_0 = 0 \tag{5.4.31}$$

There are two solutions to the quadratic equation (5.4.31) above but only one of the solutions has biological significance whiles the other violate the conservation law (5.2.17). The solutions are given by:

$$\aleph = [(A_0 + R_0)V + 1] \pm \sqrt{\frac{[(A_0 + R_0)V + 1]^2 - 4R_0 A_0 V^2}{2V^2}} \tag{5.4.32}$$

We know from equation (5.4.28) that $A_0 - (e_2 + e_3 + e_4)\aleph > 0$ since $A_0 > 0$

$$\aleph_1 = \frac{1}{2V}\left[\left(A_0 + R_0 + \frac{1}{V}\right) - \sqrt{\left(A_0 + R_0 + \frac{1}{V}\right)^2 - 4R_0 A_0}\right] \tag{5.4.33}$$

$$\aleph_2 = \frac{1}{2V}\left[\left(A_0 + R_0 + \frac{1}{V}\right) + \sqrt{\left(A_0 + R_0 + \frac{1}{V}\right)^2 - 4R_0 A_0}\right] \tag{5.4.34}$$

Analyzing the expression under the square root sign in equation (5.4.33) we have

$$\left(A_0 + R_0 + \frac{1}{V}\right)^2 - 4R_0 A_0 >$$

$$A_0^2 - 2A_0 R_0 + R_0^2 + 2(A_0 + R_0)V^{-1} + (V^{-1})^2 > 0 \tag{5.4.35}$$

$$0 \qquad (5.4.36)$$

Therefore

$$(A_0^2 - R_0^2)^2 + (V^{-1})^2 + 2(A_0 + R_0)V^{-1} > 0 \qquad (5.4.37)$$

Equation (5.4.37) is indeed a positive quantity for all $A_0 \geq 0$ and $R_0 \geq 0$.

From equations (5.2.25) the second solution to the quadratic equation violates the conservation law. Therefore, the steady state solutions of the complexes in the model are given by C_{e1}, C_{e2}, C_{e3} and א in terms of the kinetic constants (k_{ij}) and the concentrations R_0 and A_0. All the information on the kinetic constants (k_{ij}) and the initial conformations of the receptor and ligand (A_0 and R_0) at steady state are condensed in the three constants e_2, e_3 and e_4.

5.5 Effect of Ligand on Steady State

In this section the dependence of the model on the ligand at steady state is investigated. Ligand-receptor binding takes a long time to reach steady state. In this regard Segel et al. [1986] proposed that the final steady state is a linear combination of the ligand-receptor complexes. Let this linear combination be defined as

$$\Psi = \alpha_1 R A_g + \alpha_2 C_{f1} + \alpha_3 C_{f2} + \alpha_4 C_{f3} \qquad (5.5.38)$$

where the coefficients $\alpha_1, \alpha_2, \alpha_3$ and α_4 are arbitrary nonnegative real constants.

Let $\Psi = \Psi(A_0)$ such that the function Ψ is now written in terms of the ligand (A_0), and as mentioned earlier the receptor concentration is assumed to be finite (R_{tot}) whiles the ligand concentration is in abundance. The idea is to find $\lim_{A_0 \to 0} \Psi(A_0)$ and $\lim_{A_0 \to \infty} \Psi(A_0)$. Substituting for $\widetilde{C_1}, \widetilde{C_2}, \widetilde{C_3}$ in terms of e_2, e_3 and e_4, equation (5.5.38) becomes

$\Psi(A_0) = \alpha_1 R A_g + \alpha_2 e_2 \aleph(A_0) + \alpha_3 e_3 \aleph(A_0) + \alpha_4 e_4 \aleph(A_0)$ (5.5.39) From equation

(5.4.33) it holds to write $\aleph = \aleph(A_0)$, then define the function

$$\tau(A_0) := \frac{\aleph(A_0)}{A_0 - (e_2 + e_3 + e_4)\aleph(A_0)} \tag{5.5.40}$$

Equation (5.5.39) simplifies to:

$$\Psi(A_0) = \alpha_1 \tau(A_0) + (\alpha_2 e_2 + \alpha_3 e_3 + \alpha_4 e_4)\aleph(A_0) \tag{5.5.41}$$

Let

$$\omega = A_0 + R_0 + \frac{1}{V} \tag{5.5.42}$$

where $V = (e_2 + e_3 + e_4)$, then from equation (5.4.33)

$$\lim_{A_0 \to \infty} \aleph(A_0) = \lim_{A_0 \to \infty} \frac{1}{2V}\left(\omega - \sqrt{\omega^2 - 4R_0 A_0}\right) \tag{5.5.43}$$

Rationalizing equation (5.5.43) gives

$$\begin{aligned}
\lim_{A_0\to\infty} \aleph(A_0) &= \lim_{A_0\to\infty} \frac{1}{2V}\frac{(\omega-\sqrt{\omega^2-4R_0A_0})(\omega+\sqrt{\omega^2-4R_0A_0})}{\omega+\sqrt{\omega^2-4R_0A_0}} \\
&= \lim_{A_0\to\infty} \frac{1}{2V}\frac{4R_0A_0}{\omega+\sqrt{\omega^2-4R_0A_0}} \\
&= \frac{1}{2V}\frac{4R_0}{\frac{\omega}{A_0}+\sqrt{(\frac{\omega}{A_0})^2-\frac{4R_0}{A_0}}} \\
&= \frac{1}{2V}\frac{4R_0}{2} \\
&= \frac{R_0}{V} \quad \text{where we take } \lim_{A_0\to\infty}\frac{\omega}{A_0}=1
\end{aligned} \tag{5.5.44}$$

It holds that

$$\lim_{A_0\to 0} \aleph(A_0) = \lim_{A_0\to\infty} \tau(A_0) = 0 \tag{5.5.45}$$

Next we find an expression for the term $\lim_{A_0\to 0} \tau(A_0)$ by substituting for $\aleph(A_0)$.

$$\begin{aligned}
\lim_{A_0\to 0} \tau(A_0) &= \lim_{A_0\to 0} \frac{\aleph(A_0)}{A_0 - V\aleph(A_0)} \\
&= \lim_{A_0\to 0} \left[\frac{1}{2V}\left(\omega-\sqrt{\omega^2-4A_0R_0}\right)\times\left(\frac{1}{A_0-\frac{V}{2V(\omega-\sqrt{\omega^2-4A_0R_0})}}\right)\right] \\
&= \lim_{A_0\to 0} \frac{\omega-\sqrt{\omega^2-4A_0R_0}}{2V(A_0-\frac{\omega}{2}+\frac{1}{2}\sqrt{\omega^2-4A_0R_0})} \\
&= \lim_{A_0\to 0} \frac{(\omega-\sqrt{\omega^2-4A_0R_0})(A_0-\frac{\omega}{2}-\frac{1}{2}\sqrt{\omega^2-4A_0R_0})}{2V(A_0-\frac{\omega}{2}+\frac{1}{2}\sqrt{\omega^2-4A_0R_0})(A_0-\frac{\omega}{2}-\frac{1}{2}\sqrt{\omega^2-4A_0R_0})} \\
&= \lim_{A_0\to 0} \frac{1}{2V}\times\frac{A_0\omega-\frac{\omega^2}{2}-A_0\sqrt{\omega^2-4A_0R_0}+\frac{1}{2}(\omega^2-4A_0R_0)}{[(A_0-\frac{\omega^2}{2})^2-\frac{1}{4}(\omega^2-4A_0R_0)]} \\
&= \lim_{A_0\to 0} \frac{1}{2V}\times\frac{A_0(\omega-\sqrt{\omega^2-4A_0R_0}-2R_0)}{A_0(A_0-\omega+R_0)} \\
&= \lim_{A_0\to 0} \frac{1}{2V}\times\frac{-2R_0}{-\omega+R_0} \\
&= R_0
\end{aligned} \tag{5.5.46}$$

) The result in equation (5.5.46) proves that in the absence of a ligand, there are no

complexes formed and we have the initial receptor conformation R_0. A confirmation of the results in Chapter 4.

Substituting equations (5.5.46) and (5.5.44) into (5.5.41) we have

$$\lim_{A_0\to 0}\Psi(A_0)=\alpha_1 R_0,\quad \lim_{A_0\to\infty}\Psi(A_0)=\frac{(\alpha_2 e_2+\alpha_3 e_3+\alpha_4 e_4).R_0}{e_2+e_3+e_4} \tag{5.5.47}$$

The equation on the right of (5.5.47) is the fraction of concentration response at steady state defined earlier. This is a weighted average with respect to the constants e_2, e_3, e_4 and defines the capacity of the ligand to saturate the receptors. The second term on the right of equation (5.5.47) reaffirm our earlier results that for large amounts of the ligand, ($\lim_{A_0\to\infty}\Psi(A_0)$), all the receptors tends to be bounded. The first term on the left of equation (5.5.47) ($\lim_{A_0\to 0}\Psi(A_0)$) is the steady state concentration response in the absence of a ligand, when the constant$^{\alpha_1}=\frac{1}{1+M}$.

Let the steady-state affinity coefficient Θ be defined as:

$$\Theta=\frac{\lim_{A_0\to\infty}\Psi(A_0)}{\lim_{A_0\to 0}\Psi(A_0)}=\frac{(\alpha_2 e_2+\alpha_3 e_3+\alpha_4 e_4)}{\alpha_1(e_2+e_3+e_4)} \tag{5.5.48}$$

Given that α_1 6= 0, a situation which necessitate the existence of the two conformational forms of the receptor (folded and unfolded) at steady-state, then the affinity constant is well defined for each set of the coefficients in (5.5.48) above. If there is binding of the receptor and ligand then either α_2 6= 0, or α_3 6= 0 and α_4 6= 0 therefore the numerator in equation 5.5.48 is strictly positive. Notice that in a situation when no free receptor in any conformation contributes to the final steady-state activity (i.e. α_1 = 0), the steady-state affinity constant takes the value +∞. Next we show that $\aleph(A_0)$ is a strictly increasing function of A_0 by differentiating $\frac{d\aleph}{dA_0}$and checking that it is always positive. From equation (5.4.33) we have

$$\aleph_1 = \frac{1}{2V}\left[\left(A_0 + R_0 + \frac{1}{V}\right) - \sqrt{\left(A_0 + R_0 + \frac{1}{V}\right)^2 - 4R_0A_0}\right] \tag{5.5.49}$$

$$\begin{aligned}
\frac{d\aleph}{dA_0} &= \frac{1}{2V}\left[1 - \frac{1}{2}\left([A_0 + R_0 + \frac{1}{V}]^2 - 4R_0A_0\right)^{-1/2}.2\left(A_0 + R_0 + \frac{1}{V}\right) - 4R_0\right] \\
&= \frac{1}{2V}\left[1 - \frac{\left(A_0 + R_0 + \frac{1}{V} - 2R_0\right)}{\sqrt{(A_0 + R_0 + \frac{1}{V})^2 - 4R_0A_0}}\right] \\
&= \frac{1}{2V}\left[1 - \frac{A_0 - R_0 + \frac{1}{V}}{\sqrt{(A_0 + R_0)^2 + 2(A_0 + R_0)\frac{1}{V} + (\frac{1}{V})^2 - 4R_0A_0}}\right] \\
&= \frac{1}{2V}\left[1 - \frac{(A_0 - R_0 + \frac{1}{V})}{\sqrt{(A_0 - R_0)^2 + 2(A_0 + R_0)\frac{1}{V}}}\right]
\end{aligned} \tag{5.5.50}$$

From the last expression in 5.5.50, if $A_0 - R_0 + \frac{1}{V} \leq 0$, then clearly $\frac{d\aleph}{dA_0}$ is a positive quantity. Otherwise if $A_0 - R_0 + \frac{1}{V} > 0$, then notice that the negative term is of the form $\frac{p+q}{\sqrt{p^2+q^2+r}}$ where $r > 2pq$. Therefore

$$\left(\frac{p+q}{\sqrt{p^2+q^2+r}}\right)^2 = \frac{p^2+q^2+2pq}{p^2+q^2+r} < 1 \tag{5.5.51}$$

therefore $\frac{d\aleph}{dA_0}$ is strictly positive. This shows that $\aleph$ is an increasing function of A_0. Furthermore, the quantity $\tau(A_0)$ is a strictly decreasing function of A_0. Using the same procedure as we have done above, equation (5.4.29) can be rewritten as

$$\tau(A_0) + (e_2 + e_3 + e_4)\aleph(A_0) = R_0 \tag{5.5.52}$$

Differentiating equation (5.5.52) with respect to A_0 and noting that e_2, e_3, e_4 are positive constants. The right-hand side of this equation is given by the initial concentration of the receptor R_0 which is a constant therefore.

$$\frac{d\tau}{dA_0} + (e_2 + e_3 + e_4)\frac{d\aleph}{dA_0} = 0$$

$$\frac{d\tau}{dA_0} = -(e_2 + e_3 + e_4)\frac{d\aleph}{dA_0} \tag{5.5.53}$$

It is observed that $\frac{d\aleph}{dA_0} > 0$ for all A_0, and e_2, e_3, e_4 are positive constants therefore, $\frac{d\tau}{dA_0} < 0$ for all A_0. We have shown from the analysis above that for fixed receptor sites and an inexhaustible ligand, binding there will be activation and inhibition as we have shown for the model introduced in chapter 4 for WASP autoinhibition.

5.6 The Significance of Parameterized Constants

In this section we explain the biochemical significance of the parameterized constants e_2, e_3 and e_4 in the biochemical reaction network. Consider the two chemical reactions below

$$R + A \underset{k_{13}}{\overset{k_{31}}{\rightleftharpoons}} C_2$$

$$R + A \underset{k_{12}}{\overset{k_{21}}{\rightleftharpoons}} C_1$$

Let the equilibrium dissociation constants for the inactive and active complexes be K_T and K_R respectively. From the law of mass action it holds that:

$$R_t = -k_{31}AR + k_{13}C_2 \quad \text{and} \quad R_t = -k_{21}RA + k_{12}C_1. \tag{5.6.54}$$

Using the same normalization procedure as used before and remembering that e_1 is set to unity we can write

$$\frac{k_{12}}{k_{21}} = \frac{e_1}{e_2} = \frac{1}{e_2} = K_R \tag{5.6.55}$$

and

$$k_{31} = k_{13}e_3, \quad \frac{k_{31}}{k_{13}} = e_3 = \frac{1}{K_T} \tag{5.6.56}$$

Next, we consider an alternative approach to determine the constants $e_i's$ in terms of the kinetic constants k_{ij}. The steady state assumptions used here is supported by the works of Lauffenburger and Linderman [1993] (chapter 2).

From equation (5.2.24),

$$RA = \aleph \quad \text{and} \quad C_1 = \aleph e_2, \Rightarrow \frac{C_1}{RA} = e_2 = \frac{k_{21}}{k_{12}} = \frac{1}{K_R} \tag{5.6.57}$$

Equation (5.6.57) is equivalent to 5.6.55. From the scaled system of equations (5.2.125.2.14)

$$0 = -(k_{21} + k_{31}) + k_{12}e_2 + k_{13}e_3$$

$$0 = k_{21} - (k_{12} + k_{42})e_2 + k_{24}e_4$$

$$0 = k_{31} - (k_{13} + k_{43})e_3 + k_{34}e_4$$

Substituting for e_2 and solving, estimates for e_3 and e_4 are obtained as:

$$e_3 = \frac{k_{31}}{k_{13}} \qquad e_4 = \frac{k_{42}k_{21}}{k_{24}k_{12}} = \frac{k_{43}k_{31}}{k_{34}k_{13}} \tag{5.6.58}$$

The e_4 has two estimates, because it is a result of the mutually inclusive binding (see Figure 6.1). Biologically, it represents additional inputs required to fully activate WASP protein. The specific inputs that constitutes e_4 is yet not clear.

Biologically the $e^0{}_i s$ contain all the information on network routs and direct reversibility between products and reactants. Therefore, it can generally be concluded that the $e^0{}_i s$ are a generalization of the equilibrium constants in the

context of biochemical networks. The summary for estimates of the e^0*is* in terms of the kinetic and equilibrium dissociation constants are:

$$\frac{1}{K_R} = \frac{k_{21}}{k_{12}} = e_2, \quad e_3 = \frac{k_{31}}{k_{13}} = \frac{1}{K_T}, \quad e_4 = \frac{k_{42}}{k_{24}} \cdot \frac{1}{K_R} = \frac{1}{K_D K_R} = \frac{1}{K_C K_T}$$

where $K_D = \frac{k_{24}}{k_{42}}$ and $K_C = \frac{k_{34}}{k_{43}}$ are equilibrium dissociation constants. The affinity constant *C*, can therefore, be defined in terms of the e^0*is* as:

$$C = \frac{K_R}{K_T} = \frac{K_C}{K_D} = \frac{e_3}{e_2}$$

5.6.1 Computation and Comparison of Model Constants with Empirical Data

In this section the model constants are computed from empirical data and compared with existing constants computed from experimental data. Two different models of two-state ligand-receptor binding are considered in Figure 5.2 below.

Figure 5.2: The models studied by (a) Devreotes et al. (1985) and (b) Buck et. al (2004)

It must be stated, here, that all the models were proposed in order to study specific problems.

In Figure 5.2a of Devreotes and Sherring [1985], a two-state receptor conformations for the cAMP receptor of Dictyostelium was studied. Dictyostelium provides a convenient model system for the study of adaptation, a process which occurs in a wide variety of receptor-mediated responses. The affinity of the two receptor conformations for the ligand are the same and the reaction system is at steady state. Though in the present model there is no assumption on the affinities of the two

receptor conformations to be equal, it is assumed that most of the interactions between the ligand (cAMP) and its receptors can be described by the model presented in this study. Furthermore the concentration-response curve can be determined by the fraction of active complex (F_r) as a function of the ligands. It is hoped that the proposed model produces and validates results from other models of similar nature. In Devreotes and Sherring [1985], the constants determined by the authors are stated on the left and their equivalents in the present model are provided on the right.

$$k_1 = 0.012min^{-1} = k_{31}, \qquad k_{-1} = 0.104min^{-1} = k_{13}$$
$$k_2 = 0.222min^{-1} = k_{42}, \qquad k_{-2} = 0.055min^{-1} = k_{24} \tag{5.6.59}$$

The following constants can also be computed from the experimental concentration response model.

$$\begin{cases} \frac{k_{12}}{k_{21}} = 15\text{nM} = K_R, & 30\text{nM} = K_T \\ M = \frac{k_1}{k_{-1}} = \frac{[T_0]}{R_0} = 0.115, & C = \frac{K_R}{K_T} = 0.2 \\ e_2 = 6.667 \times 10^7 M^{-1}, & e_3 = 3.333 \times 10^7 M^{-1} \\ e_4 = \frac{k_{42}}{k_{24}K_R} = 2.691 \times 10^8 M^{-1} \end{cases} \tag{5.6.60}$$

From these experimental values, the corresponding fractions of active WASP complex at saturating ligand concentration $F_R(sat)$ can be computed. This is compared with the computations from the experimental concentration-response curve in Devreotes and Sherring [1985], the saturation values are:

$$\frac{[\tilde{R}_2 + \tilde{C}_2]}{R_0}(\infty) \approx 0.806, \quad F_R(sat) = \frac{1}{1 + C(1+M)} = 0.818 \tag{5.6.61}$$

where the values on the left and right of equation (5.6.61) are computations from Devreotes and Sherring [1985] and the present model respectively. The computed value 0.818 in our model compares well with the computed value from experimental data of 0.806. The ratio $M = \frac{T_0}{R_0}$ is the intrinsic intermolecular constant that controls

the steady state distribution of receptor forms in the absence of the ligand. It is computed from the interconversion step

$$R \underset{k_{-1}}{\overset{k_1}{\rightleftharpoons}} D$$

in the model of Devreotes and Sherring [1985]. K_R and K_T are the equilibrium dissociation constants for the active and inactive forms of WASP respectively, and e_2,e_3 and e_4 are constants. Equation (5.6.61) confirms that the stability of the model depends on the constant (M) (the ratio of isomeric conformation of WASP in the absence of the ligand).

The second model by Buck et al. [2004], the authors proposed a two-state allosteric model for autoinhibition of WASP. The authors report on the thermodynamic and structural analysis of WASP. Their two-state allosteric model is shown in Figure 5.2b. The protein exist in two states: an inactive and more stable T-state and a less stable but active R-state. The activating ligand is Cdc42. The major difference between the present model and that of Buck et al. [2004] is that, where as both the active and inactive conformations are embedded in R in the present model using the concept of isomerization and the intrinsic intramolecular constant M to regulate the concentrations of the two forms of WASP, they are presented as separate states in the model of Buck et al. [2004].

It should be noted, here, that this presentation is quite misleading since the protein is a single unit which behaves as an isomer (can change shape). Secondly, whereas

the present model can account for both mutually inclusive and exclusive binding, their model can only account for independent and mutually exclusive binding.

Three constructs that have been used to model WASP were thoroughly examined, GBD-C, GBD-VCA, and GBD-PVCA. These three structures have different stabilities for their autoinhibited structure because of the different linkers that join their common GBD to the C-region helix (VCA). The table below is a summary of the constructs and their dissociation constants.

In Buck et al. [2004], the following approximations for respective dissociation constants

Table 5.1: Three constructs of WASP and dissociation constants

Number	Protein construct	Dissociation constant (nM)
1	GBD Δ	22.9 ± 3.7
2	B.GBD Δ	12.8 ±2.6
3	GBD-PVCA	3200 ± 400
4	GBD-VCA	1500±700
5	GBD-C	6700±300
6	B.GBD-C	3700±300

$$K_{DT} = \frac{k_{13}}{k_{31}} = 6700 \times 10^{-9} M \quad \text{and} \quad K_{DR} = \frac{k_{12}}{k_{21}} = 22.9 \times 10^{-9} M \tag{5.6.62}$$

The equivalent dissociation constants in the present model are $K_{DT} = K_T$ and $K_{DR} = K_R$.

Also the fraction of active WASP in the absence, and at saturating concentration of the ligand were computed in their model as:

$$f_R(0) = 4.3 \times 10^{-4} \quad \text{and} \quad f_R(sat) = 0.1134 \tag{5.6.63}$$

Using the experimental approximations of dissociation constants above, we compute the fraction of active conformation of WASP complex in the absence and at saturating concentration of ligand.

$$F_r(0) = 4.346 \times 10^{-4} \quad \text{and} \quad F_R(sat) = 0.1133 \tag{5.6.64}$$

The two values in equation 5.6.64 compares very well with 5.6.63 . We can now compute the constants e_2,e_3, and e_4 from these experimental data with $M = 2300$. Once these constants are known, the fraction of active WASP in the active conformation can be determined.

$$e_2 = 4.367 \times 10^7 M^{-1}, \qquad e_3 = 1.493 \times 10^5 M^{-1}, e_4 = a e_2 \tag{5.6.65}$$

where the constant $a = \frac{K_{42}}{K_{24}}$ (not measured in experiment) and $C = \frac{e_3}{e_2} = 3.42 \times 10^{-3}$.

The values of e_2 and e_3 are consistent with experimental observations.

In the experimental work for the cAMP receptor binding in the Dickyostelium reaction, the authors Devreotes and Sherring [1985], made the observation that the binding of ligand to the receptor is very fast compared to the intermediate binding reaction. This notion is in agreement with the HMM model where $k_1, k_{-1} \gg k_2$.

This is also confirmed in the estimation of the constants (e_2,e_3) above. Further confirmation is given in the experimental work of Lauffenburger and Linderman [1993] (Chapter 2) that the constants k_{21} and k_{31} are much larger (of order 10^6,10^7) than comparable constants k_{12} and k_{13} (of order 10^{-1},10^{-2}).

CHAPTER 6

Reaction and Diffusion of Mycolactone Toxin and WASP in the cytoplasm of the cell

6.1 Introduction

Modeling a system of reaction-diffusion in a biological cell is a challenging task because of the complexity of the cytoplasm. The cytoplasm consists of nucleus, mitochondria, golgi bodies, and various subdomains that if considered will make the model computationally expensive (see Figure 2.1). Here, we discuss COMSOL Multiphysics-based methods in the study of intracellular ligand-receptor-toxin binding, and the intermediate complexes formed on the surface of the cytoplasm. The computational domain consist of two domains: an extracellular space and cytoplasm denoted by Ω_{ext} and Ω_{cell}, respectively.

In the proposed model, the WASPs, referred to as the receptor (R), are restricted to remain in the cytoplasm (subdomain Ω_{cell}), while the Cdc42, referred to as the ligand (A), and the Mycolactone, referred to as the toxin (B) are allowed to freely diffuse into the cytoplasm (Ω_{cell}) from the extracellular space (Ω_{ext}) with diffusion constants D_i, where i represents the species in the binding process. The concentrations will be denoted by u_x with the subscript (x) to indicate the reacting species and the complex(s) formed.

In the model, no reactions take place in the extracellular space of the cell. The species only bind in the cytoplasm. The ligand (A) binds with receptor to form the protein-protein complex referred to as RA in the model. The toxin can then bind this complex

to form the lipid-protein-protein complex referred to as *BRA*. It is assumed in this model that a third lipid-protein complex (*RB*) is formed when the toxin binds the receptor (hydrophobic region) directly.

It is reasonable to assume that *R* and its complexes formed do not also diffuse out of the cytoplasm, but rather, there is accumulation of these complexes on the surface of the cytoplasm.

By this approach the total amount of complexes that are produced to bind Arp2/3 complex to initiate actin polymerization can (approximately) be computed.

The complexes (*RA,RB* and *BRA*) are assumed to be activators of the Arp2/3 complex in the cytoplasm to initiate actin filament polymerization. It is important to note that over production of these complexes in the cell will lead to cytoskeletal rearrangement and eventual cell death through apoptosis or necrosis (as in BU patients).

The concentration of receptors in the cytoplasm is assumed to be constant. This implies that a saturation level is reached in the complexes formed when all binding sites on the receptors are fully bound. Such situations lead to a simple linear dynamics for the reactions terms.

In Chaudry et al. [2012], Kreamer et al. [2009], Hamilton [2003], the standard procedure of adsorption and desorption of surface reactions on cytoplasm membrane have been considered for polycyclic aromatic hydrocarbons using homogenization methods.

Mathematically, the ligand-receptor or ligand-receptor-toxin binding in the cytoplasm can be modelled by a set of Partial Differential Equations (PDEs). We employ numerical methods to solve the problem to determine the complexes formed on a 2D domain. The COMSOL Multiphysics with its predefined equations and in-built

material libraries offer several approaches to model ligand-receptor binding with an additional opportunity to restrain complexes/species and reactions to specific compartments whiles coupling the species to other reactions.

6.2 Modeling BU Spread as a Diffusive Process

Diffusion is the phenomenon of transportation of molecules from a region of higher concentration to a region of lower concentration. The diffusion of chemicals in an arbitrary domain follows classical diffusion process, and therefore, Fick's Law of diffusion applies. Important to us is to find the relation between the concentration of the diffusing species (C) and the flux J in an arbitrary domain Ω . An applicable constitutive law states that the steady state diffusive flux (J) is proportional to the concentration gradient. Let D denote the diffusion coefficient in this thesis.

$$J \propto \frac{d}{dx} C(\underline{X}, t) \Longrightarrow J = -D \frac{d}{dx} C(\underline{X}, t) \tag{6.2.1}$$

The value of D depends on the size of C, as well as the medium in which it is diffusing with dimension of $(length)^2/time$. $\underline{X}$ is a vector. In three dimensions, when D is a constant, the flux is of the form,

$$J = -D\nabla C \tag{6.2.2}$$

where $\nabla C = (\frac{dC}{dx}, \frac{dC}{dy}, \frac{dC}{dz})$. The diffusion equation without reaction terms can generally be written as:

$$\frac{dC}{dt} = -\nabla.(D\nabla C). \tag{6.2.3}$$

Reaction-diffusion Mechanism

Considering a general situation involving a reaction-diffusion process, the governing equations can be derived from balance laws as follows: Let $\Omega \subset R^3$ denote an open, bounded and smooth region of a cell, say, with boundary $\partial\Omega$. let S be an arbitrary surface enclosing a volume $V \subset \Omega$. If C is allowed to move randomly by passing through the volume surface S, the rate of change of material within the volume, according to the conservation law, is given by

$$\frac{d}{dt}\int_V C(\underline{X},t)dV = -\int_{S'} J.ndA + \int_V f\left(\underline{X},k,t,C(\underline{X},t)\right)dV. \tag{6.2.4}$$

where J is the flux of material, dA is the surface integration element, n is the outward normal vector to the boundary. The presence of $C(\underline{X},t)$ in the source term allows for the possibility that the rate of production of C depends upon itself as in an enzymatic reaction. Then from the divergence theorem, the surface integral can be replaced by the volume integral as:

$$\int_{\partial\Omega} C.ndx = \int_{\Omega} \nabla.Cdx \tag{6.2.5}$$

The flux integral in (6.2.4) becomes:

$$\int_{S_0} J.ndA = \int_V \nabla.JdV. \tag{6.2.6}$$

Therefore,

$$\frac{d}{dt}\int_V C(\underline{X},t)dV = -\int_V \nabla.JdV + \int_V f\left(\underline{X},k,t,C(\underline{X},t)\right)dV \tag{6.2.7}$$

where ∇ is the divergence operator. If the function $C(\underline{X},t)$ is smooth enough, then integration and differentiation can be interchanged, and equation (6.2.7) can be written as:

$$\int_V \left[\frac{dC(\underline{X},t)}{dt} + \nabla.J - f\left(\underline{X},k,t,C(\underline{X},t)\right)\right]dV = 0 \tag{6.2.8}$$

Since the volume V is arbitrary, the integrand can be equated to zero.

$$\frac{dC(\underline{X},t)}{dt} + \nabla.J - f\,(\underline{X},k,t,C(\underline{X},t)) = 0 \quad . \tag{6.2.9}$$

Equation (6.2.9) is called a reaction-diffusion equation. It holds for a general flux transport *J*, whether diffusion or some other related processes. Here, $\nabla.J$ is the diffusion term which describes the movement of the chemical species *C* within the domain (Ω), and $f(\underline{X},t,C(\underline{X},t))$ is the reaction term which describes the reaction occurring inside the domain (Ω). Substituting equation (6.2.2) into (6.2.9) gives the parabolic equation:

$$\frac{dC(\underline{X},t)}{dt} = \nabla.\,(D\nabla C) + f\,(\underline{X},k,t,C(\underline{X},t)) \quad . \tag{6.2.10}$$

As described in chapters 3 and 4, the reaction term f will be determined from the binding of Cdc42 and *Mycolactone* to WASP in the cytoplasm of the cell.

6.3 General Modeling Approach

The equations are formulated as a coupled reaction-diffusion equations of the form

$$\frac{dX_i}{dt} = \nabla.(D_i \nabla X_i) + S_i \tag{6.3.11}$$

where S_i denote the reaction terms, S_i couples the equations for the different species X_i. D_i is the diffusion constant for component *i* and ∇ is the nabla operator.

The following reactions will be considered in the cell cytoplasm.

$$R + A \xrightarrow[}{k_a} C$$

$$C + B \xrightarrow[}{k_b} C_2$$

$$R + B \xrightarrow{k_b} C_3$$

where R, A and B denote the receptor protein (WASP), ligand and the toxin respectively whiles C, C_2 and C_3 represent active complexes of WASP. The k_a and k_b are reaction rate constants. It is assumed that the toxin bind to the receptor protein (R) and the protein complex (C) at the same rate (k_b).

The governing equations in the different subdomains are written as reaction-diffusion system though some of the reactions could be described by simple Ordinary Differential Equations (ODEs). These species are allowed to diffuse in the cytoplasm since their diffusion does not alter the total concentrations as we want to compute. Based upon the description in section 6.1 we propose the following:

Subdomain One (Extracellular space)

$$\begin{cases} \frac{du_A}{dt} = \nabla.(D_A \nabla u_A) \\ \frac{du_B}{dt} = \nabla.(D_B \nabla u_B) \end{cases} \tag{6.3.12}$$

Subdomain Two (Cytoplasm)

$$\begin{cases} \frac{du_A}{dt} = -k_a u_A u_R + \nabla.(D_A \nabla u_A). \\ \frac{du_R}{dt} = -k_a u_A u_R - k_b u_B u_R + \nabla.(D_R \nabla u_R) \\ \frac{du_C}{dt} = k_a u_A u_R - k_b u_C u_B + \nabla.(D_C \nabla u_C). \\ \frac{du_{C_2}}{dt} = k_b u_C u_B + \nabla.(D_{C_2} \nabla u_{C_2}). \\ \frac{du_{C_3}}{dt} = k_b u_B u_R + \nabla.(D_{C_3} \nabla u_{C_3}). \\ \frac{du_B}{dt} = -(u_C + u_R) k_b u_B + \nabla.(D_B \nabla u_B) \end{cases} \tag{6.3.13}$$

Boundary and Initial conditions

On geometry one, define Neumann boundary condition (see Figure 6.4)

$$n.\nabla u_A = -k_a u_A u_R, \quad \text{and} \quad n.\nabla u_B = -k_b u_B u_R \quad \text{on} \quad \partial Y_{cell} \tag{6.3.14}$$

Geometry two, (cell membrane is represented as a separate compartment, Figure 6.4(b)). Assuming concentration on both sides of the cell membrane are in rapid equilibrium, we define concentration

$$\begin{cases} \frac{dU_i}{dt} - \nabla.(D_i \nabla U_i & \\ & U_i \\ & U_i \\ & n.\nabla U_i = h \end{cases}$$

$u_{Acell} = u_{Aext}$ and $u_{Bext} = u_{Bcell}$ on ∂Y_{cell}. (6.3.15)

The model problem can be written in compact form as

$$\begin{aligned}) &= F_i \quad \text{in} \quad \partial Y \\ &= 0 \quad \text{on} \quad \partial Y \times [0,T] \\ &= g \quad \text{on} \quad Y_{cell} \times \{t = 0\} \\ &\quad \text{on} \quad \partial Y_{cell} \times [0,T] \end{aligned} \tag{6.3.16}$$

where n is the outward normal vector, ∇ is the two dimensional nabla operator, g is the Dirichlet data of initial concentration of species in the cytoplasm and h is the flux on the boundary. U_i is a vector of the reacting species with the subscript i indicating the species and F_i is a vector of all the reaction terms. The terms in the vector F_i couples the systems of reacting species. In the numerical treatment, we consider two geometrical representations of the cell. The problem in equation (6.3.16) can not be solved analytically therefore, the problem is solved numerically. The finite element method is used and it is based on a discrete representation of the weak form of equation (6.3.16). The numerical treatment will consider only one cell, since it is

assumed that the tissue is a periodic arrangements of cells. This reduces memory requirements and computational time.

Next the topological setup of the model

6.4 Topological Setup of the Tissue in the Model

The setup below describes the simplified model of the tissue. Let $\Omega \subset R^N$ be a bounded Lipschitz domain with periodic arrangements of cells and the reference unit cell $Y = (0,1)^N$ be an open set in R^N, where $N = 2$. Lattice of copies of Y spans the entire region of Ω as shown on the left of figure 6.1. By this representation Ω, represents a layer of tissue.

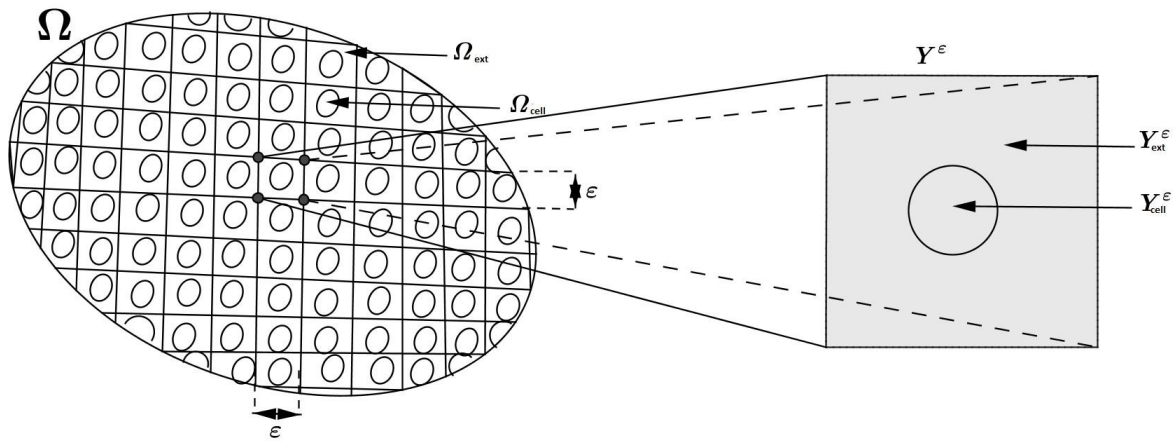

Figure 6.1: Left Periodic domain and Right unit cell

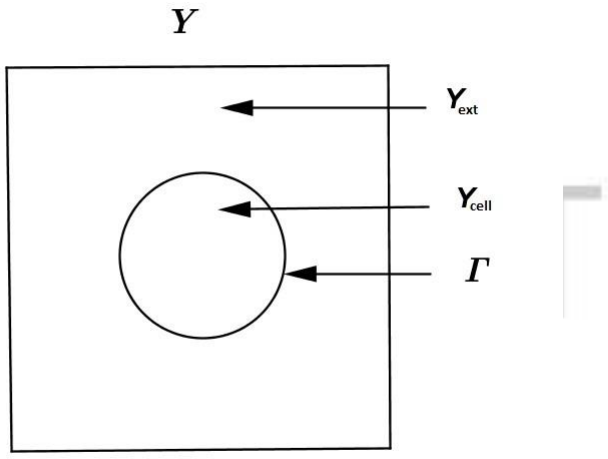

Figure 6.2: unit cell

Within the unit cell Y, we define a geometrical structure Y_{cell} (see Figure 6.2) as the cytoplasm (i.e. a closed subset of Y) and $Y_{ext} := Y \setminus Y_{cell}$ the extracellular space. To distinguish the complexes and reacting species in the two domains (Y_{cell} and Y_{ext}), we supplement the concentrations with the indices *cell* and *ext* to indicate cytoplasm and extracellular space respectively. Example by u_{Bcell}, we mean the concentration of the lipid toxin in the cytoplasm.

Also we assume that any two neighboring subdomains Y_{cell} do not touch each other and the two parts of the unit cell satisfy $\overline{Y}_{cell} \cap \overline{Y}_{ext} = \Gamma$. $\Gamma \subset Y$ is a one-dimensional boundary (cell membrane) that separates Y into two connected components Y_{cell} and Y_{ext}. Therefore $\Gamma = \partial Y_{cell}$, $\overline{Y}_{cell} \subset Y$ and such that $Y = Y_{ext} \cup Y_{cell} \cup \Gamma$. It is reasonable to assume the surface of the one-dimensional boundary (cell membrane) to be amphipathic in nature that has hydrophobic and hydrophilic regions.

The following assumptions and conditions are useful:

1. Y_{cell} and Y_{ext} have strictly positive measure in Y with $\overline{\partial Y_{cell}} \cap \partial Y = \emptyset$.

2. Y_{ext} is an open set with a local Lipschitz boundary.

3. The concentrations of the ligand and toxin on the cell membrane boundary are in rapid equilibrium.

4. The Continuum hypothesis is adopted to enable molecules in the cell and extracellular space to be described using concentrations u_{xi}.

5. The cytoplasm and the cell membrane have constant physical and chemical properties.

6. The flux through the membrane is normal to the surface of the membrane.

7. A layer of tissue constitutes an aggregation of similar cells.

Assumptions **4**-**6** are modifications from [Dreij et al., 2011, Chaudry et al., 2012].

One elementary cell (Y) consists of both the cytoplasm and extracellular space as depicted in Figure 6.2, assumption **1**. If the boundary of the extracellular space (Y_{ext}) is sufficiently regular, the second assumption **2** is fulfilled. The binding species (R, A, and B) and all the active complexes in the model are denoted by their concentrations, assumption **4** with the species as subscripts (i.e. u_R,u_B,u_A,u_{RA},u_{RB} and u_{BRA}). Next the periodic arrangement of the cells in the domain.

For a small parameter $\varepsilon > 0$, we generate copies of cells εY of regular mesh of size ε to span the domain $\Omega \subset R^N$. Denote each re-scaled cell by $Y_i^\varepsilon = (0,\varepsilon)^N$ (see Figure6.1) where $N = 2$ in this model, $1 \leq i \leq N(\varepsilon)$. The number of cells in the domain of Ω is given by $N(\varepsilon) = \varepsilon^{-1} \mid \Omega \mid$. Then each cell now become homeomorphic to Y, by a linear homeomorphism $\Pi^\varepsilon{}_i$ with ratio of magnification ε^{-1}. It holds that

$$Y^\varepsilon_{cell_i} = (\Pi^\varepsilon_i)^{-1}(Y_{cell}). \tag{6.4.17}$$

$$Y^\varepsilon_{ext_i} = (\Pi^\varepsilon_i)^{-1}(Y_{ext}). \tag{6.4.18}$$

It holds further that $\Omega^{\varepsilon} = \Omega^{\varepsilon}_{cell} \cup \Omega^{\varepsilon}_{ext}$, and $Y^{\varepsilon} = Y^{\varepsilon}_{cell} \cup Y^{\varepsilon}_{ext} \cup \Gamma^{\varepsilon}_{cell}$.

The extracellular space $\Omega^{\varepsilon}_{ext} \subset \Omega$ is obtained by removing the periodically distributed cells. That is

$$\Omega_{\varepsilon ext} = \Omega \setminus \left[\bigcup_{i=1}^{N(\varepsilon)} Y_{i\varepsilon}. \right. \tag{6.4.19}$$

and

$$\Omega_{\varepsilon cell} = \left[\bigcup_{i=1}^{N(\varepsilon)} Y_{i\varepsilon}. \right. \tag{6.4.20}$$

Also define the boundary of the extracellular space by

$$\partial\Omega^{\varepsilon}_{ext} = \partial\Omega \cup \partial\Omega^{\varepsilon}_{cell}. \tag{6.4.21}$$

where $\partial\Omega^{\varepsilon}_{cell} = \Gamma$ is the cell membrane boundary.

For $T > 0$, let $S := (0,T)$ denote the time interval. The space-time domains then becomes

$$Q := S \times \Omega \qquad \text{and } Q^{\varepsilon}_{z} := \mathbb{S} \times \Omega^{\varepsilon}_{z}, \quad \forall z \in \{ext, cell\}.$$

The domains $\Omega^{\varepsilon}_{ext}$ and $\Omega^{\varepsilon}_{cell}$ are assumed to be extracellular space and cytoplasm of cell respectively.

It suffices to state that the domain Y^{ε}_{cell} as well as the domain Y^{ε}_{ext} of this repetition are Y-periodic in the language of Homogenization Theory. Through this concept, periodic Homogenization Methods can also be used to compute solutions for the problem. Some basic ideas of the Finite Element Method related to this study is introduced next.

6.5 Elements of Function Spaces

The finite element method depends on assumptions on regularity of solution. Therefore, the classes of functions with specific differentiability and integrability

called function spaces are very essential. This section is devoted to summarizing the elements of the theory of function spaces and reviewing some basic definitions and results from the theory of partial differential equations related to this work. The concepts and notational conventions introduced here will be used systematically throughout the rest of the thesis. (see for example, Dietrich [2007], Philippe [1987], Jacob and Ted [2007], Brenner and Scott [1994], Johnson [1990] for a comprehensive introduction to finite element methods).

Function Spaces

The definitions of some function spaces

Definition 6.5.1. Let the domain $\Omega \subset \mathbb{R}^n$ be Lebesgue measurable with non-empty interior. The class of all measurable functions u is defined as:

$$L^p(\Omega) := \{u : \Omega \to \mathbb{R} \mid \int |u|^p dx < +\infty\}, (\quad 1 \leq p < +\infty). \ \Omega \tag{6.5.22}$$

$$p = 2, \quad L^2(\Omega), \qquad p = \infty, \qquad L^\infty(\Omega) = \{u : \Omega \to \mathbb{R}, measurable\} \tag{6.5.23}$$

Remark: u is essentially bounded if

$$ess.\sup_{\Omega} \mid u \mid := \inf\{k > 0 :\mid u(x) \mid \leq k \quad \text{or nearly all} \quad x \in \Omega\} < \infty \tag{6.5.24}$$

$L^p(\Omega)$ is a Banach space and these spaces are equipped with the norms:

$$\| u \|_{0,p} := \left(\int_\Omega \mid u \mid^p dx \right)^{1/p}, \quad 1 \leq p < \infty \tag{6.5.25}$$

and

$$\|u\|_{0,\infty} = ess.\sup_{\Omega} \mid u \mid \tag{6.5.26}$$

$L^2(\Omega)$ is a Hilbert space with scaler product

$$(u,v) := \int_\Omega uv dx \tag{6.5.27}$$

with support of

$$u : \Omega \to \mathbb{R} \tag{6.5.28}$$

$$\text{sup}u := \{x \in \Omega \mid u(x) \neq 0\} \tag{6.5.29}$$

The space of non-empty test function is defined by:

$$C_0^\infty = \{u \in C_c^\infty \quad \text{Support of u is compact}\} \tag{6.5.30}$$

As an example

$$u_\varepsilon(x) = \begin{cases} \exp\left(-\frac{\varepsilon^2}{\varepsilon^2 - |x|^2}\right), & |x| < \varepsilon \\ 0, & \text{otherwise} \end{cases} \tag{6.5.31}$$

6.6 Notation

The weak derivative

D^α for $\alpha = (\alpha_1, ..., \alpha_n) \in \mathbb{N}_0^n, \quad \alpha_i \geq 0$, with $|\alpha| = \sum_{j=1}^{n} \alpha_j$ is given by

(6.6.32)

$$D^\alpha u = \partial_{x_1}^{\alpha_1}, ..., \partial_{x_n}^{\alpha_n} := \frac{\partial^{|\alpha|} u}{\partial_{x_1}^{\alpha_1}, ..., \partial_{x_n}^{\alpha_n}} \tag{6.6.33}$$

Definition 6.6.1. A function in $u \in L^2(\Omega)$ is called weakly differentiable with index α if there is a function $w \in L^2(\Omega)$ such that:

$$\int_\Omega u D^\alpha v dx = (-1)^{|\alpha|} \int_\Omega w v dx, \quad \forall \quad v \in C_0^\infty(\Omega) \tag{6.6.34}$$

Equation (6.6.34) is called the partial integration.

Also important are vector subspaces of $L^p(\Omega)$, termed as the Sobolev spaces

Definition 6.6.2. Let $m \geq 0$ and $p \geq 1$ the space $W^{m,p}(\Omega) := \{u \in L^p(\Omega) : D^\alpha u \in L^p(\Omega), |\alpha| \leq m\}$ is called a Sobolev space

The Sobolev space $W^{m,p}(\Omega)$ is equipped with the norm:

$$\| u \|_{m,p} := \left(\int_\Omega \sum_{|\alpha| \leq m} | D^\alpha u |^p \, dx \right)^{1/p} \tag{6.6.35}$$

Correspondingly, a semi-norm on this space is defined as:

$$| u |_m := \left(\int_\Omega \sum_{|\alpha| \leq m} | D^\alpha u |^2 \, dx \right)^{1/2} \tag{6.6.36}$$

respectively

$$\| u \|_{m,\infty} := \max_{|\alpha| \leq m} \| D^\alpha u \|_{0,\infty} \tag{6.6.37}$$

Remark

The functions in $W^{m,p}(\Omega)$ are the functions from $L^p(\Omega)$ whose weak derivatives are in $L^p(\Omega)$. For $p = 2$, it holds that $H^m(\Omega) := W^{m,2}(\Omega)$. Define the scalar product defined on $H^m(\Omega)$ as

$$(u,v)_m := \sum_{|\alpha| \leq m} (D^\alpha u, D^\alpha v)_0. \tag{6.6.38}$$

Of great use will be $H^1_\Gamma(\Omega)$ a closed subspace of $H^1(\Omega)$ defined as:

$$H^1_\Gamma(\Omega) = \{ v \in H^1(\Omega) \mid v = 0 \quad \text{on} \quad \Gamma \}. \tag{6.6.39}$$

It consists of square integrable functions whose trace vanishes on the boundary Γ.

We define $W_0^{m,p}$ as the completion of $C_0^\infty(\Omega)$ with respect to the norm

$$\| \cdot \|_{m,p}, \quad W^{m,p} = \overline{C_0^\infty}^{\| \cdot \|_{m,p}} \tag{6.6.40}$$

Theorem 6.1. *For $m \geq 1$, $p \geq 1$*

The space $(W^{m,p}(\Omega), \| \cdot \|_{m,p})$ is a Banach space

The space $(H^m(\Omega), (.,.)_m)$ is a Hilbert space

Note that functions in a Sobolev space need not be continuous but for large m and p Sobolev functions are continuous.

For the model problem, because of the nature of the extracellular space and the cytoplasm, we need more smoothness on the boundaries. Here, we limit ourselves to only Lipschitz domains

Definition 6.6.3. : A bounded domain $\Omega \in \mathbb{R}^n$ has Lipschitz boundary, if for every $x \in \partial\Omega$ there is a sphere $B(x)$ which lies in an open set $O_i, i = 1,...,M$. Such that $O_i \cap \Omega = O_i \cap \Omega_i$ where

$$\Omega_i = \{(x_1,x_2) \in \mathbb{R}^n : x_1 \in \mathbb{R}^{n-1}, x_2 \in \mathbb{R}, \quad x_2 < \varphi_i(x_1)\} \tag{6.6.41}$$

where the functions φ_i are Lipschitz continuous. That is $|\varphi_i(x)-\varphi_i(y)| \leq L\,|x-y|$, for some constant $L > 0$.

Theorem 6.2. *(Trace-mapping Theorem)*

Let Ω be bounded with Lipschitz boundary and let $p \geq 1$, then there exist a unique continuous mapping $tr : W^{1,p}(\Omega) \to L^p(\partial\Omega)$ such that $tr(u) = u\,|\partial\Omega$, $\forall\, u \in C^1(\overline{\Omega})$, such that $tr(u)$ is called the generalized boundary of u.

From Theorem 6.2 we have the following identities.

Theorem 6.3. *: $W^{1,p} = \{u \in W^{1,p} \mid \quad tr(u) = 0\}$*

$$H_0^1(\Omega) = \{u \in H^1 \mid \quad tr(u) = 0\} = \overline{C^\infty}^{\|\cdot\|_0}$$

Then the following Lemma holds (Poincare- Friedreich's Inequality). Let $\Gamma \subseteq \partial\Omega$ have a non-vanishing $(n-1)$-dimensional measure. Then, there exist constants, depending only on Ω and Γ, such that for $u \in H^1(\Omega)$,

$$\| u \|^2_{L^2(\Omega)} \leq C_1 \mid u \mid^2_{H^1(\Omega)} + C_2 \| u \|^2_{L^2(\Gamma)} \tag{6.6.42}$$

If u vanishes on Γ,

$$\| u \|^2_{L^2(\Omega)} \leq C_1 \mid u \mid_{H^1(\Omega)} \tag{6.6.43}$$

and thus

$$\mid u \mid^2_{H^1(\Omega)} \leq \| u \|^2_{H^2(\Omega)} \leq (C_1 + 1) \mid u \mid^2_{H^1(\Omega)} \tag{6.6.44}$$

See for example Andrea and Olof [2005], Lawrence and Evans [2002] for the proof.

Next we describe the existence and uniqueness solutions of the model problem.

6.7 General Second-Order Parabolic PDEs

The general parabolic equation for a uniformly elliptic operator L on $\Omega \times (0,T)$ is given by

$$u_t + Lu = f \tag{6.7.45}$$

where the divergence form of L is given by

$$L = -\sum_{i,j=1}^{n} \partial_i \left(a^{ij} \partial_j u \right) + \sum_{j=1}^{n} b^j \partial_j u + cu \tag{6.7.46}$$

where the coefficients $a^{ij}(x,t), b^j(x,t), c(x,t)$ are coefficient functions with $a^{ij} = a^{ji}$. In equation (6.7.46), it is assumed that there exist $\beta > 0$ and $\xi \in R^n$ such that

$$\sum_{ij=1}^{n} a^{ij}(x,t)\xi_i\xi_j \geq \beta \mid \xi \mid^2, \forall \quad (x,t) \in \Omega \times (0,T \tag{6.7.47}$$

Equation 6.7.45 is complete with the addition of initial and boundary values. The model problem is obtained if $b^j = 0 = c$.

Variational Formulation

In order to apply the finite element method, we must develop a computable form of our problem, the so called weak form. For simplicity we do the variational formulation for the initial/ boundary value problem (IBVP) of the receptor in the cytoplasm of the cell. The IBVP can be written as

$$\begin{aligned} u_{Rt} &= \nabla.(D_R \nabla u_R) + f \\ u_R &= 0 \quad \text{on} \quad \partial Y_{cell} \\ u_R &= R_0 \quad \text{on} \quad Y_{cell} \end{aligned} \tag{6.7.48}$$

where $f = -(k_a u_A u_R + k_b u_B u_R)$ is a sink. The variational formulation of the model in equation (6.7.48) with the Dirichlet boundary is formulated. From now we omit the subscripts on the concentration and write u instead of u_R.

We first suppose that the domain Y, the diffusion coefficients and the solution are smooth. The equation (6.7.48) is multiplied by a test function $v \in C_c^\infty(\Omega)$, and integrated over Y, and the divergence theorem applied. This gives

$$(u_t, v)_{L^2} + a(u(t), v : t) = (f(t), v)_{L^2} \quad \text{for} \quad 0 \le t \le T \tag{6.7.49}$$

where $(.,.)_{L^2}$ denote the L^2-inner product

$$(u, v)_{L^2} = \int_Y u(x)v(x)dx \tag{6.7.50}$$

and the associated bilinear form a is given by

$$a(u, v; t) = \sum_{ij=1}^{n} \int_Y a^{ij}(x, t)\partial_i u(x)\partial_j v(x \tag{6.7.51}$$

In equation (6.7.49) we mean $u(t) = u(.,t)$ and to generalize the weak solution, it is assumed that $Y \subset R^n$ is bounded and open for $T > 0$

Then

- The diffusion coefficient $a^{ij} \in L^{\infty}(Y \times (0,T))$; • $a^{ij} = a^{ji}$ and the condition in 6.7.47 is satisfied

- $f \in L^2(0,T;H^*(Y))$ and $g \in L^2(Y)$.

Here f is allowed to take values in $H^*(Y) = H_0^1(Y)$, where $H^*(Y)$ is the dual space of $H_0^1(Y)$. The duality pairing between $H^*(Y)$ and $H_0^1(Y)$ is denoted by

$$\langle ., . \rangle : H^*(Y) \times H_0^1(Y) \to R \tag{6.7.52}$$

The coefficient of a are uniformly bounded in time, therefore it holds that

$$a : H_0^1(Y) \times H_0^1(Y) \times (0,T) \to R \tag{6.7.53}$$

If there exist constants $C > 0$ and $\alpha \in R$ such that for each $u, v \in H_0^1(Y)$

$$C \parallel u \parallel_{H_0^1}^2 \leq a(u,v;t) + \alpha \parallel u \parallel_{L^2}^2 \quad \text{and}$$
$$| a(u,v;t) | \leq C \parallel u \parallel_{H_0^1} \parallel v \parallel_{H_0^1} \tag{6.7.54}$$

Let u be associated with the mapping

$$u : [0,T] \to H_0^1(Y) \tag{6.7.55}$$

defined by

$$[u(t)](x) := u(x,t) \qquad (u \in Y, 0 \leq t \leq T) \tag{6.7.56}$$

Now u is not considered as a function of x and t together but as a mapping u of t into the space $H_0^1(Y)$ of functions of x.

Then in problem equation (6.7.48) we can similarly define

$$f: [0,T] \to L^2(Y) \tag{6.7.57}$$

by

$$[f(t)](x) := f(x,t) \qquad (x \in Y, 0 \le t \le T) \tag{6.7.58}$$

This guarantees the choice of $v \in H_0^1(Y)$ for a weak solution

We can now define the weak solution to the model problem in equation (6.7.48) as:

Definition 6.7.1. A function $u : [0,T] \to H_0^1(Y)$ is a weak solution to (6.7.48) if: $u \in L^2(0,T;H_0^1)$ and $u_t \in L^2(0,T;H^*(Y))$ and for every $v \in H_0^1(Y)$

$$\mathrm{h}u(t),v\mathrm{i} + a(u(t),v;t) = \mathrm{h}f(t),v\mathrm{i} \tag{6.7.59}$$

for t pointwise almost everywhere in $[0,T]$ and $u(0) = R_0$ in the cytoplasm **Remark** *It is not clear how to interpret the time derivative of a function which is in L^2 and also $u(0) = R_0$ (measure zero)* The following theorem holds:

Theorem 6.1. *Suppose* $u \in L^2(0,T;H_0^1(Y))$ *with* $u^0 \in L^2(0,T;H^*(Y))$, *then*

(i) $u \in C([0,T];L^2(Y))$ (6.7.60)

after possibly being redefined on a set of measure zero,

(ii) *The mapping*

$$t \,7\!\to \mathrm{k}\, u(t)\, \mathrm{k}^2_{L^2(Y)} \tag{6.7.61}$$

is absolutely continuous with

$$\frac{d}{dt} \parallel u(t) \parallel^2_{L^2(Y)} = 2\langle u'(t), u(t)\rangle \tag{6.7.62}$$

for almost everywhere $0 \le t \le T$

Furthermore, we have the estimate

$$\max_{0\le t\le T} \| u(t) \|_{L^2(Y)} \le C(\| u \|_{L^2(0,T;H_0^1(Y))} + \| u' \|_{L^2(0,T;H^*(Y))}) \quad (6.7.63)$$

The constant C depends on T only.

See for example Lawrence and Evans [2002] for the proof of Theorem 6.1. Furthermore, from the evolution triple (Golfand triple), we have for example

$$H_0^1(Y) \subset L^2(Y) \subset (H_0^1)^* = H^*(Y) \quad (6.7.64)$$

Comment: For $u \in w(0,T;V) = \{V \in L^2(0,T;V) \mid V^0 \in L^2(0,T;V^*)\}$ and $V = H_0^1$, we have $u = [0,T] \to L^2$ is continuous nearly everywhere. Then $u(0) = R_0$ make sense.

Theorem 6.2. *Suppose that the condition in Theorem 6.1 are satisfied, then for every* $f \in L^2(0,T;H^*(Y))$ *and* $R_0 \in H_0^1$ *there is a weak solution*

$$u \in C([0,T]; L^2(Y)) \cap L^2(0,T; H_0^1(Y)) \quad (6.7.65)$$

of 6.7.48 with $u_t \in L^2(0,T;H^*(Y))$ Next we

proceed as follows:

1. Partition the domain (Y) into triangles.

2. Construct a finite dimensional subspace (V_h) consisting of piecewise-polynomials, and

3. Define the transition conditions

6.7.1 Triangulation

Let $Y \subset R^d$ be a bounded domain with a Lipschitz continuous boundary. A triangulation or mesh is a non-overlapping partition of Y into elements.

Definition 6.7.2. Let $Y \subset R^d$ be a bounded domain. A partition Z_h of Y into subsets $T \in Z_h$ is called a triangulation if the following are satisfied

1. For each $T \in Z_h$, T is closed and T° 6= 0, and connected. Where $T^\circ = T \backslash \partial T$ denote interior of T.

2. $\bar{Y} = \mathrm{S}_{T \in Z_h} T$.
3. If $G = T_i^\circ \cap T_j^\circ = \emptyset$, $\forall\ T_i, T_j \in Z_h$, i 6= j, then G is a common edge, face or vertex of T_1 and T_2.

4. $Z_h = \{T_1, \ldots . T_M\}$.

5. $h = \max_i diam(T_i)$, $\forall\ T_i \in Z_h$.

Now we can assume that the domain Y and all T_i are polyhedron.

Then Z_h is called a triangulation of $\bar{Y}$ [Chamakuri, 2007]. h is called the diameter of Z_h, and the family Z_h satisfying the above properties is said to be geometrically conforming.

Definition 6.7.3. A triangulation Z_h is called admissible if each edge of T_i is either the edge of another T_j or part of ∂Y .

Definition 6.7.4. A finite element in R^d is a triple $(T, P_T, {}^{\mathrm{P}}{}_T)$ satisfying the following properties:

- T is a closed subset of R^d with a non empty interior and a Lipschitz continuous boundary.

- P_T is a finite dimensional function space defined on T and $N = \dim P_T$.

- ${}^{\mathrm{P}}{}_T$ consists of linearly independent functionals, or it is a set of degrees of freedom. such that a function $v \in P_T$ is determined by the degrees of freedom ${}^{\mathrm{P}}{}_T$.

The nodal basis function Φ_i is now defined by

$$\mathrm{P}_i(a_j) = \delta_{ij} \equiv \begin{cases} 1 & \text{if if} \quad i = j \\ 0 & \text{if} \quad i \,6{=}\, j \end{cases} \tag{6.7.66}$$

6.8 Finite Dimensional Space

The finite-element method is a numerical implementation of the Galerkin method which uses a space V_h of piecewise polynomial functions that are supported on elements. Finite-element basis functions, are supported on a small number of adjacent elements. Furthermore, one can approximate functions on domains with

complicated geometry in terms of the finite-element basis functions by subdividing the domain into smaller elements, and refine the decomposition in regions where higher resolution is required. The finite-element basis functions are not exactly orthogonal, but they are almost orthogonal since they overlap only if they are supported on nearby elements. As a result, the associated Galerkin equations involve sparse matrices, which is crucial for their efficient numerical solution. The basic idea of the existence

of a solution is to approximate, $u; [0,T] \to H_0^1(Y)$ by functions u_h;[0,T] → V_h that take values in a finite-dimensional subspace $V_h \subset H_0^1(Y)$. To obtain the u_h, we project the PDE onto V_h, meaning that we require that u_h satisfies the PDE up to a residual which is orthogonal to V_h. This gives a system of ODEs for u_h, which has a solution by standard ODE theory. Each u_h satisfies an energy estimate of the same form as the a priori estimate for solutions of the PDE.

$$\dim V_h = \frac{1}{h} < \infty, \quad \text{and} \quad V_h \in H \tag{6.8.67}$$

In more detail, the existence of uniform bounds implies that the sequence {u_h} is weakly compact in a suitable space and hence, by the Banach-Alaoglu theorem, since the PDE and the approximating ODEs are linear, linear functionals are continuous with respect to weak convergence. Therefore, the weak limit of the solutions of the ODEs is a solution of the PDE.

6.9 Finite Element

6.9.1 Weak form

$$\frac{d}{dt}(u(t),v)+a(u(t),v)=(f(t),v), \qquad V=H_0^1(Y), \quad V_h$$: finite dimentional subspace (6.9.68)

Find $u_h(t) \in V_h$ with $u_h(0) = I_hR(0)$, such that

$$\frac{d}{dt}(u_h(t),v_h)+a(u_h(t),v_h)=(f(t),v_h) \quad \forall v_h \in V_h \tag{6.9.69}$$

V_h = Span{Φ_1.....Φ_N} → basis function (6.9.70) M $u_h(t,x)$ = $\sum_{i=1}^{N} u_i(t)\Phi_i(x)$ (6.9.71)

$v_h = \Phi_j$

$$\frac{d}{dt}\left(\sum_i^N u_i(t),\Phi_i;\Phi_j\right)+a(\sum_i^N u_i\Phi_i.\Phi_j)=(f,\Phi_j) \tag{6.9.72}$$

$$\sum_{i=1}^{N} u_i'(t)(\Phi_i,\Phi_j) + \sum_{i=1}^{M} u_i(t)a(\Phi_i,\Phi_j) = (f,\Phi_j) \tag{6.9.73}$$

Then

$$A=(a(\Phi_i,\Phi_j)), \qquad F=(f,\Phi_j), \qquad u=(u_i)_i \in R^m, \qquad M=(\Phi_i,\Phi_j)_{i,j} \tag{6.9.74}$$

and

$$Mu^0 + Au = F, \qquad u = u(t) \in R^m \tag{6.9.75}$$

where M is the mass matrix, A is the stiffness matrix. A is large, sparse and positive definite. See for example Thomee [1984] for a detail discussion on the lumping of

the mass matrix and further reading in [Axelsson and Barker, 2001, Dautray and Luis,

1988].

The direct method (noniterative) of solving finite element computations is used in this study.

In Comsol Multiphysics, there are three stages in solving the problem using the direct solve namely: Get an initial solution on a coarse mesh, Estimate, and Refine mesh.

- We get an initial solution of the finite element discretized problem on a coarse mesh.

- Set a tolerance $TOL > 0$. Then the global discretization error denoted by $\| E \|$ is estimated using the local discretization error denoted by $\| E \|_T$.

$$\underbrace{\| u - u_h \|^2}_{GlobalError} = \sum_{T \in Z_h} \underbrace{\| u - u_h \|^2}_{LocalError} \tag{6.9.76}$$

where

$$\| E \|_T = \| u - u_h \|_T \leq TOL \tag{6.9.77}$$

- The mesh is refined by subdividing the elements into finer mesh. This procedure is repeated until the error tolerance level is reached by every element in the discretized domain.

6.10 Numerical formulation

Galerkin Finite Element Method (GFEM) is used for the discretization, with triangular elements used for the discretization of the domain. The system of equations obtained from the GFEM is solved using a direct solver. The discretization

of the governing PDEs by the GFEM scheme result in a set of linear equations. The core of the resulting coupled system of equations is the solution of sparse linear system, which is the most intensive part of the solver.

The numerical algorithm can broadly be classified into three categories:

- Numerical formulation with finite element discretization.
- Solution strategy for solving the resultant linear equations.
- Solution of the linear system.

The solution of the linear system is the most difficult part in terms of computational time and memory requirement. Next, an overview of one of the sparse direct solvers (UMFPACK) used in this work.

6.11 The Solver

6.11.1 Sparse direct solver (UMFPACK)

The UMFPACK is a routine developed for solving sparse linear systems using the Unsymmetric MultiFrontal method. The Multifrontal method is the upgraded version of the frontal method developed for solving finite element problems of symmetric positive definite systems by Amestoy and Duff [1989]. It was later further improved to include unsymmetric systems by Davis [2004]. This implies the matrix A need not be symmetric. COMSOL Multiphysics has in-built direct and iterative solvers which can be selected depending on the type of problem being solved, and the symmetric

nature of the matrix. The UMFPACK solver automatically select different strategies for pre-ordering the rows and columns in the matrix [Raju and Khaitan, 2009].

The direct solver solves

$$Ax = b \tag{6.11.78}$$

where the matrix A is large, sparse and typically ill-conditioned. It computes a decomposition of A (e.g. LU decomposition). Sparse, direct solvers have the advantage of saving memory and CPU time. They are very robust and the work grows as

$$0(N_{1+2(d-1)/d}) \tag{6.11.79}$$

where d is the dimension and thus we have the system here growing as $0(N^2)$ on a $2d$.

Furthermore, the memory also grows as:

$$0(N_{1+(d-1)/d}) \tag{6.11.80}$$

that gives $0(N^{3/2})$ for $2d$.

6.12 Computational Details

The model is implemented in COMSOL 3.5 using the coefficient form PDE with the variables fully coupled. The description of the ligand-receptor-toxin binding lead to a system of PDEs. These problems are difficult to solve analytically therefore we find approximate solution to the problem numerically. The COMSOL Multiphysics software is based on the finite element method (FEM) described earlier by subdividing the solution domain of the problem into a large number of finite elements to find approximate solution to the governing equation(s) Figure 6.5. FEM

method uses simple piecewise linear, or quadratic functions to compute solutions for the unknown variables. This way, the error in the approximation can be determined by substituting the piecewise approximation function for the unknown to compute the residuals.

COMSOL uses a predefined equation system, users can not change the numerical methods but can modify the variables to suit a specific problem. COMSOL Multiphysics has an integrated environment with a variety of model libraries for solving single and coupled system of stationary or transient first, second and third order in space PDEs on one, two or three dimensional domains. Modeling in COMSOL Multiphysics follow the steps below.

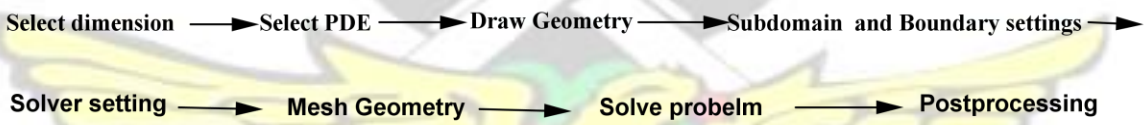

Figure 6.3: Steps in COMSOL modeling

6.13 Choice of PDE

The coefficient form of PDE in comsol Multiphysics can be written as:

$$d_a \frac{du}{dt} + \nabla.(-c\nabla u - \eta u + \gamma) + \beta\nabla u + au = f \tag{6.13.81}$$

with the following boundary conditions

$$hu = r$$

$$n.(c\nabla u + \eta u - \gamma) + qu = g - h^T\mu$$

where n is the unit normal perpendicular to the membrane and $d_a, c, \eta, \gamma, \beta, a, f, h, g$ are scalar function. The model problem is realized by setting $e_a = \eta = \beta = \gamma = a = 0$ **6.14**

Geometry

In the numerical analysis, we compare two geometrical representation of the cell. The two geometries are different in the implementation of the cell membrane boundary. First the cell membrane is implemented as one-dimensional boundary Figure

6.4a and second as a separate subdomain Figure 6.4b. The two boundaries differ in the coupling of the equations on the cell membrane boundary. We use the features in COMSOL to define flux on the boundary of the first geometry and concentration on the boundary of the second geometry.

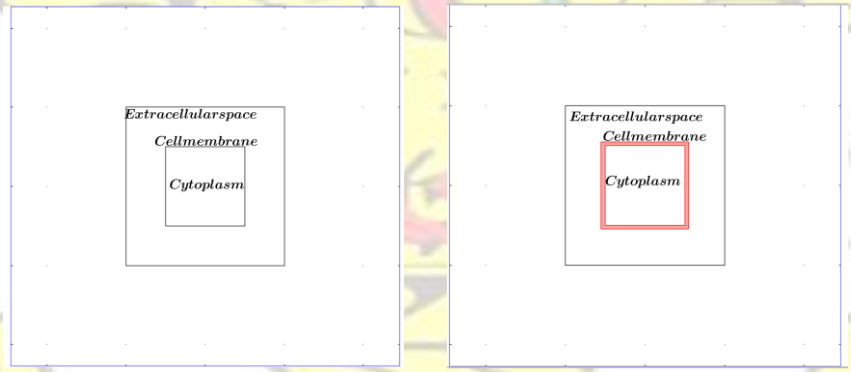

(a) (b)

Figure 6.4: Schematic representation of geometries (a) membrane as 1D boundary (b) membrane as a separate compartment / subdomain

We find in the numerical simulations that the system of equations is reaction dominant. Although the complexes formed could be described by ODEs, for the sake

of the geometrical comparison, all the evolution equations are written as reaction-diffusion equations (6.3.12-6.3.13). Note that only the ligand and the toxin are allowed to freely diffuse in the extracellular space and the cytoplasm. All other species are restricted to the cytoplasm. By this approach the numerical results are not affected since we are interested in the total concentration of all complexes formed. An integral of the concentration over the subdomains gives the total concentration of the species. Therefore, the diffusion of a species in a subdomain does not affect the result.

6.15 Coupling of the Subdomains

In COMSOL, the model can be implemented in two ways: first using a set of global PDEs with different parameters in the different domains. Secondly separate PDEs can be defined in the different domains and suitably coupling the species in the different subdomains. These approaches have been used in Menshykau and Iber [2012], Vollmer et al. [2013]. In this study we implement a simple 2D model as described above using the second approach to solve the system of equations in (6.3.12-6.3.13). In the cytoplasm the concentration of the ligand (u_{Acell}), the toxin (u_{Bcell}) and the receptor (u_{Rcell}) are being consumed and there is formation of the complexes (u_{Ccell},u_{C2cell},and u_{C3cell}).

The 2D geometry used in the numerical simulation is shown in Figure 6.4. Figure 6.4a consists of an extracellular space (Ω_{ext}), a one dimensional cell membrane boundary and the inner subdomain representing the cytoplasmic surface (Ω_{cell}). Figure 6.4b differ from Figure 6.4a in the implementation of the cell membrane as a separate compartment. The extracellular space and the cytoplasm are represented by squares of size 1 and 0.5, respectively. The thickness of the cell membrane in Figure 6.4b is

0.05.

6.16 Model implementation in COMSOL

In this section we compare the two approaches in modeling the cell membrane. The cell membrane separates the extracellular space from the cytoplasm. In both geometries the species are coupled between the extracellular space and the cytoplasm.The numerical solution are computed using three direct solvers namely: UMFPACK, SPOOLES (Sparse object oriented linear equation solver) and PARDISO (Parallel direct sparse solvers). The performance of these solvers with respect to the computational time and memory requirement on a $64-bit$ windows HP-Z1 workstation machine with 16GB RAM is evaluated.

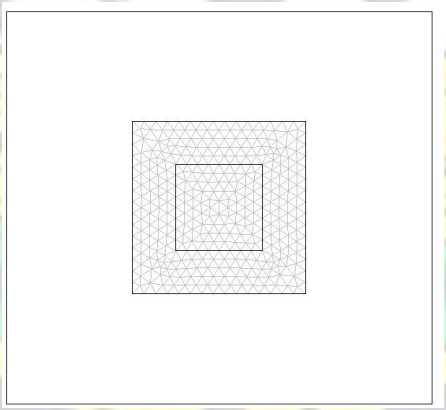

Figure 6.5: Meshed Geometry

In Y_{cell} the following parameters were used $D_R = D_C = D_{C2} = D_{C3} = 1$, $k_b = 0.1$, $k_a = 0.5$ and $D_A = 100$.

In the extracellular space (Y_{ext}), $D_R = D_C = D_{C1} = D_{C2} = 0$.

The initial concentrations are $u_C = u_{C2} = u_{C3} = 0$ in all compartments. Since the complexes formed are restricted to the cytoplasm,

$$n.\nabla u_C = n.\nabla u_{C_2} = n.\nabla u_{C_3} = 0. \quad \text{on} \quad \partial Y_{cell} \tag{6.16.82}$$

For the ligand, *Mycolactone* toxin and receptor, we have

$$\int_{Y_{ext}} u_A dA = 2 \tag{6.16.83}$$

$$\int_{Y_{ext}} u_B dA = 0.5 \tag{6.16.84}$$

$$\int_{Y_{cell}} u_R dA = 1 \tag{6.16.85}$$

as initial conditions respectively. This implies that, at time zero ($t = 0$) concentrations of the ligand and receptors are present in Y_{ext} and Y_{cell} respectively. The PDEs are coupled on the boundary by imposing the condition $u_{Acell} = u_{Aext}$ and $u_{Bcell} = u_{Bext}$ on ∂Y_{cell} in geometry 2. By this we mean the concentration of the ligand on the cell membrane are always in rapid equilibrium (assumption 3). An alternative boundary condition for geometry 2 is:

$$\frac{\partial S_{ext}}{\partial n_{ext}} + \frac{\partial S_{cell}}{\partial n_{cell}} = 0 .$$

where $S = u_A, u_B$ and $n_{ext} = -n_{cell}$.

6.17 Numerical results

In this section the numerical result from the simulations are presented. The numerical solutions presented here were obtained by integrating over respective subdomains or compartments. In the plots, the ligand, toxin and receptor will be represented by black, deep dashed purple and deep blue lines whiles the complexes formed (C, C_2 and C_3) are represented by red, dashed red or dashed-dotted light blue,

and dashed purple lines respectively. For simplicity $u_x(t) = xt$, on the legend where x denote the specie. The other concentrations are represented similarly on the ligand.

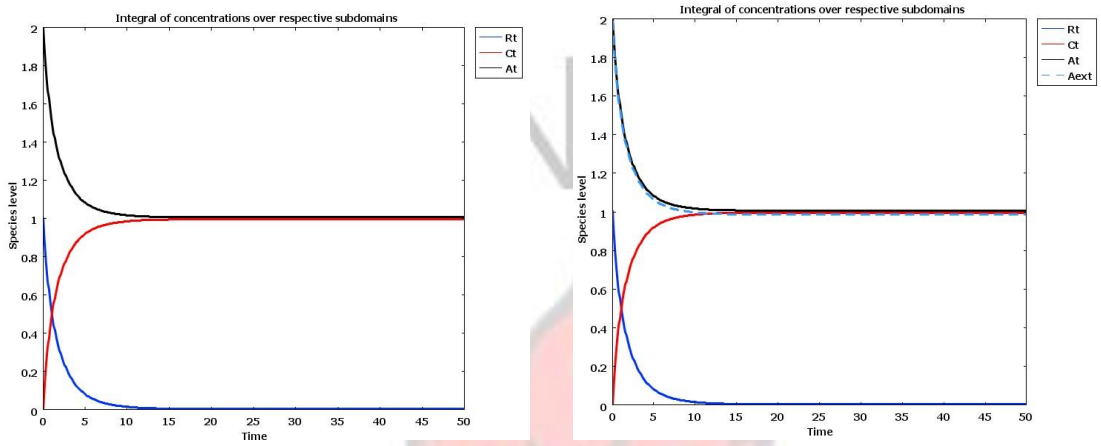

(a) (b)

Figure 6.6: Numerical solution for concentration of complex C formation

Figure 6.6 shows the numerical results for ligand (A) receptor (R) binding to form the complex (C). The plots in Figure 6.6a and Figure 6.6b shows the result for implementation of membrane as boundary (1D) and membrane implemented as separate compartment respectively. The results agree for the two geometries. The only difference is the coupling of the equations on the boundary. Note that the ligand and the receptor are consumed in the binding process to form the complex (C). After the value 15 on the time axis, notice that the ligand, receptor and complex are at steady state.

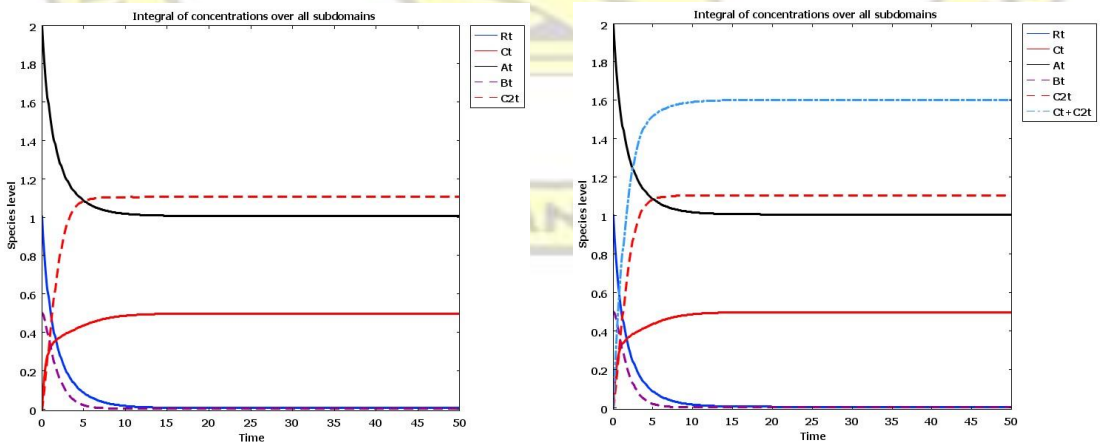

(a) (b)

Figure 6.7: Numerical solution for concentration of species (a) Shows depletion of ligand and receptor concentration and formation of complexes C and C_2, (b) Sum of C and C_2 is shown in dashed-dotted blue line

Figure 6.7 shows the numerical solution for five coupled PDEs from ligand-receptortoxin binding and formation of the complexes C and C_2. The results in Figure 6.7 is without the toxin (B) binding directly to the receptor. In Figure 6.7b the sum of the two complexes formed C+C_2 is shown. The light blue dashed-dotted line is the integral of the two complexes over the cytoplasm. The formation of the complexes C and C_2 are restricted to the cytoplasm. The numerical results show an increase in active WASP complex with the introduction of the toxin as shown by the dashed-dotted blue line. Next the binding rate of the ligand and toxin are investigated.

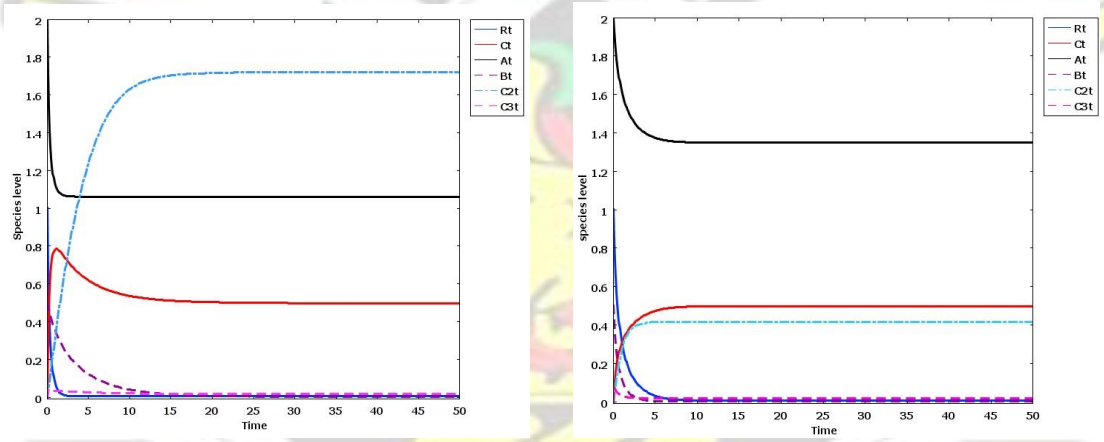

(a) (b)

Figure 6.8: Time course for ligand-receptor binding (a) K_a = 0.5, K_b = 0.1, (b) K_a = 0.1, K_b = 0.5

Figure 6.8a shows the effect of an increase in the binding rate of the ligand over the binding rate of the toxin. There is a significant rise in the formation of the complex C_2. Furthermore there is a sharp increase in the formation of the complex C followed by a decrease and becomes steady as time increase. In Figure 6.8b shows a reverse in the binding rates with the toxin binding faster than the ligand. Notice the

significant drop in the formation of the complexes C and C_2. The ligand is not consumed as in Figure 6.8a though this is expected. The formation of the complex C_3 appear to be small compared to C and C_2. This supports the information in the literature that WASP is autoinhibited in its basal form and the autoinhibited domain is relieved on binding to the ligand Cdc42 which then exposes the hydrophobic region for the toxin binding and hyperactivation.

In the next plot we study the behavior of the solution if the binding rates of both ligand and toxin are kept equal and the initial concentration of the toxin is increased.

The rate at which both ligand and toxin bind the receptor are made equal ($K_a = K_b = 0.1$) in Figure 6.9. In Figure 6.9b the initial concentration of B is increased from 0.5 to 1 (i.e. $\int_{Ycell} u_B dA = 1$). It is found that formation of the complex (C_2)

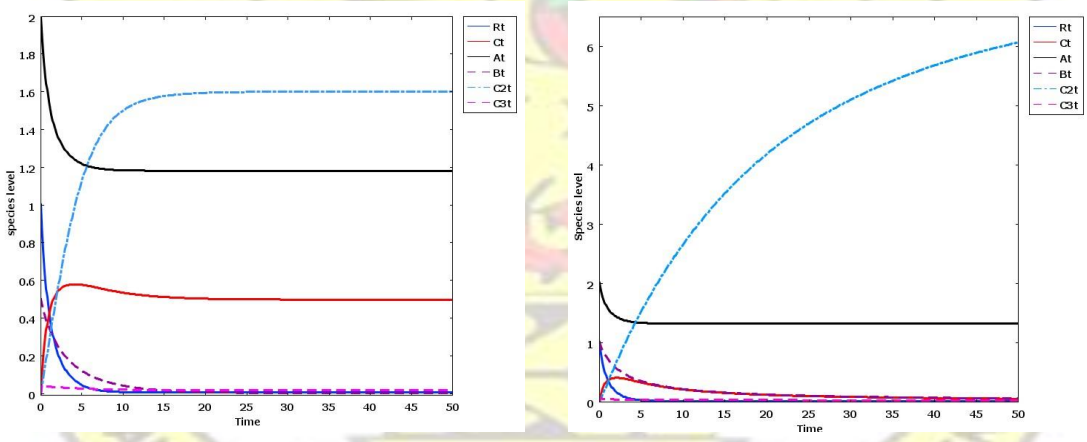

(a) (b)

Figure 6.9: Numerical solution for concentration of species (a) $k_a = 0.1$, $k_b = 0.1$, (b) $k_a = 0.1$, $k_b = 0.1$

exceed the initial concentrations of the ligands and the receptor. This supports the fact that a small amount of the toxin can disrupt the functions of WASP in the cell. It

gives an idea of how these complexes activate Arp2/3 complex leading to the over production of actin filament in the cytoplasm.

Figure 6.10 shows the surface plots of the concentration of ligand (u_A) in $2D$ and $3D$ views in Figure 6.10a and Figure 6.10b respectively. It is found that the direction of the concentration of ligand in Figure 6.10a and the highest concentration is at the center of the cytoplasm. The plot in Figure 6.10b is one of the features in COMSOL Multiphysics where a 3D plot can be obtained from a 2D model.

The plot shows the concentration distribution of the ligand (A) on the surface of the cytoplasm. The numerical solution show the concentration of A is maximum at the center of he domain as shown in both Figure 6.10a and Figure 6.10b.

Figure 6.11a show numerical solution in the second geometry where the membrane is implemented as a separate compartment. The numerical solution in Figure 6.11a is equal to Figure 6.8b for implementation of the membrane as a one-dimensional boundary. Figure 6.11b shows the surface plot for the formation of the complex C

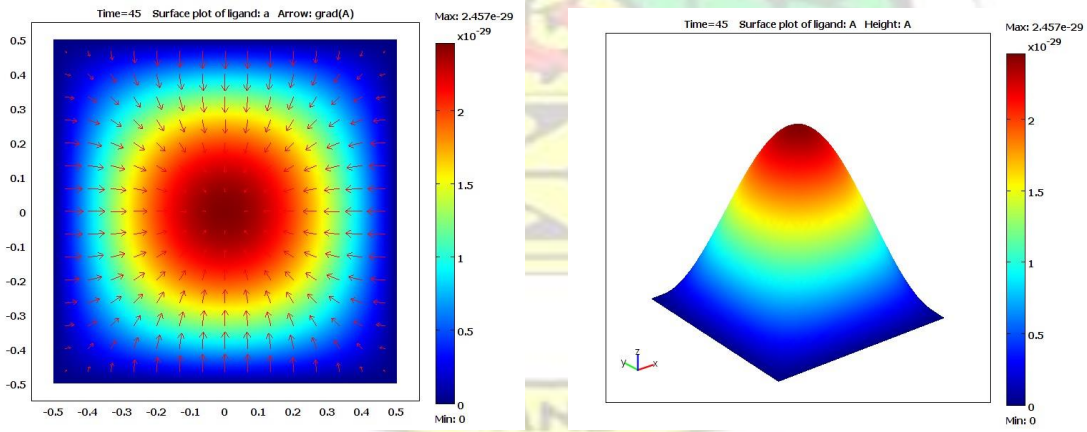

(a) (b)

Figure 6.10: Surface plot of concentration (a) 2D surface plot of u_A (A) (b) 3D surface plot of u_A

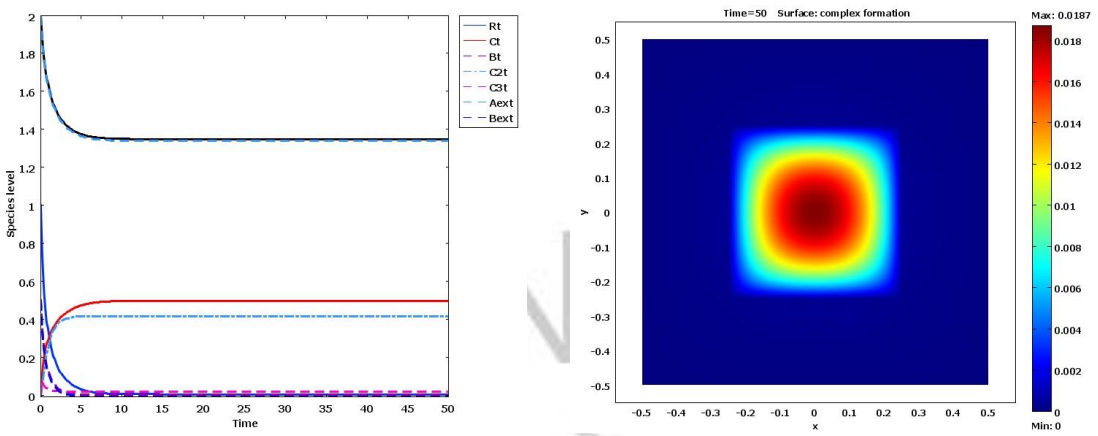

(a) (b)

Figure 6.11: Concentration and surface plot (a) Numerical solution for the concentration of species (b) 2D initial surface plot of complex C

restricted to the cytoplasm of the cell. An important result in this work is the surface plots in Figure 6.10a, Figure 6.10b and Figure 6.11b, that given the right parameters, the extent of diffusion of any of the reacting species and most especially the toxin in the tissue can be predicted. This result is crucial in the treatment of BU disease. The numerical results confirm the report in the literature that the concentration of the *Mycolactone* toxin decreases from the center to the margin of the BU (see Figure 6.12). In Laure et al. [2013], experimental epithelial cells show that *Mycolactone*induced stimulation of Arp2/3 concentrated in the perinuclear region of the cell, resulting in defective cell migration and adhesion followed by rapture.

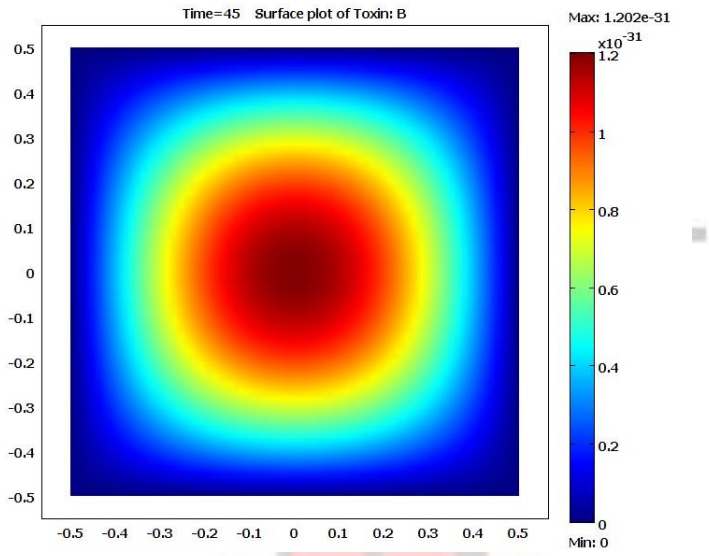

Figure 6.12: Surface plot of toxin

Next we numerically solve the reversible reactions given below in the cell.

$$[R] + [A] \underset{k_{-1}}{\overset{k_1}{\rightleftharpoons}} [C]$$

$$[C] + [B] \underset{k_{-2}}{\overset{k_2}{\rightleftharpoons}} [C_2]$$

$$[R] + [B] \underset{k_{-3}}{\overset{k_3}{\rightleftharpoons}} [C_3]$$

The evolution equations for the coupled reaction-diffusion system are:

$$\begin{cases} \frac{du_R}{dt} &= -k_1 u_R.u_A - k_3 u_R.u_B + k_{-3}u_{C_3} + k_{-1}u_C + D_R\nabla^2 u_R \\ \frac{du_A}{dt} &= -k_1 u_R.u_A + k_{-1}u_C + D_A\nabla^2 u_A, \\ \frac{du_C}{dt} &= k_1 u_R.u_A - k_{-1}u_C - k_2 u_C.u_B + k_{-2}u_{C_2} + D_C\nabla^2 u_C, \\ \frac{du_{C_2}}{dt} &= k_2 u_C.u_B + k_{-2}u_{C_2} + +D_{C_2}\nabla^2 u_{C_2}, \\ \frac{du_{C_3}}{dt} &= k_3 u_R.u_B - k_{-3}u_{C_3} + D_{C_3}\nabla^2 u_{C_3}, \\ \frac{du_B}{dt} &= -(k_2 u_B + k_3 u_R)u_B + k_{-2}u_{C_2} - k_{-3}u_{C_3} + D_B\nabla^2 u_B \end{cases} \quad (6.17.86)$$

where $k_{\pm i}$ $i \in \{1,2,3\}$ are reaction rate constants. The description of the equations follow as in section 6.3. The boundary conditions, initial conditions, and the constant diffusion coefficients used in section 6.3 remain the same. The rate constants used in the numerical simulations are shown under Figure 6.13. The numerical solution for the formation and depletion of the species in the binding or reaction process is as shown in Figure 6.13.

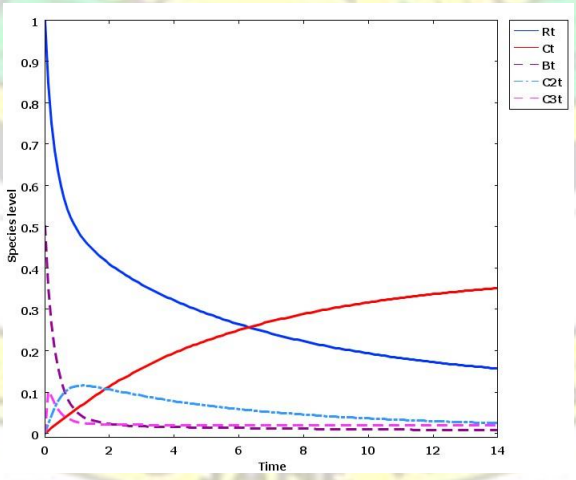

Figure 6.13: Numerical solution for the concentration of species, $k_1 = 0.5, k_{-1} = 0.01, k_2 = 0.1, k_{-2} = 0.25, k_3 = 1, k_{-3} = 0.02$

Figure 6.13 is the numerical solution for solving the coupled system of reversible reaction-diffusion equations (6.17.86). It is observed in the numerical analysis that though the number of degrees of freedom solved for remains the same, the time and memory requirements are increased about two times and six times respectively due to the inclusion of the reversible part (values not shown). The red, light dashed-dotted blue, and purple lines represent the complexes C, C_2 and C_3 respectively whiles the blue line represents the receptor R. The point where the red line meets the blue line is an equilibrium point. At this point the formation of C equals the depletion of R. The point where the red line meet the deep purple line is the equilibrium between the complex C and the toxin B. The formation of C equalize the depletion of B faster than with R at the respective equilibrium points. We also find that the equilibrium points between C and C_2, C and C_3 decrease with time respectively. The numerical results confirms that the toxin binds WASP faster than the ligand.

The table below is a summery of the performance of the three direct solvers in terms of solution time, memory usage, number of degrees of freedom solved for, and number of elements in the mesh.

Table 6.1: Performance of solvers on a coarse mesh

Solver	*J* dof's	Time (sec.)	Memory (GB)	Elements
UMFPACK	42440	131.804	566	648
SPOOLES	42440	87.961	596	648
PARDISO	42440	36.339	595	648

Table 6.2: Performance of solvers on a fine mesh

Solver	*J* dof's	Time (sec.)	Memory (GB)	Elements
UMFPACK	42440	134.774	701	2592
SPOOLES	42440	88.78	712	2592
PARDISO	42440	35.726	665	2592

The tables 6.1 and 6.2 show the performance of the solvers. In the numerical simulation, about 95% of the time used by the solvers were used in the matrix factorization step. The general observation is that the number of degrees of freedom solved for are the same in both meshes (coarse and fine). An increase in the number of mesh elements increases the computational time and memory requirement increase which is expected.

The UMFPACK solver takes the longest time to solve the linear system of equations. It is more than three times slower than the time taken by PARDISO and about one and a half times slower than the SPOOLES solver. In terms of memory requirement, the SPOOLES solver requires the largest memory and UMFPACK rquires the least in the coarse mesh. There is a little deviation when the mesh elements increased from 648 to 2592. The SPOOLES solver still requires the largest amount of memory followed by UMFPACK and PARDISO respectively. From tables 6.1 and 6.2 it can be observed that in terms of memory requirement and computational time, the PARDISO solver performs better than SPOOLES and UMFPACK although on a coarse mesh the UMFPACK requires less memory.

CHAPTER 7

Conclusions Recommendations and future work

Understanding the functions of WASP in eukaryotic cells is a major step in understanding the etiology of many diseases, including Buruli ulcer and Wiskott-Aldrich syndrome.

In this thesis, the mechanism of ligand-receptor and ligand-receptor-*Mycolactone* toxin binding and associated reaction-diffusion mechanisms is studied. The aim of the work was to develop a mathematical model for the Buruli Ulcer disease. A new model has been formulated to mimic the binding mechanism, operation and functions of WASP with its activators. The idea of isomerization was used to develop a concentration-dependent model for WASP. The isomeric structure of WASP allowed us to model mutually exclusive and mutually inclusive binding of proteins, and most importantly, account for other inputs to fully activate WASP.

From the modeling approach used, the fractional response of WASP complex at varying concentrations of Cdc42 and *Mycolactone* toxin in the cytoplasm, can be determined. From this, an idea of how actin filament polymerization in the cell is manifested is realized. The results show differences in fraction of active bound WASP complexes, and fraction of bound WASP complexes.

In the absence of a ligand, it is found that the fraction of active WASP complex is controlled by the intrinsic isomeric equilibrium constant M whiles at saturating concentration of the ligand (Cdc42), it is controlled by the affinity constant C, and M.

From the analysis, it is shown that there is a lag phase in the ligand-protein-toxin binding process. Biologically this is explained as the period for breaking of bonds (i.e. when the ligand binds and displaces the intramolecular interaction between the GBD and the VCA of WASP). Also, Egidio et al. [2007] explain this lag phase as a delay-type hypersensitivity response in BU patience in accordance with cell mediated development.

From the steady state analysis, parameterized constants and expressions were obtained for the fraction of species in terms of the kinetic and equilibrium constants. Biologically, the parameterized constants ($e^0{}_i s$) contained all the information of network routs and direct reversibility between products and reactants. It is concluded that the $e^0{}_i s$ are a generalization of the equilibrium constants in the context of biochemical networks. The reaction rates, equilibrium constants, fraction of active WASP in the absence, and at saturating concentration of the ligand, compare well with experimental results (see for example Buck et al. [2004], Devreotes and Sherring

[1985]).

For the numerical treatment of reaction-diffusion systems in the cell, a periodic geometry for computing quasi-periodicity in tissue modeling is introduced. This technique allows us to simulate one cell as a true representation of the tissue, and drastically reduced computational costs and CPU memory. The coupled system of reactiondiffusion equations were solved in the cytoplasm of the cell. The two geometrical representations of the cell membrane produced similar results. The numerical results confirm that the concentration of the toxin is highest at the center and decreases as it moves towards the boundary of the domain.

Importantly, the extent of diffusion of the toxin in the tissue is predicted with time. This is very crucial in the treatment of the BU (see Figure 6.12).

The numerical results show that though *Mycolactone* can solely activate WASP, the toxin binds well when the hydrophobic region on WASP is exposed as a result of Cdc42-GBD interaction. The performance of three direct solvers were compared. The PARDISO solver was found to perform better in terms of computational time and CPU memory usage.

Finally, it is concluded that the results obtained in this thesis are unique; it confirms existing experimental results, and give further insights into the etiology of BU disease. In Figure 4.11(a) and Figure 6.9b, an idea of what happens to the actin filament polymerization process when the concentration of *Mycolactone* toxin increases in the cell is given. Furthermore, the analysis confirm the result in Laure et al. [2013], that competitive inhibitors of *Mycolactone* toxin are needed to prevent the toxin from binding the hydrophobic region of WASP for effective treatment of BU.

7.0.1 Recommendations and Future work

In this study, the numerical simulation in a square domain of the cell cytoplasm was considered. In future, it will be necessary to extend the model to include other geometrical representations of the cell. Secondly, the system of reaction-diffusion equations can be coupled with heat equation to investigate the effect of temperature on the model. The model can be extended to include a moving mesh boundary.

Work has already started to solve the model problem using the idea of periodic homogenization. It is also important to get an experimentalist on board to verify some of the parameters in the model.

REFERENCES

et al. Abdul-Manan, N. B. Aghazadeh. Structure of cdc42 in complex with the gtpasebinding domain of the wiskott-aldrich syndrome protein. *Nature.*, 399(6734):379– 383., 1999.

N. Abdul-Manan, B. Aghazadeh, G. A. Liu, A. Majumdar, O. Ouerfelli, K. A. Siminovitch, and M. K. Rosen. Structure of cdc42 in complex with the gtpase-binding domain of the wiskott-aldrich syndrome protein. *Nature*, 399:379–383, 1999.

P. R. Amestoy and I. S. Duff. Vectorization of a multiprocessor multifrontal code. *Int.J. Suppercomputer Appl*, 3(3):41–59, 1989.

G.K. Amofah, F. Bonsu, and C. Tetteh. Buruli ulcer in ghana: results of a national case search. *Emerg Infect Dis.*, 8:167–170., 2002.

T. Andrea and B. W. Olof. *Domain Decomposition Methods-Algorithms and Theory. Springer series in Computational Mathematics.* Springer-Verlag Berlin Heidelberg, third edition., 2005.

O. Axelsson and V. A. Barker. *Finite element solution of boundary problems theory and computations;. Chapter 6.* 2001.

S. H. Belinda, H. Kirsti, M. Michael, O. Joy, H. Stephen, E. W. Anne, and E. S. Rachel. The pathogenic mechanism of the mycobacterium ulcerans virulence factor, mycolactone, depends on blockade of protein translocation into the er. 2014.

N. Bindslev. Strategies of biological regulation. 18, 2008.

J. J. Blum. The enzymatic interaction between myosin and nucleotides. *Arch Biochem Biophy*, 55:486–511, 1955.

M. Boguski and F. McCormick. Protein regulating ras and its relatives. *Nature*, 366: 643–654, 1993.

M. Boleira, O. Lupi, L. Lehman, and K. B. Asiedu. Buruli ulcer. an bras. dermatol. 85(3):281–301, 2010.

C. Bozzo. A mycobacterium ulcerans toxin, mycolactone, induces apoptosis in primary human keratinocytes and in hacat cells. *Microbes Infect.*, 12(14-15):1258–1263, 2010.

R.A. Bradshaw and E. A. Dennis. *Handbook of cell signalling*. Elsevier: st Louis, 2003.

S. Braxmeier, M. Hellmann, A. Beck, A. Umboock, G. Pluschke, T. Junghanss, and H. Weinlaeder. Phase change material for thermotherapy of buruli ulcer : modelling as an aid to implementation. *Journal of medical engineering and technology*, 33: 559–566, 2009.

S. Brenner and R. Scott. *The Mathematical Theory of Finite Element Methods*. Springer-Verlag,, 1994.

G. Bretzel, K.L. Huber, B. Kobara, M. Beissner, E. Piten, and Herbinger K. H. Laboratory confirmation of buruli ulcer disease in togo 2007-2010. *PLos Negl.Trop. Dis*, 5(7) e1228, 2011.

A. Bruce, J. Alexander, L. Julian, R. Martin, R. Keith, and W. Peter. *Molecular Biology of The Cell.* Garland Science, Taylor and Francis Group, 2008.

M. Buck, Xu. Wei, and K. R. Michael. Global disruption of the wasp autoinhibited structure on cdc42 binding. ligand displacement as a novel method for monitoring amide hydrogen exchange. 2001.

M. Buck, X. Wei, and K. R. Michael. A two-state allosteric model for autoinhibition rationalizes wasp signal integration and targeting. 2004.

P. D. Burbelo, D. Drechsel, and A. Hall. A conserved binding motif defines numerous candidate target proteins for both cdc42 and rac gtpases. *Biol. Chem*, 270(49): 29071–29074, 1995.

R.P. Bywater, A. Sorensen, P. Rogen, and P.G. Hjorth. Construction of the simplest model to explain complex receptor activation kinetics. *Theor. Biol.*, 218:139–147, 2002.

M.F. Carlier, A. Ducruix, and D. Pantaloni. Signaling to actin, the cdc42-n-wasparp2/3 connection. *Chem.Bio*, 6:R235–R240, 1999.

N. Chamakuri. *Adaptive Numerical Simulation of Reaction Diffusion Systems*. PhD thesis, Otto-Von-Guericke University of Magdeburg, Germany, 2007.

Q.A. Chaudry, M. Hanke, K Deij, and R. Morgenstern. Mathematical modeling of reaction diffusion systems in a cell including surface reactions on the cytoplasmic membranes. 2012.

H. Chen, B.W. Bernstein, and J. R. Bamburg. Regulating actin-filament dynamics in vivo. *Trends Biochem. Sci.*, 25:19–23, 2000.

J. Clancey, R. Dodge, and H. F. Lunn. Study of a mycobacterium causing skin ulceration in uganda. *Annales de la societe Belge de medicine tropica*, 42:585–590,

1962.

J. Invest. Clin. Mycolactone activation of wiskott-aldrich syndrome proteins underpins buruli ulcer formation. 123(4):1501–1512, 2013.

R. Dautray and Lions J. Luis. *Mathematical Analysis and Numerical Methosd for Science and Technology, Functional and Variational Methods*. Spriger-Verlage. vol. 2, 1988.

T. Davis. A column pre-ordering strategy for the unsymmetric-pattern multi-frontal method. *ACM. Trans. Math. Software*, 30(2):165–195, 2004.

C. Demangel, T.P. Stinear, and S. T. Cole. Buruli ulcer: Reductive evolution enhances pathogenicity of mycobacterium ulcerans. *Nat Rev Microbiol*, 7:50–60, 2009.

J. M. Derry and H. D.. Ochs. Isolation of a novel gene mutated in wiskott- aldrich syndrome. *Cell.*, 78(4):635–644, 1994.

P. N. Devreotes and J. A. Sherring. Kinetics and concentration dependence of reversible camp-induced modification of the surface camp receptor in dickyostelium. *biological chemistry*, pages 6378–6384, 1985.

K. Devriendt, A. S. Kim, G. Mathijs, S. G. Frints, and M. Schwartz. Constitutively activating mutation in wasp causes x-linked severe congenital neutropenia. *Nat. Genet.*, 27:313–317, 2001.

B. Dietrich. *Finite Elements.* Cambridge University Press, 3rd edition, 2007.

K. Dreij, Q.A. Chaudhry, B. Jernstro¨m, R. Morgenstern, and M. Hanke. A method for efficient calculation of diffusion and reactions of lipophilic compounds in complex cell geometry. *PLoS ONE*, 6(8), 2011.

T. Egidio, G. F. Alexandra, and G.C. Antonio. Evidence for intramacrophage growth phase of mycobacterium ulcerans. *American Soc. for Micr.*, pages 977–987, 2007.

M. Feinberg. The existence and uniqueness of steady-states for a class of chemical reaction networks. *Arch. Rat. Mech. Anal.*, 132:311–370, 1995.

K. George, M.D. Chatterjee, G. Gunawardana, D. Welty, J. Hayman, R. Lee, andSmall. L. C. P. Mycolactone a polyketide toxin from mycobacterium ulcerans required for virulence. *Science*, (5403), 8547:854–857, 1999.

K.M. George, L. Pascopella, D.M. Welty, and P.L. Small. A mycobacterium ulcerans toxin, mycolactone,causes apoptosis in guinea pig ulcers and tissue culture cells. *nfect Immun*, 68(2):877–883, 2000.

J.B.S. Haldane. *Enzymes.* Green and Co., 1930.

A. Hall. Rho gtpase and the actin cytoskeleton. *Science*, 279:509–514, 1998.

J. A. Hamilton. Fast flip-flop of cholestrol and fatty acids in membranes: implications for membrane transport proteins. *Lipidol*, 14:263–271, 2003.

B. T. Helfand, L. Chang, and R. D. Goldman. The dynamic and motile properties of intermediate filaments. *Annu Rev cell Dev Biol*, 19:445–467, 2003.

H. N. Higgs and T. D. Pollard. Regulation of actin-filament network formation through arp2/3 complex, activation by a diverse array of proteins. *Annual. ReV. Biochem*, 70:649–676, 2001.

H.N. Higgs and T.D. Pollard. Activation by cdc42 and pip(2) of wiskott-aldrich syndrome protein (wasp) stimulates actin nucleation by arp2/3 complex. *Cell Biol.*, 150:1311–1320., 2000.

T.L. Hill and M. W. Kirschner. Bioenegetics and kinetics of microtuble and actin filament assembly-disassembly. *Int. Rev. Cytol*, 78:1–125, 1982.

T. Hillen and A. L. Mark. *Mathematical ecology of cancer.* Springer Int. Publ. Switzaland, 2014.

H. Hong, C. Demangel, S. J. Pidot, P. F. Leadlay, and T. Stinear. Mycolactones: immunosuppressive and cytotoxic polyketides produced by aquatic mycobacteria. *Nat Prod Rep*, 25(3):447–454, 2008.

J. Howard. Mechanics of motor proteins and cytoskeleton. *Sunderland MA Sinauer*, 2001.

N. K. Hussain and S. . Jenna. Endocytic protein intersectin-l regulates actin assembly via cdc42 and n-wasp. *Nat Cell Biol.*, 3(10):927–932, 2001.

M. Imran and Smith. Hal. The pharmacodynamics of antibiotic treatment. *Comp. and Math. methods in med.*, 7 No. 4., 2006.

F. Jacob and B. Ted. *A First Course in Finite Elements.* John Wiley and Sons., 2007.

A. B. Jaffe and Hall A. Rho gtpases: biochemistry and biolog. *Annu Review Cell. Dev Biol.*, 21:247–269, 2005.

C. Jean-Pierre. 50 years of allosteric interactions, the twists and turns of the models. *Nature Reviews Molecular Cell Biology*, 14:819–829, 2013.

C Johnson. *Numerical Solution of Partial Differential Equations by the Finite Element Method.* 1990.

D. I. Johnson. Cdc42 an essential rho-type gtpase controlling eukaryotic cell polarity. *Microbiol. Mol. Biol. ReV*, 63:54–105, 1999.

M. Kathleen, P. George, Lisa, M. Diane, Welty, and P. L. C. Small. A mycobacterium ulcerans toxin, mycolactone, causes apoptosis in guinea pig ulcers and tissue culture cells. 68, No. 2:877–883, 2000.

A.S. Kim, L. T. Kakalis, N. Abdul-Manan, G. A. Liu, and M. K. Rosen. Autoinhi-bition and activation mechaism of the wiskott-aldrich syndrome protein. *Nature*, 404(6774):151–158, 2000a.

A.S. Kim, L.T. Kakalis, N. Abdul-Manan, G.A. Liu, and Rosen. M.K. Autoinhibition and activation mechanisms of the wiskott-aldrich syndrome protein. *Nature*, 404(6774):151–158, 2000b.

S. D. Kreamer, D. Lombardi, and A Primorac. Lipid-bilayer permeation of drug-like compounds. *Chem. Biodivers*, 6:1900–1916, 2009.

K. J. Laidler. General steady-state equations in enzyme and other catalyzed reactions. *Trans Faraday Soc.*, 52:1374–1382, 1956.

K.J. Laidler. *The Chemical Kinetics of Enzyme Action.* London: Oxford University Press., 1958.

N. N. Lamarche and Tapon. Rac and cdc42 induce actin polymerization and g1 cell cycle progression independently of p65pak and the jnk/sapk map kinase cascade. *Cell*, 87(3):519–529., 1996.

D.A. Lauffenburger and J.J. Linderman. *Receptors: Models for Binding, Trafficking, and Signaling.* Oxford University Press, New York, 1993).

C. Laure, G. Florent, A. Francois, Le. B. Agnes, and Laxmee et. al. Mycolactone activation of wiskott-aldrich syndrome proteins underpins buruli ulcer formation. *Clin inest.*, 123(4):1501–1512, 2013.

G. Laure, C. Florent, A. Fran¸cois, Le. B. Agn`es, C. Laxmee, Di. B. Vincenzo, F. F. Arnaud, B. Georges, and D. Caroline. Mycolactone impairs t cell homing by suppressing microrna control of l-selectin expression. 2011.

C. Lawrence and Evans. *Partial differential equations;. Graduate studies in mathematics Vol. 19, pg 287-288.* 2002.

M. Lei, W. Lu, W. Meng, M. C. Parrini, M. J. Eck, B. J. Mayer, and S. C. Harrison. Structure of pak1 in an autoinhibited conformation reveals a multistage activation switch. *Cell*, 102(3):387–397, 2000.

A. Leo, C. Hansch, and D Elkins. Partion coefficinet and their uses. *Chem Rev.*, 71: 525–616, 1971.

D.W. Leung and M. K. Rosen. The nucleotide switch in cdc42 modulates coupling between the gtpasebinding and allosteric equilibria of wiskott-aldrich syndrome protein. *Proc Natl Acad Sci U S A.*, 102(16):5685–5690, 2005.

K. Luby-Phelps. Cytoarchitecture and physical properties of cytoplasm: olume, viscosity, diffusion intracellular surface area. *Int. Rev. cytol*, 192:189–221, 2000.

L.M. Machesky and R. H. Insall. Signaling to actin dynamics. *Cell Biol*, 146: 267–272, 1999.

Q. N. Martinez, R. Rohatgi, I.M. Anto´n, M. Medina, S.P. Saville, H. Miki, T. Yamaguchi, H. Takenawa, J.H. Hartwig, R.S. Geha, and N. Ramesh. Wip regulates n-wasp-mediated actin polymerization and filopodium formation. 2001.

Brunori. Maurizio. Allostery turns 50 is the vintage yet attractive. 2011.

P. J. C. McCallum, G. Tolhurst, H. A. Buckle, G. Sissons, Buckle, and J. C. Tolhurst. A new mycobacterial infection in man. *Pathol. Bacteriol*, 60:93–122, 1948.

D. Menshykau and D. Iber. Simulation in comsol: Deforming and interacting domains. 2012.

M. W. Meyers. Mycobacterium ulcerans infection (buruli ulcer): first reported patient in togo. *British journal of Dermatolog*, 134:1116–1121, 1996.

H. Miki, T. Sasaki, Y. Takai, and T. Takenawa. Induction of filopodium formation by a wasp-relatedactin-depolymerizing protein n-wasp. *Nature*, 391(6662):93–96, 1998.

A. P. Miles, J. G. Barbara, and Graves. Autoinhibitory domains: Modular effectorsof cellular regulation. *Annu. Rev. Cell Dev. Biol*, 18:421–462, 2002.

T. J. Mitchison. Evolution of a dynamic cytoskelton philos. *Trans R. Soc. Lond B Biol Sci*, 349:299–304, 1995.

J Monod, J.P. Changeux, and F. Jacob. Allosteric proteins and cellular control systems. *Mol Biol.*, 6:306–29, 1963.

J. Monod, J. Wyman, and J.P. Changeux. On the nature of allosteric transitions: A plausible model. *Mol Biol.*, 12:88–118, 1965.

A. Morreale, M. Venkatesan, H. R. Mott, D. Owen, D. Nietlispach, P. N. Lowe, and E. D. Laue. Structure of cdc42 bound to the gtpase binding domain of pak. *Nat.Struct. Biol*, 7(5):384–383, 2000.

H. R. Mott, D. Owen, D. Nietlispach, P. N. Lowe, E. Manser, L. Lim, and E. D. Laue. Structure of the small g protein cdc42 bound to the gtpase-binding domain of ack. *Nature*, 399(6737):384–388, 1999.

S. M. Munter, Way, and et. al. Signaling during pathogen infection. *Science*, 2006.

J. D Murray. *Mathematical Biology: An Introduction*. 2001.

G. Palade. Intramolecular aspects of the process of protein synthesis. *Science*, 189: 347–358., 1975.

S. C. D. Panchal, Kaiser, and et. al. A conserved amphipathic helix in wasp/scar protein is essential for ctivation of arp2/3 complex. *Nat. struct. Biol.*, 10(8):591– 598, 2003.

G. Ciarlet Philippe. *The Finite Element Methods for Elliptic Problems.* NorthHolland Publishing Company, Amsterdam New York, Oxford, Tokyo, first edition., 1987.

T. D. Pollard and J. A. Cooper. Actin, a central player in cell shape and movement. *Science*, 326(5957):1208–1212, 2009.

F. Portaels, Johnson. P. M., and Meyers W. Buruli ulcer diagnosis of mycobacterium ulcerans disease. In *A manual for health care providers W.H.O report*, 2001.

Qiagen. Globe pathways-actin nucleating by arp-wasp complex.

M. P. Raju and S.K. Khaitan. High performance computing of three-dimensional finite element codes on a 64-bit machine. 2009.

W. M. Richard, M. B. Eric, and L.C.S . Pamela. Unraveling an emerging diease associated with disturbed aquatic environments: The case of buruli ulcer. *Frontiers in Ecology and the Environment,*, 3, No. 6. .:323–331, 2005.

M. Schunk, T. William, E. Klutse, N. Joerg, and K. Opare-Asamoah. Outcome of patients with buruli ulcer after surgical treatment with or without antimycrobacterial treatment in ghana. *Am J. Trop. Med. Hyg*, 81(1),:75–81, 2009.

Seer. *Seer*. URL http://training.seer.cancer.gov.

L.A. Segel, A. Goldbeter, P.N. Devreotes, and B.E. Knox. A mechanism for exact sensory adaptation based on receptor modification. *Theor. Biol*, 120:151–179., 1986.

Y. L. Shih and L. Rothfield. The bacterial cytoskeleto. *Microbiol Mol Biol. Rev*, 70: 729–754, 2006.

V. Siegmund, O. Adjei, P. Rac, C. Berberich, E. Klutse, F. van Vloten, T. Kruppa, B. Fleischer, and Bretzel G. Dry-reagent-based pcr as a novel tool for laboratory conformation of clinically diagnosed mycobacterium ulcerans-associated disease in areas in the tropics where m. ulcerans is endermic. *JCM*, 43.1:271–276, 2005.

R. Simona, E. Mensah-Quainoo, T. Junghanss, and G. Pluschke. What does detection of mycobacterium ulcerans dna in the margin of an excised bu lesion tell use. *journal of clinical microbiology*, 44(11):4273–4275, 2006.

A. D. Siripala and Welch. M. D. Snapshot: actin regulators ii. *Cell*, 128(5), 2007.

D.S. Snyder and P. L. Small. Uptake and cellular actions of mycolactone, a virulence determinant for mycobacterium ulcerans. *Microb Pathog*, 34(2):91–101, 2003.

J. M. Stevens, E. E. Galyov, and M.P. Stevens. Actin-dependent movement of bacterial pathogens. *Nat Review Microbiol.*, 4(2):91–101, 2006.

D. M. S. Stewart and Treiber-Held. Studies of the expression of the wiskott- aldrich syndrome protein. *Clin. Invest.*, 97(11):2627–2634, 1996.

V. Thomee. *Galerkin finite element method for parabolic problems; pg 166.* Springer-Verlag, 1984.

N. Volkmann, K.J. Amann, and S. Stoilova-McPhie. Structure of arp2/3 complex in its activated state and in actin filament branch junctions. *Science*, 293:456–59., 2001.

J. Vollmer, D. Menshykau, and D. Iber. Simulating organogenesis in comsol: Cellbased signaling models. 2013.

WHO. URL www.who.int/buruli/photos/small-ulcers/en/.

WHO. Buruli ulcer diagnosis of the mycobacterium ulcerans disease. 2001.

WHO. Report of the 7th advisory group on buruli uncer. 2004.

P.J. Woolf, T.P. Kenakin, and J.J. Linderman. Uncovering biases in high throughput screens of g-protein coupled receptors. *Theor. Biol.*, 208:403–418., 2001.

J. Zalevsky, I. Grigorova, and R. D. Mullins. Activation of the arp2/3 complex by the listeria acta protein. acta binds two actin monomers and three subunits of the arp2/3 complex. *Biol. Chem*, 276:3468–75, 2001a.

J. Zalevsky, L. Lempert, H. Kranitz, and R. D. Mullins. Different wasp family proteins stimulate different arp2/3 complexdependent actin-nucleating activities.

Curr. Biol., 11:1903–1913, 2001b.